How Do Interactions Between Cytotoxic T Cells and Targets Shape the Functional Response Describing Target Cell Death?

Saikrishna Gadhamsetty

Reading committee:	Prof. dr. Becca Asquith
	Prof. dr. Vitaly V. Ganusov
	Prof. dr. Hans Heesterbeek
	Prof. dr. Roeland M.H. Merks
	Prof. dr. Roland R. Regoes
Promotor:	Prof. dr. Rob J. de Boer
Co-promotor:	Prof. dr. Joost B. Beltman

Cover: Illustration of the different types of CTL-target interactions considered in the thesis. Assistance of Alessia Peviani and Bram van Dijk is gratefully acknowledged.
Printed by: CPI – Koninklijke Wöhrmann B.V., Zutphen, The Netherlands
ISBN: 978-94-6203-937-7

How Do Interactions Between Cytotoxic T Cells and Targets Shape the Functional Response Describing Target Cell Death?

Hoe bepalen interacties tussen cytotoxische T en target cellen de functionele response van target cel sterfte?
(met een samenvatting in het Nederlands)

Proefschrift

ter verkrijging van de graad van doctor aan de Universiteit Utrecht op gezag van de rector magnificus, prof.dr. G.J. van der Zwaan, ingevolge het besluit van het college voor promoties in het openbaar te verdedigen op woensdag 21 oktober 2015 des middags te 4.15 uur

door

Saikrishna Gadhamsetty

geboren op 5 december 1985 te Nellore, India

Promotor: Prof. dr. R.J. de Boer
Copromotor: dr. J.B. Beltman

The studies described in this thesis were financially supported by the Computational Life Sciences program of the Netherlands Organization for Scientific Research (NWO), grant number 819.03.009, by the "Virgo consortium," funded by the Dutch government [project number FES0908] and the "Netherlands Genomics Initiative (NGI)", project number 050-060-452].

Contents

Chapter 1

Introduction and Overview

1.1 Preface

Cytotoxic T lymphocytes (CTLs) play an important role in the control of virus infections and tumors by killing virus-infected and tumor cells (which is contact-dependent), and by secreting soluble factors (which is contact-independent) [1–4]. CTL-mediated killing generally involves four steps: localization of the target cell; formation of a specialized junction with the target (called a cytotoxic synapse); delivery of effector molecules, such as perforin and granzymes; and detachment from the dying target, followed by resumption of the search for new target cells, which may also be accompanied by the production of soluble factors [1, 5, 6].

An important parameter in determining the efficiency of CTL-mediated control is the rate at which they kill the target cells. There have been numerous attempts to quantify the CTL-mediated killing rates involving different pathogens and tumors, using different experimental setups [7–13], and several determinants of the CTL-mediated killing rates have been identified (density of expressed pMHC [7, 9, 12, 14], speed of migration [15], killing time [15, 16]). However, there is no clear agreement on how CTL-mediated killing varies with CTL and target cell densities [11, 17].

The central question we address in this thesis is the general functional form expected for how CTL-mediated killing depends on CTL and target cell numbers in various different scenarios, and how different factors alter this function. We find that a double saturation function with two different saturation constants in general describes the CTL-mediated killing well. Although the double saturation function describes the data from two independent cytotoxicity assays in collagen-gels, our results show that in such experiments it may be difficult to identify the underlying mechanisms of CTL-target cell interactions.

1.2 Assays to determine CTL-mediated killing rates

1.2.1 In vitro assays

In early experiments, CTL-mediated killing was measured by so-called '^{51}Cr-release' assays, in which CTLs are co-incubated with targets labeled with radio-active chromium [17, 18]. Typically after 4 hours of co-incubation, the amount of chromium released into the supernatant is measured, which was considered as an indirect measure of the CTL-mediated killing efficiency. The chromium is only released when the target cell membranes are lysed by the CTLs, and this release into the supernatant is likely not to be instantaneous [17]). Hence, the released chromium might not be a reliable indicator of the number of target cells killed, but it is unclear whether this assay over- or underestimates the killing rates. Since this assay is conducted in liquid suspensions, it cannot take some of the essential steps of CTL killing into account like finding target cells and synapse formation [2, 19, 20]. In summary, the CTL efficiency measured with this assay

is likely not representative of the *in vivo* situation.

Recently, collagen-gel assays have been developed which overcome many of the shortcomings of the ^{51}Cr-release assays [7, 21]. Most importantly, collagen gels support the migration of T cells [21, 22], and thus the killing rate realized from these assays includes the efficiency of CTLs to scan for target cells and form conjugates with them. The killing efficiency of CTLs is typically determined from the difference between the number of target cells surviving in the absence and in the presence of CTLs typically at about 20-30 hours. In such assays, the number of surviving target cells can be measured by flow cytometry [21], by bright field imaging (unpublished; see Chapter 6), or by clonogenic assays [7]. One of the potential drawbacks of this approach is that the number of targets present at the beginning and at the end of the assay is not measured within the same gel, as it has to be digested to determine the number of cells [7] (for bright field imaging a contrasting agent has to be added [21]). Therefore, if there is a high degree of variation between experimental replicates, this tends to result in inaccurate estimations of CTL-mediated killing rates. Time-lapse imaging of collagen gels [21] can help in circumventing this problem, as well as in identifying the mode of CTL-target interactions.

1.2.2 In vivo assays

In addition to the above *in vitro* assays, the CTL-mediated killing efficiency *in vivo* can be estimated from 'adoptive transfer' assays [12, 23–25]: Typically, equal numbers of peptide-pulsed target cells and unpulsed cells are transferred into mice, and the ratio of surviving pulsed and unpulsed target cells are measured at defined time intervals. As the peptide-pulsed target cells are killed by CTLs, the ratio of pulsed to unpulsed targets decreases, which can be used to estimate killing rates. However, these adoptive transfer assays do not provide information on whether all CTLs are functionally active, and on where the killing predominantly occurs.

Alternatively, killing rates have been determined from the rates at which the viral load changes following perturbations of the steady state viral load during chronic infection, or from the rate at which escape mutants replaces the wild type virus (see Chapter 7 for more details and potential misinterpretations). Fortunately, the rise in the usage of time-lapse two-photon microscopy imaging is promising for more direct, accurate estimates of CTL-mediated killing efficiencies and the underlying cellular interactions during killing [2, 19, 26].

1.3 Overview of killing rates

The killing efficiency of CTLs is often reported either as per-capita killing rates, or as the CTL-mediated death rate. The per-capita killing rate, k, is the rate at which each CTL kills a target, and the CTL-mediated death rate, K, is the rate at which a target

cell dies due to CTL-mediated killing. The CTL-mediated death rates can be used to compare the quality of CTL responses. As per-capita killing and death rates provide complementary information, it is important to know both metrics. The precise relation between the per-capita killing and the death rate depends on the functional response of CTL-mediated killing. Additionally, depending on the design of the experiment, studies report these parameters either for a CTL response targeting a single epitope, or for all responses together. Finally, the half-life of targets, $t_{\frac{1}{2}}$ is sometimes used a measure of the CTL killing pressure [17, 27], which is simply defined as $t_{\frac{1}{2}} = ln[2]/K$.

Elemans *et al.* [11] recently performed a meta-analysis of several studies and recomputed the death rates from per-capita killing rates (Table 1.1; see their supplementary text for the calculation details). These recomputed death rates likely provide ball-park estimates, as they were computed assuming mass-action killing kinetics, for which there is only limited evidence [9, 10, 15]. In one of the early adoptive transfer assays involving lymphocytic choriomeningitis (LCMV), the CTL-mediated death rates of target cells pulsed with LCMV-peptide NP396 were found to be 126.4-499.1/day [8, 9]. From the same studies, the death rates for GP276-specific response were 21.2-71.3/day. This difference in the epitope-specific killing rates occurs because NP396 elicits a dominant CTL response. Note that the variation in the estimates of killing rates for a peptide depend on whether or not target cells are considered to also die from preparation techniques of experiments (i.e., death independent of the CTLs).

In the case of polyomavirus (PyV) infection, Ganusov *et al.* [9] found CTL-mediated death rates of target cells pulsed with peptide MT389 during acute and chronic infections of 67.7/day and 21.6/day respectively, which are similar to the GP276-specific death rates during LCMV infection. In contrast to the above estimates, Hogan *et al.* [14] find much lower CTL-mediated death rate for T cells pulsed with influenza peptide NP38, about 5.67-18.4/day, and about 30% lower killing rates for B cells pulsed with the same peptide (except at the lowest peptide densities; compare the lower bounds in Table 1.1). The differences in the death rates of B and T cells suggest that these cells differ in their susceptibilities to killing. Taken together, the estimated death rates vary about 100-fold, even though all mentioned studies employ similar adoptive transfer assays and techniques to measure numbers of surviving target cell (and similar doses for peptide pulsing). Recently, Garcia et al. [12] found that CTL-mediated killing rates increase only about 10-fold when the dose of peptide-pulsing is increased 1000-fold. Thus, the role of peptide dose is limited for CTL killing, and can explain only a part of the large variability in estimated death rates.

Table 1.1. Summary of published estimates of CTL-mediated death rates. When killing rates are estimated for a specific peptide, the peptide and the target cell type used are shown in parentheses.

	CTL-mediated death rates, K/day			
Pathogen (Peptide; Target cells)	Acute	Chronic	Functional response	Reference
LCMV (NP396; Splenocytes)	126.4-499.1	-	Mass-action	[8, 10, 27]
LCMV (GP276; Splenocytes)	21.2-71.3	-	Mass-action	[8, 10, 27]
PyV (MT389; Splenocytes)	67.7	21.6	Mass-action	[9]
Influenza (NP38; T cells)	5.7-13.7	-	Mass-action + Peptide decay	[14]
Influenza (NP38; B cells)	6.1-11.3	-	Mass-action + Peptide decay	[14]
HTLV	-	0.05-0.1	-	[11]
BLV	-	1.98	-	[11]
HIV	4	-	-	[28]
HIV	-	4.4-9.8	-	[13]
HIV	0.2	-	-	[29]

Interestingly, Elemans *et al.* [11] found much lower median death rates of 1.60/day and 0.10/day during human lymphotropic virus (HTLV) (in humans) and bovine leukemia virus (BLV) infections (in sheep), respectively. The death rates during HTLV-infection were estimated from the viral decay following therapy, whereas for BLV they were determined from the difference in the surviving infected cells with and without the inhibition of CTL responses. Further, the estimates for the CTL-mediated death rates of HIV-infected cells vary over 10-fold, and there is no consensus on whether CTLs are predominantly responsible for the death of infected cells or not [13, 29–32]. The inferred death rates determined from the viral load decline critically depend on what is the rate limiting step during viral replication (see Chapter 7 for more details and for the killing rates observed during HIV-1-infection).

Overall, it appears that the estimates for the rate at which CTLs mediate killing of pathogen-infected cells are quite variable, and it remains unclear to what extent this variation in the estimated killing rates truly reflects differences in the strength of the CTL responses.

1.4 Functional response of CTL-mediated killing

Analogous to the concept in ecology, the functional response of CTL mediated killing is defined as the rate at which single CTLs kill target cells, as a function of the CTL and the target cell densities [16, 33, 34]. Multiplying the functional response with the density of CTLs gives the total number of target cells killed per unit of time. Knowledge of the functional response of CTL-mediated killing, and how it varies with different factors, can help in determining to what extent the qualitative and quantitative differences in the functional response can explain the variation in the observed killing rate estimates.

Several studies examined the functional response of CTL mediated killing. The methods to determine the functional response can be classified into three categories: using quantitative analysis of cytotoxicity assay data [8–10, 12, 14], using the analogy of enzyme-substrate kinetics [16, 33, 35], or using simulations of CTL-mediated killing [15]. With the latter two approaches one can build a theoretical expectation for the form of the functional response, and the first approach identifies the functional response observed in experimental systems. For instance, CTL-mediated killing of target cells in both the LCMV and PyV studies followed mass-action kinetics [9, 10, 15], implying that the rate at which the target cells are killed increases linearly both with increases in CTL and in target cell densities. Generally, functional responses that were mechanistically derived and those determined from simulation studies suggest saturation of CTL-mediated killing [15, 16]. In the following sections, we provide more details on these approaches to determine the expected functional response.

1.4.1 Mechanistic derivation of the functional response

Using an analogy to the Michealis-Menten (MM) model for enzyme-substrate kinetics, the expected functional response can be derived analytically assuming that a CTL can kill one target cell at a time, and that a target cell can only be killed by one CTL [16, 17, 35]. The 'reaction scheme' of CTL-mediated killing is given by

$$E + T \underset{k_{-1}}{\overset{k_1}{\rightleftharpoons}} [ET] \xrightarrow{k_2} E + T^* \ , \tag{1.1}$$

where k_1 and k_{-1} are the rates of conjugate formation and dissociation, k_2 is the killing rate (which is inversely related to the average time required for killing a target, t_D), and E, T, $[ET]$, and T^* represent free cognate CTLs, free target cells, CTL-target conjugates, and dead targets, respectively. The dynamics of conjugates, $[ET]$, free CTLs, free targets, and killed targets are then given by

$$\begin{aligned} \frac{dC}{dt} &= k_1 ET - (k_2 + k_{-1})C \ , \\ \frac{dT^*}{dt} &= k_2 C \ , \end{aligned} \tag{1.2}$$

where C and T^* represent, respectively, the number of conjugates, $[ET]$, and the number of cells killed.

Notably, Borghans *et al.* [16] used the total quasi-steady state assumption (which considerably extends the validity of quasi-steady state assumption over a larger domain of initial conditions) to derive the functional response. Following their derivation, the conservation equations for effectors and targets are given by

$$\begin{aligned} \bar{E} &= E + C, \\ \bar{T} &= T + C, \end{aligned} \tag{1.3}$$

where $\bar{E}$ and $\bar{T}$ are the total CTL and target cell numbers. From Eqs. (1.2) and (1.3), the dynamics of conjugates are given by

$$\frac{dC}{dt} = k_1(\bar{E} - C)(\bar{T} - C) - (k_2 + k_{-1})C \ , \tag{1.4}$$

By making a quasi-steady state (QSS) assumption for C (i.e., $\dfrac{dC}{dt} = 0$), we obtain the following quadratic equation in terms of the total number of conjugates, C:

$$C^2 - (h + \bar{E} + \bar{T})C + \bar{E}\bar{T} = 0, \tag{1.5}$$

where $h = (k_2 + k_{-1})/k_1$ is the Michaelis-Menten constant. Solving the above quadratic equation, we can obtain the expression for C (which we hereafter refer to as the full QSSA solution), given by

$$C = \frac{1}{2}\left(h + \bar{E} + \bar{T} - \sqrt{(h + \bar{E} + \bar{T})^2 - 4\bar{E}\bar{T}} \right) \ . \tag{1.6}$$

The full QSSA model can be further simplified using a Padé approximation, which is a rational approximation of a function, to obtain the following expression for C:

$$C = \frac{\bar{E}\bar{T}}{h + \bar{E} + \bar{T}} \ . \tag{1.7}$$

From Eqs. (1.7) and (1.2), the number of cells killed per unit time (the total killing rate) is given by

$$\frac{dT^*}{dt} = \frac{k_2 \bar{E}\bar{T}}{h + \bar{E} + \bar{T}} = K(\bar{E}, \bar{T})\bar{T} = f(\bar{E}, \bar{T})\bar{E} \ , \tag{1.8}$$

where $K(\bar{E}, \bar{T}) = \dfrac{k_2 \bar{E}}{h + \bar{E} + \bar{T}}$ is the CTL-mediated death rate, and $f(\bar{E}, \bar{T}) = \dfrac{k_2 \bar{T}}{h + \bar{E} + \bar{T}}$ is the functional response of CTL-mediated killing. This functional response saturates with increases in target cell densities, but decreases with increasing CTL densities. The total killing rate (i.e., number of cells killed per unit time) saturates similarly with both an increase in CTL and target cells—i.e., a double saturation function. Further, the CTL-mediated death rate saturates to the same extent with increases in CTL or target cell densities.

In recent in vitro studies, it was shown that a single CTL can polarize lytic granules towards multiple target cells simultaneously [36], and that multiple CTLs can interact with a single target cell at the same time [37]. Thus, killing is probably not 'monogamous' in all circumstances, and the above-mentioned functional response need not apply for regimes of killing that involve different cellular interactions. Although Merrill [33] heuristically determined a functional response for cases where multiple CTLs bind and jointly kill a target cell, it remained unclear whether this can be analytically derived, and whether a general functional response exists for various scenarios of CTL-target cell interactions.

1.4.2 Simulation approach to determine the functional response

Instead of applying the analogy to enzyme-substrate kinetics, the expected functional response can be determined using computer simulation models that mimic the *in vivo* observed migration properties, in which the CTL-mediated killing rates at different CTL and target cell densities are measured. Graw and Regoes [15] simulated a region of a lymphoid tissue using agent-based model to determine the functional response, and in contrast to Borghans *et al.* [16] they found that the CTL-mediated killing saturated at much lower CTL than target cell densities, which breaks the symmetry of Eq. 1.8 derived by Borghans *et al.* [16]. However, in their simulations CTLs could kill multiple target cells simultaneously, whereas a target cell could only be killed by a single CTL even if it is contact with many CTLs. Thus, it remained unclear whether the onset of saturation in killing at lower CTL densities is due to these particular CTL-target interactions. Moreover, the importance of other factors in the simulations was unclear, such as whether killing takes place in 2D or 3D environments and the stability of conjugates.

In summary, at the start of this PhD project it was unclear what to expect for a general functional response, and how different factors influence the functional response.

1.5 Thesis outline

In the first part of this thesis (**Chapters 2-4**), we investigate the functional response of CTL-mediated killing of target cells, and how various factors like the mode of CTL-target cell interactions, stability of the conjugates, and tissue dimensionality, influence the functional response. We employ computational and mathematical models to determine the expected general functional response from the various CTL-target cell interactions. In the second part of the thesis (**Chapters 5-6**), we analyze the experimental data from two cytotoxicity assays to determine which functional responses occur under different experimental conditions. Finally, in the third part of the thesis (**Chapters 7-8**), we review the importance of CTL-mediated killing in HIV infection, and provide a summarizing discussion and outlook.

In **Chapter 2**, we investigate why different studies found different functional responses of CTL-mediated killing, and attempt to determine a general functional response using 2D simulations of CTL-target cell interactions. We considered four simple scenarios of such cellular interactions that differ in the types of conjugate allowed, and in all simulations we find that the CTL-mediated killing saturates both with increasing CTL and target cell densities, although the relative extent of saturation depends on the nature of the CTL-target interactions. We show that CTL-mediated killing resulting from the simulations of all the CTL-target cell interactions can be well described by a double saturation (DS) model with two different saturation constants—one for saturation in CTLs and the other for saturation in target cells.

The simulations from which the general functional response was derived had conjugates with quite stable CTL-target cell interactions. Thus, usually a conjugate with a single CTL led to their death, i.e., these represented 'single-stage' killing models. In **Chapter 3**, we examine how the functional response changes if the target cell needs to transit through multiple stages before dying (i.e., multi-stage killing). The onset of saturation occurs at much higher densities of CTL and target cells, but we find similar relative onsets of saturation in the CTL and target cell densities as observed in single-stage killing (Chapter 2). Furthermore, we again find that the DS model describes the CTL-mediated killing well for all the modes of CTL-target interactions, and we explain this delay mechanistically with a mathematical derivation in a model describing the binding site dynamics.

The DS model can be mechanistically derived for cases in which target cells are only killed by a single CTL at a time, and for other cases it is still a good approximation and provides a semi-mechanistic description. Therefore, the functional response of CTL-mediated killing is expected to qualitatively remain the same between 2D and 3D spaces. However, quantitatively there may be differences due to factors such as the number of cells that can bind in 2D versus 3D spaces, and differences in the scanning efficiency. In

Chapter 4, we study the quantitative changes of the functional response in 2D and 3D spaces, and show that the saturation in killing rate indeed depends on the dimensionality of the tissue. We find that the saturation sets in at lower densities in the 3D than in the 2D simulations, and that this is due to higher encounter rates between cells in 3D environments.

Having developed a general expectation for the functional response in various circumstances, we apply it to data from *in vitro* cytotoxicity assays in collagen gels to determine the functional responses observed experimentally. In **Chapter 5**, we re-analyze published data from CTL-mediated killing of melanoma cells in collagen gels [7], and extensively compare the performance of multiple competing models that offer different explanations. Although a phenomenological square root function describes the CTL-mediated killing statistically better than a saturation model, it fails to describe the critical T cell concentration required to balance the growth. Therefore, we conclude that the saturation model is currently the best mechanistic descriptor of the CTL-mediated killing of melanoma cells in these gels. Furthermore, in **Chapter 6** we examine an independent data set from similar cytotoxicity assays of ovarian cancer cells, which have a different spatial distribution of cells compared to the assays in Chapter 5. In this data set, we again find that saturation is stronger with CTL than with target cell density. We also investigate whether this allows for a conclusion about the nature of CTL-target interactions for the particular spatial configuration of the assays. In contrast to the experiments, we always found in our simulations that CTL-mediated killing saturates more strongly with target than CTL density, irrespective of the mode of the CTL-target cell interactions. Interestingly, this suggests that we incompletely understand the interactions, and that there may be additional mechanisms at play that result in saturation at lower CTL densities.

In **Chapter 7**, we review published estimates of CTL-mediated death rates in HIV-1 infections and examine the importance of the CTL-mediated killing in HIV control. Besides highlighting potential misinterpretations of the CTL-mediated killing rates during HIV-1 infection, we conclude that CTLs may be killing the majority of virus-producing cells. This is consistent with all experimental studies. Finally, in **Chapter 8**, we summarize the results from all the chapters of the thesis, and conclude with an outlook for better estimates of CTL-mediated killing rates and functional responses.

Chapter 2

A General Functional Response of Cytotoxic T Lymphocyte Mediated Killing of Target Cells

Saikrishna Gadhamsetty, Athanasius F.M. Marée, Joost B. Beltman and Rob J. de Boer

Biophys. J. 106:1780–1791.

Abstract

Cytotoxic T lymphocytes (CTLs) kill virus-infected cells and tumor cells, and play a critical role in immune protection. Our knowledge on how the CTL killing efficiency varies with CTL and target cell numbers is limited. Here, we simulate a region of lymphoid tissue using a cellular Potts model to characterize the functional response of CTL killing of target cells, and find that the total killing rate saturates both with the CTL and the target cell densities. The relative saturation in CTL and target cell densities is determined by whether a CTL can kill multiple target cells at the same time, and whether a target cell can be killed by many CTLs together. We find that all the studied regimes can be well described by a double saturation function with two different saturation constants. We show that this double saturation model can be mechanistically derived for the cases where target cells are killed by a single CTL. For the other cases, a biological interpretation of the parameters is still possible. Our results imply that this double saturation function can be used as a tool to predict the cellular interactions in cytotoxicity data.

2.1 Introduction

Cytotoxic T lymphocytes (CTLs) are critical to control and to eliminate viral infections and tumors. Adoptive transfer of *in vitro* activated CTLs has been shown to successfully induce tumor regression both in mice [2, 38, 39] and in humans [40]. The rate at which a CTL kills target cells, as well as the variation of the killing rate when CTL and target cell densities change, are poorly characterized. Knowledge of these CTL killing efficiency parameters is important to estimate the critical CTL density required for sterilizing immunity to tumours and viral infections [7, 10, 41, 42].

Analogous to the concept in ecology, the functional response of CTL mediated killing is defined as the rate at which single CTLs kill targets, as a function of the CTL and the target cell densities [16, 33]. Multiplying the functional response with the density of CTLs gives the total killing rate, i.e., the total number of target cells killed per unit of time. Several studies examined the functional response of CTL mediated killing [10, 15, 16, 33]. Using an analogy to the Michealis-Menten (MM) model for enzyme-substrate kinetics, Borghans *et al.* [16] derived a functional response assuming that a CTL can kill one target cell at a time, and that a target cell can only be killed by one CTL. They found for such 'monogamous killing' that the total killing rate should saturates to the same extent with an increase in either CTL or target cell densities. In recent *in vitro* studies, it was shown that a single CTL can polarize lytic granules towards multiple target cells simultaneously [36], and that multiple CTLs can interact with a single target cell at the same time [37]. Thus, killing is probably not monogamous in all circumstances, and the above-mentioned functional response might not apply for regimes of killing that involve different cellular interactions.

A number of theoretical studies examined the functional response of CTL killing resulting from non-monogamous killing regimes. In an early study, Merrill [33] extended the enzyme-substrate kinetics analogy by allowing multiple CTLs to bind and independently kill single target cells. He found that the total killing rate in this model saturates at lower target cell densities than CTL densities. Contrary to these results, Graw and Regoes [15] found that CTL killing efficiency does not saturate with increasing target cell densities in their agent-based model simulations, but saturates with increasing CTL densities. Adding to the confusion, Ganusov et al. [10] analyzed *in vivo* cytotoxicity data [23] and concluded that mass-action kinetics (i.e., no saturation) describe the CTL mediated killing well. Taken together, it remains unclear how the CTL killing rates vary with CTL and target cell densities, and why we observe mass-action kinetics in some studies [10] and saturation in CTLs and/or targets in others [15, 16, 33].

In this study, we examine whether the differences in the functional responses of the different studies can be due to differences in the underlying CTL-target cell interactions. To address this question, we first create simulated data on well-defined killing regimes that differ in the allowed CTL-target cell interactions. For this purpose, we perform cellular Potts model (CPM) [43, 44] simulations of a densely packed cellular environment (like in a lymph node or spleen). Next, for each of the simulated killing regimes, we

examine whether a functional response can be mechanistically derived. Strikingly, we find that the total killing rate for all the killing regimes can be unified into a double saturation function with two saturation constants, one for the target cells and another for the CTLs. The saturation constants for the CTLs and the target cells turn out to depend on the killing regime, and can hence be used to infer the cellular interactions that underly *in vivo* and *in vitro* cytotoxicity assay data.

2.2 Materials and Methods

2.2.1 Cellular Potts model

We simulate a region of a spleen or a lymph node using the 2-dimensional CPM formalism. Similar to our previous studies [45, 46], we consider a field representing the T-cell zone of a lymph node, which is composed of fibroblastic reticular cells [47] forming a reticular network (RN; ≈17% of the field), B cells as target cells (≈39%), and CTLs (≈39%), and let the rest of the field (≈5%) be extracellular matrix (ECM). Following the initialization of the RN, both B cells and CTLs are initialized at empty random positions as a square of 9 μm^2, which subsequently grow to their target area of 44 μm^2, corresponding to a diameter of almost 8 μm [7]. Changes in the cell configuration and movements of the cells occur due to minimization of the surface energy of the cells. At each time step, all pixels are considered for extension into a random neighboring site, and the change in surface energy due to an extension is calculated by the difference in Hamiltonians H of two configurations. The Hamiltonian is given by

$$H = \sum_{ij} \sum_{i'j'} J_{\tau(\sigma_{ij}),\tau(\sigma_{i'j'})} \left(1 - \delta_{\sigma_{ij},\sigma_{i'j'}}\right) + \sum_{\sigma} \lambda (a_\sigma - A_{\tau(\sigma)})^2 \,, \tag{2.1}$$

where $J_{\tau(\sigma_{ij}),\tau(\sigma_{i'j'})}$ is the surface energy associated between a cell site (of state σ_{ij} and cell type $\tau(\sigma_{ij})$) and the neighboring lattice site (of state $\sigma_{i'j'}$ and cell type $\tau(\sigma_{i'j'})$), λ is the inelasticity, δ is the Kronecker delta, a_σ is the actual area of the cell σ, and $A_{\tau(\sigma)}$ is the target area of cells of type $\tau(\sigma)$. The first term in Eq. 2.1 represents the sum of all surface energies, and the second term is an area constraint applied to maintain the size of the cells close to their target area. The probability that a lattice site is copied into the neighboring site obeys a Boltzmann equation, i.e., is 1 if $\Delta H < 0$, and $e^{-(\Delta H)/D}$ otherwise, where D represents the membrane fluctuation amplitude of cells. The entire model is implemented in the C programming language.

2.2.2 Motility of cells in the simulations

Naïve T and B cells in lymph nodes migrate in a consistent direction for several minutes, but exhibit no preference for directional migration in the long term, i.e., they perform a persistent random walk [26, 48]. Previously, we showed that a self-adjusting motility of T

cells is sufficient to explain these dynamical properties of T cells in lymph nodes [45, 46], and we here adopt the same algorithm. Briefly, the extensions of a lattice site along a 'target direction' are made more likely than in other directions by extending ΔH for B cells and CTLs as follows:

$$\Delta H = -\mu cos(\alpha) \, , \tag{2.2}$$

where μ is the directional propensity of cells, and α is the angle between the target direction and the direction of the considered displacement. At the start of the simulation, the target direction of cells is assigned randomly from a uniform distribution of $[-\pi, \pi]$, and it is asynchronously updated thereafter every 180 seconds based on its direction of recent migration. Immotile cells tend to be circular, whereas migrating cells are slightly elongated with an extended tail.

For the employed model parameters (described below), we find mean speeds of simulated CTLs and target cells of about 9.5 μm/min and 5.6 μm/min, respectively (representative speed profiles are shown in Fig. S1A-D in the supplementary information). Using Fuerth's equation [49], the motility coefficients of CTLs and B cells are estimated to be 66.3 μm^2/min and 25.9 μm^2/min respectively (Fig. S1E), which are close to experimental findings [26, 48, 50]. The mean square displacement (Fig. S1E) confirms that the target cells and CTLs in our model roughly perform persistent random walks [26, 45, 51].

2.2.3 Killing algorithm

When a CTL and a target cell come into contact, they form a conjugate based on the rules of the killing regime(see Supplementary Figure S4 for algorithms of simulations). To keep cells in a conjugate together, we up-regulate the adhesion between a CTL and its target immediately upon conjugate formation, that is, decrease the surface tension for these cells by $\gamma_{adhesion} = 60$. Thus, the effective surface tension between CTLs and targets in a conjugate γ_{conj} becomes $\gamma_{CTL,tgt} - \gamma_{adhesion}$. In addition to the up-regulation of adhesion, we stop the active migration of both CTLs and targets in conjugates by setting the directional propensities μ of all conjugated cells to zero. Cells in a conjugate have a flattened interface zone due to the strong adhesion. Unless otherwise mentioned, we do not restrict the number of binding sites on CTLs and target cells, but the finite surface area of the cells naturally limits the maximum number of synapses that cells can form.

We perform simulations for four well-defined killing regimes: monogamous, joint, simultaneous, and mixed killing (Fig. 2.1A). For monogamous killing, conjugates of only one CTL and one target cell are allowed to occur, whereas conjugates of any number of CTLs and target cells can be formed during mixed killing. In the joint killing regime, multiple CTLs are allowed to bind and jointly kill a target cell. Conversely, multiple targets can be killed by a single CTL in the simultaneous killing regime. Conjugates are followed throughout the simulation to count the duration of contact for all target cells in conjugates. For monogamous and simultaneous regimes, target cells are killed if their duration of contact with a CTL reaches the 'kill time' t_D. With respect to simultaneous killing, we

considered CTLs to be able to kill multiple target cells all with the same kill time (each in t_D minutes), i.e., killing of individual targets does not slow down when a CTL kills multiple targets at the same time. We chose this simplest case due to the lack of experimental data concerning such changes in t_D. For the other 2 types of killing regimes (i.e., joint and mixed), we consider the killing rate of a target cell to be proportional to the number of CTLs bound to it, which is achieved by keeping track of the cumulative contact duration with all conjugated CTLs of a target. This implies that the time required to kill a target cell decreases linearly with the number of CTLs in a conjugate (e.g., two CTLs bound to a target would kill it in $t_D/2$ mins, i.e., half the time required for single CTL to kill a target cell). When the duration of contact for target cells in a conjugate reaches the kill time t_D, the target cell disappears in a few seconds (by setting its target area to -1 μm^2), and the CTL resumes its migration, if it is not conjugated to any other target cell. In all our simulations, CTLs can also serially kill any number of targets, i.e., CTLs require no "re-arming" time required between killing two consecutive targets. To maintain a constant target cell density in the field throughout the simulation, we introduce a new target cell at a random position as soon as the area of the killed cell has reached zero. To prevent new target cells from being created inside another cell, this randomly chosen point for introducing a target cell is required to be either in the ECM, or at the membrane between two cells. If conjugates break despite a strong adhesion preference, target cells remember the elapsed contact duration, i.e., upon renewed contact with the same or another CTL the kill signal accrues on the existing signal. After break-up of a conjugate, the CTL and the target resume their migration in the field if they are not conjugated to other cells.

To speed up the approach to steady state, CTLs are allowed to form conjugates (yet do not kill target cells) during an initialization period of 4 mins. At the end of this initialization period, we draw a random number from a uniform distribution of [0 min, t_D min), to represent the time already elapsed in the conjugate. Conjugate formation during the initialization period, together with elapsed conjugate time assignment, results in a rapid approach to a quasi steady state (QSS) of killing dynamics, which is characterized by a constant number of conjugates during our simulations. We discard the initialization period in all analysis and plots. Following initialization we run each simulation for 600 minutes, i.e., 40 times the kill time t_D. To maintain similar migration properties at different frequencies of CTLs and target cells, we vary the number of antigen-bearing target cells, $\bar{T}$, and cognate CTLs, $\bar{E}$, while keeping the total number of T and B cells in the field constant. To make sure that the measured killing occurs at QSS, the number of cells killed are counted over the last 75 mins of the simulation, and is averaged over 6 independent simulations for all CTL and target cell densities. Our analysis with 6 independent simulations resulted in a robust data set with little variability, as can be appreciated from the very low standard deviations (e.g., Figs. 3-5). Each simulation took about 3 hours of CPU time on a single processor of Intel Xeon 3.33 GHz with 48 GB of memory.

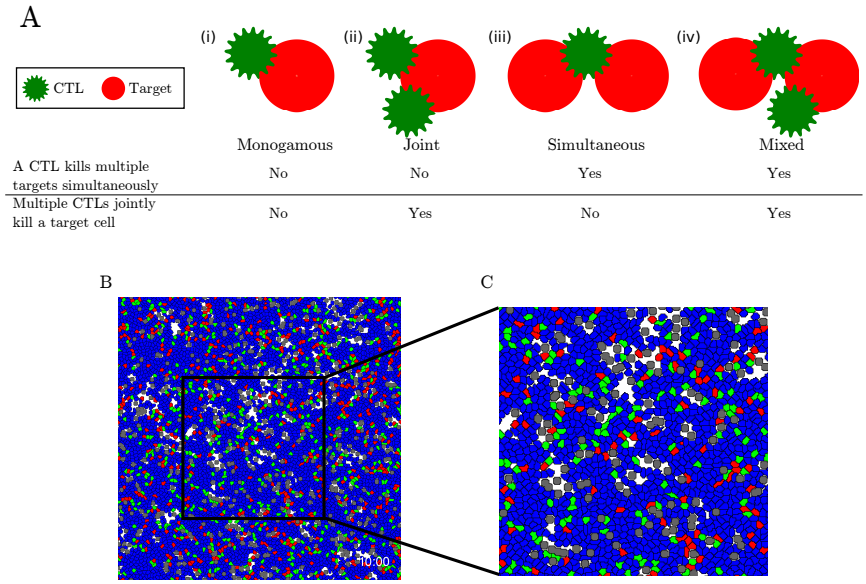

Figure 2.1. Illustration of the model. Panel A illustrates the killing regimes. Panel B depicts a snapshot of a 2-dimensional simulation, and panel C shows a magnified view of a region of the field. CTLs and target cells are depicted in green and red, respectively, and the reticular network is shown in grey. Non-specific target cells and CTLs are shown in blue. The snapshots shown in (B) and (C) are from simulations in the absence of killing with $\bar{E} = 500$ cells and $\bar{T} = 500$ cells.

2.2.4 Default model parameters

All the simulations are performed using the parameters described below (see Table 2.1 for a summary of the simulation parameters). We consider a 2-dimensional torus of 500 pixels$\times$500 pixels, where the length of each lattice site equals 1μm. One time step in the simulation (i.e., attempting to update all the lattice sites) corresponds to 1 second in real time. CPM is a phenomenological model [43, 44], and its parameters have no biophysical meaning. We tuned CPM parameters such that the simulations captures *in vivo* migration properties of CTLs and B cells, a fraction of which are target cells. The surface energies J and the surface tensions γ are chosen such that the non-cognate interactions between any pair of cells (including the RN) are neutral (see Table 2.2), i.e., there is no preferential adhesion. Other default parameters used in the simulations: t_D = 15 min [15, 26], μ_{CTL} = 450 for CTLs, $\mu_{\ mathittgt}$ = 220 for targets, $\lambda = 200$, and $D = 6$.

2.2.5 Non-linear regression (or fit) to the data

All the regression analyses of models to the data from simulations are performed using the function *nlinfit* in MATLAB (The MathWorks Inc., Natick, MA), which uses the

Table 2.1. Summary of simulation parameters used. Parameters are chosen such that the simulated CTLs and B cells recapitulate migration properties observed *in vivo*. Surface energy parameters are mentioned in Table 2.2.

Parameter	Symbol	Value used (units)
Time required to kill a target	t_D	15 mins [15, 26]
Inelasticity of the cells	λ	200
Membrane fluctuation amplitude of cells	D	6
Directional propensity of CTLs	μ_{CTL}	450
Directional propensity of targets	μ_{tgt}	220
Target direction update interval	-	3 mins
Number of static elements representing RN	-	1050
Diameter of the rod	-	8μm
Total number of CTLs	-	2250
Total number of target cells	-	2250
Target area of CTLs and target cells	A	44μm^2

Table 2.2. Default surface energies and surface tensions used in the simulations. Surface energies are represented by J, and γ are the surface tensions in arbitrary units.

	ECM	RN	CTL	Target (tgt)
ECM	$J_{ECM,ECM} = 0$	$\gamma_{ECM,RN} = 0$	$\gamma_{ECM,CTL} = 0$	$\gamma_{ECM,tgt} = 0$
RN	$J_{RN,ECM} = 0$	$J_{RN,RN} = 0$	$\gamma_{RN,CTL} = 150$	$\gamma_{RN,tgt} = 150$
CTL	$J_{CTL,ECM} = 150$	$J_{CTL,RN} = 300$	$J_{CTL,CTL} = 300$	$\gamma_{CTL,tgt} = 0$
tgt	$J_{tgt,ECM} = 150$	$J_{tgt,RN} = 300$	$J_{tgt,CTL} = 300$	$J_{tgt,tgt} = 300$

Levenberg-Marquardt algorithm. Log-transformed numbers of cells killed were used for all the regressions to prevent skewing of the fit to the killing observed at high CTL and target cell densities.

2.3 Results

2.3.1 Cellular Potts model simulations

To determine the killing efficiency for different killing regimes, a CPM of simulated CTL and target cell (B cells in our case) migration in the T cell zone of a lymphoid tissue was constructed. The CPM is a grid-based model, in which each biological cell consists of multiple lattice sites (see Materials and Methods for details). Similar to our previous work on the migration of T cells and their interactions with dendritic cells [45, 46], we consider a finite, wrapped two-dimensional (2D) space. Spleen and lymph nodes (LNs) have a complex topology and constitute different cell types, but we consider for simplic-

ity a space filled with static elements representing the fibroblastic reticular network (RN) that is present in LNs (≈17% of the space), 2250 CTLs, and 2250 target cells (representative snapshots of simulations are shown in Fig. 2.1B-C). Note that the field is densely packed with RN, CTLs, and targets, and only about 5% of the space is extracellular matrix (ECM). We perform simulations with different numbers of antigen-bearing target cells and their cognate CTLs, while keeping the total number of CTLs and target cells constant (2250 cells each). All the CTLs and targets exhibit the same migration properties, irrespective of their antigen status. This approach restricts confounding effects of different motility patterns that may arise when antigen-specific cell numbers are varied. CTLs and target cells perform a persistent random walk according to a set of well-defined migration rules (see Materials and Methods for details), which result in a realistic cell migration (see Fig. S1 in the supplementary information) and cellular interactions [45, 46].

Recent imaging studies suggested that multiple CTLs can jointly kill a target, and one CTL can kill multiple targets simultaneously [36, 37]. To identify a general functional response, we therefore perform simulations for four different killing regimes: monogamous, joint, simultaneous, and mixed killing (Fig. 2.1A; note that this nomenclature is chosen from the viewpoint of the CTL). In the *monogamous* killing regime, conjugates of just one CTL and one target cell are allowed to form. In the *mixed* killing regime, a CTL can induce death of multiple target cells simultaneously, and a target cell can be killed by multiple CTLs. Joint and simultaneous killing regimes are intermediates between monogamous and mixed. For *joint* killing, a CTL can kill only a single target cell at a time, but a target cell can be killed by many CTLs acting together (similar to the case Merrill [33] considered). Conversely, in the *simultaneous* regime, a CTL can induce death of multiple target cells simultaneously, but a target cell can be killed by a single CTL only. It is unknown how the killing time t_D varies with the number of CTLs and target cells in a conjugate. For simplicity, we therefore make the killing rate proportional to the number of synapses formed per target cell, and the rate at which CTLs kill individual targets does not decline with the number of synapses they have with target cells. Note that rather than explicitly modeling the binding sites [33], the finite surface area of CTLs and target cells in the CPM naturally restricts the maximum number of synapses that cells can form, unless otherwise specified.

A killing time t_D of 15 minutes is used in all the simulations. After an initial transient of 4 mins, the number of cells killed over 5 minute intervals, and the number of synapses that target cells have with CTLs, are recorded every 5 mins (Fig. 2.2) to assess quasi steady state (QSS). Because we want to fit mathematical models to our artificial data after the system has reached QSS, we only use the number of cells killed during the final 75 mins of the simulation, which was sufficient to approach to QSS for all regimes. For a given CTL and target cell density, the total number of synapses with targets are the lowest for the monogamous killing regime (Fig. 2.2A) as only one CTL can be in synapse with a target cell. Another factor that likely plays a role in the rather subtle differences between joint, simultaneous and mixed killing, is that in our simulations CTLs migrate faster than targets, and conjugates do not actively migrate. In the mixed killing regime, we observe more synapses than there are target cells because multi-cellular conjugates of several CTLs and several targets can occur (Fig. 2.2A). Since killing takes 15 minutes

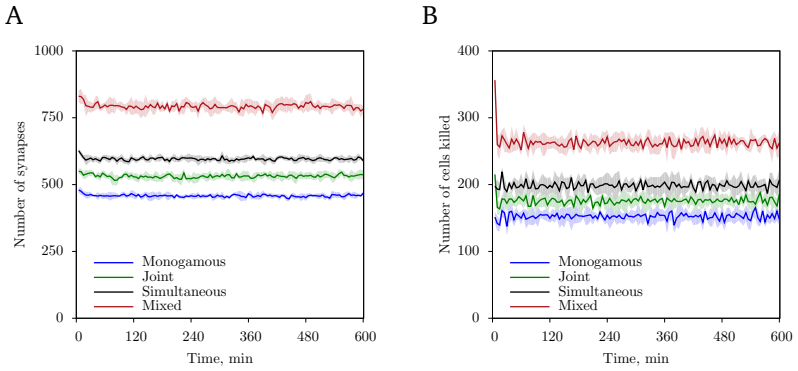

Figure 2.2. The total number of synapses with target cells (A) and the number of cells killed (B) over 5 minute intervals during simulations with $\bar{E} = 750$ cells and $\bar{T} = 750$ cells for the four killing regimes. Solid lines indicate the average from 6 independent simulations, and the shaded regions indicate standard deviations over these 6 observations. The dynamics of conjugates and cells killed during the initialization period are not shown (i.e., time $t = 0$ denotes the time point after this initialization. The dynamics of conjugates and cells killed does not exhibit any correlation with time (Spearman's correlation $|\rho_S| < 0.09$, $P > 0.23$).

in the monogamous killing case, and the number of cells killed is recorded over 5 minute intervals, the number of cells killed is about one-third of the number of conjugates at QSS (Fig. 2.2B).

2.3.2 Monogamous killing

In our monogamous killing simulations (see Movie S1 in the Supporting Material for a representative simulation), CTLs and targets form 'complexes' that dissociate after a contact duration $t_D = 15$ mins into a free CTL and a dying target cell (see Fig. S4 for a simplified simulation algorithm). For this scenario, Borghans *et al.* [16] followed the Michaelis-Menten (MM) analogy to derive an expression for CTL mediated killing:

$$E + T \underset{k_{-1}}{\overset{k_1}{\rightleftharpoons}} ET \xrightarrow{k_2} E + T^* \,, \tag{2.3}$$

where k_1 and k_{-1} are the rates of conjugate formation and dissociation, k_2 is the killing rate, and E, T, ET, and T^* represent free cognate CTLs, free target cells, CTL-target conjugates, and dead targets, respectively. In this model, the killing rate k_2 is assumed to be exponentially distributed, which is different from a fixed time required to kill a target t_D used in our CPM simulations.

In brief, they used a total quasi steady state approximation (tQSSA) to find that the number of cells killed over a time period Δt is given by

$$K_{full} = k_2 \Delta t C = k_2 \Delta t \, \frac{h + \bar{E} + \bar{T} - \sqrt{(h + \bar{E} + \bar{T})^2 - 4\bar{E}\bar{T}}}{2} \,, \tag{2.4}$$

where C is the number of conjugates, $\bar{E}$ and $\bar{T}$ are the total number of cognate CTLs and target cells respectively, k_2 is the killing rate of target cells, and h is the Michaelis constant defined as $\frac{k_2 + k_{-1}}{k_1}$. Hereafter this model is referred to as the 'full QSSA model'. Borghans *et al.* [16] further showed that a simplified expression can be derived by using a Padé approximation of Eq. 2.4 (hereafter referred to as 'Padé model'):

$$K_{Padé} = k_2 \Delta t C = \frac{k_2 \Delta t \bar{E} \bar{T}}{h + \bar{E} + \bar{T}} \ . \tag{2.5}$$

This Padé model can be rearranged to a conventional double saturation (DS) model with a single saturation constant:

$$K_{DS} = \frac{k' \Delta t \bar{E} \bar{T}}{1 + \bar{E}/h + \bar{T}/h} \ , \tag{2.6}$$

where $k' = k_2/h$. This function is known in ecology as the Beddington functional response [34, 52]. Note that for $h \to \infty$ the DS model approaches the classical mass-action model:

$$K_{mass} = k' \Delta t \bar{E} \bar{T}. \tag{2.7}$$

Thus, k' in Eq. 2.6 is the mass-action killing rate.

As expected from both the full QSSA and the DS models, our monogamous killing simulations show that the number of cells killed saturates to a similar extent when we increase target cell or CTL densities (Figure 2.3: symbols). Fitting the DS model to our simulations, we find that it describes the data fairly well (sum of squared residuals (SSR)=1.4×10^6; see Table 2.3 for best fit parameters; Fig. 2.3A: lines). Because the DS approximation poorly describes the data at high densities, whereas we expected the simulation model to be described well by the total Michaelis-Menten model, we examined whether the full QSSA (Eq. 2.4) describes the data better at high cell densities. Indeed, the full QSSA model describes the simulation data well at all CTL/target numbers (SSR=1.07×10^5; Fig. 2.3B: lines). Since the DS and full QSSA models have the same number of parameters, the lower SSR indicates that the full QSSA provides a better description of the data. The excellent fit of the full QSSA model suggests that the total Michaelis-Menten model is indeed an appropriate mechanistic description of the monogamous interactions between killers and targets, and that the poor performance of the DS model at high densities is due to the Padé approximation used to derive the functional response [53]. Thus, the full QSSA model represents an excellent mechanistic functional response for the monogamous killing regime, yet the DS model performs almost as well as long as cognate cell densities remain sufficiently low.

2.3.3 Joint killing

In our simulations for the joint killing regime, multiple CTLs jointly kill a target cell, as was recently suggested (see supplementary movies of ref. [37]). For such joint killing, Merrill [33] also used the Michaelis-Menten analogy and derived a model similar to the

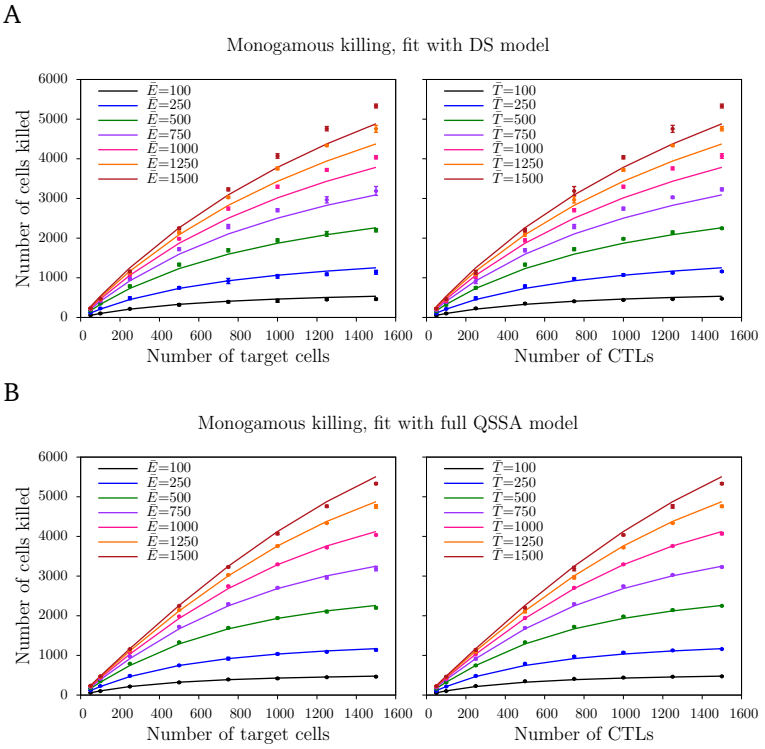

Figure 2.3. Number of target cells killed for monogamous killing. The total number of cells killed over 75 mins of simulation as a function of target cell (left panels) and CTL (right panels) densities for the monogamous killing regime. Markers indicate the average over 6 independent runs, error bars indicate the standard deviations, and the solid lines indicate the predictions obtained by fitting the DS model (A) and the full QSSA (B) with the best fit parameters. Parameter estimates: $k = 1.808 \times 10^{-4}$ cells^{-1} min^{-1} and $h = 571$ cells for the DS model, and $k = 8.113 \times 10^{-2}$ cells^{-1} min^{-1} and $h = 391$ cells for the full QSSA model.

Table 2.3. Best fit parameters (95% confidence intervals shown in the parentheses) of the double saturation (DS) model for different killing regimes.

Regime	k' (cells^{-1} min^{-1})	h_E (cells)	h_T (cells)
Monogamous	$1.808(\pm 0.143) \times 10^{-4}$	$571(\pm 68)$	$571(\pm 68)$
Joint	$1.845(\pm 0.40) \times 10^{-4}$	$2051(\pm 144)$	$458(\pm 15)$
Simultaneous	$1.812(\pm 0.81) \times 10^{-4}$	$523(\pm 36)$	$2979(\pm 561)$
Mixed	$1.735(\pm 0.047) \times 10^{-4}$	$1945(\pm 131)$	$1945(\pm 131)$

Padé model (Eq. 2.6), allowing multiple CTLs to bind and jointly kill a single target cell. He considered the rate of synapse formation to be proportional to the number of free binding sites on CTLs and target cells, and proposed the dynamics of the number of occupied binding sites on target cells, i.e., synapses (C_b), to be given by

$$\frac{dC_b}{dt} = k_1(\bar{E} - C_b)(n\bar{T} - C_b) - (k_{-1} + k_2)C_b \ , \tag{2.8}$$

where k_1 and k_{-1} are respectively the rates of conjugate formation and dissociation, k_2 is the killing rate, n is the number of binding sites per target cell, and $\bar{E}$ and $\bar{T}$ are, as before, the total number of cognate CTLs and target cells present at time t. Using the tQSSA, Merrill found that for $C_b \ll n\bar{T}$, the total killing rate, $K_{merrill}$, is given by a double saturation function, with a stronger saturation of killing in target cells than in CTLs (hereafter referred to as Merrill's model):

$$K_{merrill} = \frac{nk_2\bar{E}\bar{T}}{K_m + \bar{E} + n\bar{T}} \ , \tag{2.9}$$

where $K_m = (k_2 + k_{-1})/k_1$. The above equation can be rearranged into a conventional double saturation (DS) model with two different saturation constants:

$$K_{merrill} = \frac{k'\bar{E}\bar{T}}{1 + \bar{E}/h_E + \bar{T}/h_T} \ , \tag{2.10}$$

where $k' = nk_2/K_m$ is a mass-action killing rate, and $h_E = K_m$ and $h_T = K_m/n$, respectively, the saturation constants in CTLs and in targets.

To identify the conditions for which Merrill's model is valid, we attempt to deduce it from a full cell-based model. In joint killing, multiple CTLs sequentially bind to target cells, and the transitions that can occur for this case are given by the following reaction scheme:

$$\begin{aligned} E + T &\underset{k_{-1}}{\overset{nk_1}{\rightleftharpoons}} E_1T \xrightarrow{k_2} E + T^* \ , \\ E_1T + E &\underset{2k_{-1}}{\overset{(n-1)k_1}{\rightleftharpoons}} E_2T \xrightarrow{2k_2} 2E + T^* \ , \\ &\vdots \\ E_{n-1}T + E &\underset{nk_{-1}}{\overset{k_1}{\rightleftharpoons}} E_nT \xrightarrow{nk_2} nE + T^* \ , \end{aligned} \tag{2.11}$$

where k_1 and k_{-1} are the rates of conjugate formation and dissociation, k_2 is the killing rate, and E, T, and T^* represent the free cognate CTLs, the free target cells, and the dead targets, respectively. For conditions limited by synapse formation rather than limited by encounters between CTLs and target cells, the conjugates E_1T form at a rate nk_1. Similarly, since conjugates E_nT have n synapses, they can dissociate at a rate nk_{-1} to give rise to a conjugate $E_{n-1}T$ and a free CTL. Consistent with Merrill's model, we consider CTLs in conjugates E_nT to act independently and together kill the target cell in

E_nT at a rate nk_2. The dynamics of the conjugates are thus given by

$$\begin{aligned}
\frac{dC_1}{dt} &= nk_1 \overbrace{(\bar{E} - \sum_{i=1}^{n} iC_i)}^{\text{free CTLs}} \overbrace{(\bar{T} - \sum_{i=1}^{n} C_i)}^{\text{free targets}} - (k_2 + k_{-1})C_1 - (n-1)k_1C_1(\bar{E} - \sum_{i=1}^{n} iC_i) \\
&\quad + 2k_{-1}C_2 \ , \\
\frac{dC_2}{dt} &= (n-1)k_1C_1(\bar{E} - \sum_{i=1}^{n} iC_i) - 2k_2C_2 - 2k_{-1}C_2 - (n-2)k_1C_2(\bar{E} - \sum_{i=1}^{n} iC_i) \\
&\quad + 3k_{-1}C_3 \ , \\
&\vdots \quad \vdots \\
\frac{dC_n}{dt} &= k_1C_{n-1}(\bar{E} - \sum_{i=1}^{n} iC_i) - nk_2C_n - nk_{-1}C_n \ ,
\end{aligned} \tag{2.12}$$

where C_1, C_2, and C_n represent the number of conjugates E_1T, E_2T, and E_nT, respectively, $\bar{E}$ and $\bar{T}$ are the total number of CTLs and target cells, respectively, and $\sum_{i=1}^{n} iC_i$ and $\sum_{i=1}^{n} C_i$ are the total number of CTLs bound to target cells and the total number of targets bound to at least one CTL, respectively.

The total number of synapses C_b equals the number of CTLs in conjugates, i.e., $\sum_{i=1}^{n} iC_i$. Therefore, the dynamics of synapses is given by

$$\begin{aligned}
\frac{dC_b}{dt} &= nk_1(\bar{E} - \sum_{i=1}^{n} iC_i)(\bar{T} - \sum_{i=1}^{n} C_i) - (k_2 + k_{-1})C_1 - (n-1)k_1C_1(\bar{E} - \sum_{i=1}^{n} iC_i) \\
&\quad + 2k_{-1}C_2 + 2\Bigg((n-1)k_1C_1(\bar{E} - \sum_{i=1}^{n} iC_i) - 2k_2C_2 - 2k_{-1}C_2 \\
&\quad - (n-2)k_1C_2(\bar{E} - \sum_{i=1}^{n} iC_i) + 3k_{-1}C_3 \Bigg) + \dots \\
&\quad + n\Bigg(k_1C_{n-1}\bar{E} - \sum_{i=1}^{n} iC_i) - nk_2C_n - nk_{-1}C_n \Bigg) \ .
\end{aligned} \tag{2.13}$$

Replacing $\sum_{i=1}^{n} iC_i$ with C_b and rearranging, we get

$$\frac{dC_b}{dt} = k_1(\bar{E} - C_b)(n\bar{T} - C_b) - (k_2 + k_{-1})C_b - k_2 \sum_{i=2}^{n} (i^2 - i)C_i \ , \tag{2.14}$$

which has an additional term $-k_2 \sum_{i=2}^{n} (i^2 - i)C_i$ compared to Merrill's equation (Eq. 2.8) for the dynamics of the synapses. Thus, unless $C_i \to 0 \ \forall \ i \geq 2$, this model cannot be

written entirely in terms of C_b. Surprisingly, Merrill's equation can be deduced from the full model if the killing rate of the target cell in E_nT conjugates is the same as that in a conjugate E_1T (see Supporting Material).

We simulated the joint killing regime (see Movie S2) by allowing target cells to be in conjugate with multiple CTLs at the same time and by increasing the speed at which a target is killed when it is to multiple CTLs (see Fig. S4). Interestingly, we found that the number of cells killed saturates as a function of the target cell density, but increases almost linearly with the CTL density (Fig. 2.4A), which is consistent with Merrill's model [33]. To determine whether Merrill's analysis can provide a phenomenological description of our simulation data, we fit the DS model (Eq. 2.10) and find that this model describes the data quite well (Fig. 2.4A; see Table 2.3 for parameters). We find a 4.5-fold difference in the saturation constants, which according to Merrill's model [33] gives an approximate number of binding sites (i.e., maximum number of synapses per cell; see Fig. S2 in the Supporting Material for distributions of binding sites). The difference in the saturation constants after fitting with the DS model with two different saturation constants can thus help us to distinguish the joint killing from other regimes.

2.3.4 Simultaneous killing

Wiedemann *et al.* [36] experimentally observed that individual CTLs can also simultaneously kill multiple target cells at the same time. Our simulations (see Movie S3 and Fig. S4) for such a simultaneous killing regime show that there is little saturation of CTL killing with target cell density and strong saturation with CTL density (Fig. 2.4B), i.e., saturation is reversed compared to joint killing. This finding is consistent with the simulations by Graw and Regoes [15], in which the functional response saturates with CTL density only. In their simulations, conjugates of multiple targets and multiple CTLs are allowed, however. But, although multiple CTLs can bind to a target cell, only one is allowed to kill it, i.e., the killing time, t_D, does not decrease with the number of CTLs bound to the target. This implies that the killing regime of Graw and Regoes [15] is similar to our simultaneous killing regime, thus explaining why our results are consistent with theirs.

Next, we examine whether an analytical functional response can be mechanistically derived from a cell-based model. Similar to our analysis for joint killing regime, we consider single CTLs to bind sequentially to m target cells for binding-limited conditions, so the transitions for this case are given by the following reaction scheme:

$$\begin{aligned} E + T &\underset{k_{-1}}{\overset{mk_1}{\rightleftharpoons}} ET_1 \xrightarrow{k_2} E + T^* \,, \\ ET_1 + T &\underset{2k_{-1}}{\overset{(m-1)k_1}{\rightleftharpoons}} ET_2 \xrightarrow{2k_2} ET_1 + T^* \,, \\ &\vdots \\ ET_{m-1} + T &\underset{mk_{-1}}{\overset{k_1}{\rightleftharpoons}} ET_m \xrightarrow{mk_2} ET_{m-1} + T^* \,, \end{aligned} \tag{2.15}$$

where k_1 and k_{-1} are the rates of conjugate formation and dissociation, k_2 is the killing rate, and E, T, and T^* represent the free cognate CTLs, the free target cells, and the dead targets, respectively. We consider the target cells in conjugates ET_m to be killed independently by the CTLs. Therefore, the conjugates ET_m are lost when any of the m target cells is killed, i.e., at a rate mk_2. Because CTLs have m binding sites, ET_1 conjugates form at a rate mk_1, and ET_m conjugates dissociate into ET_{m-1} and a free T at a rate mk_{-1}. Therefore, the dynamics of conjugates are given by

$$\begin{aligned}
\frac{dD_1}{dt} &= mk_1 \overbrace{(\bar{E} - \sum_{i=1}^{m} D_i)}^{\text{free CTLs}} \overbrace{(\bar{T} - \sum_{i=1}^{m} iD_i)}^{\text{free targets}} - (k_2 + k_{-1})D_1 - (m-1)k_1 D_1(\bar{T} - \sum_{i=1}^{m} iD_i) \\
&\quad + 2k_{-1}D_2 + 2k_2 D_2 \ , \\
\frac{dD_2}{dt} &= (m-1)k_1 D_1(\bar{T} - \sum_{i=1}^{m} iD_i) - 2k_2 D_2 - 2k_{-1}D_2 - (m-2)k_1 D_2(\bar{T} - \sum_{i=1}^{m} iD_i) \\
&\quad + 3k_{-1}D_3 + 3k_2 D_3 \ , \\
&\vdots \qquad \vdots \\
\frac{dD_m}{dt} &= k_1 D_{m-1}(\bar{T} - \sum_{i=1}^{m} iD_i) - mk_2 D_m - mk_{-1}D_m \ , \qquad (2.16) \\
& \qquad (2.17)
\end{aligned}$$

where D_1, D_2, and D_m represent the number of ET_1, ET_2, and ET_m conjugates, respectively.

The total number of synapses $C_b = \sum_{i=1}^{m} iD_i$. Therefore, the dynamics of synapses is given by

$$\begin{aligned}
\frac{dC_b}{dt} &= mk_1(\bar{E} - \sum_{i=1}^{m} D_i)(\bar{T} - \sum_{i=1}^{m} iD_i) - (k_2 + k_{-1})D_1 - (m-1)k_1 D_1(\bar{T} - \sum_{i=1}^{m} iD_i) \\
&\quad + 2k_{-1}D_2 + 2k_2 D_2 + 2\Bigg((m-1)k_1 D_1(\bar{T} - \sum_{i=1}^{m} iD_i) - 2k_2 D_2 - 2k_{-1}D_2 \\
&\quad - (m-2)k_1 D_2(\bar{T} - \sum_{i=1}^{m} iD_i) + 3k_{-1}D_3 + 3k_2 D_3 \Bigg) + \dots \\
&\quad + m\Bigg(k_1 D_{m-1}(\bar{T} - \sum_{i=1}^{m} iD_i) - mk_2 D_m - mk_{-1}D_m \Bigg) \ . \qquad (2.18)
\end{aligned}$$

Replacing $\sum_{i=1}^{m} iD_i$ with C_b and rearranging, we get

$$\frac{dC_b}{dt} = k_1(m\bar{E} - C_b)(\bar{T} - C_b) - (k_2 + k_{-1})C_b \ , \qquad (2.19)$$

which is similar to Merrill's equation for joint killing (Eq. 2.8). Interestingly, we can mechanistically derive Merrill's equation - hence an analytical functional response - for simultaneous killing from a cell-based model.

Following the approaches of Merrill [33] and Borghans *et al.* [16], we can formally derive the functional response starting from Eq. (2.19). Since every synapse induces death of target cells, the rate at which target cells are killed is given by

$$\frac{dT^*}{dt} = k_2 C_b \ . \tag{2.20}$$

We can find an analytical expression for the killing rate in a similar way as for monogamous killing. Thus, in order to derive the full solution for the functional response we first make a tQSSA and subsequently simplify using a Padé approximation. The functional response resulting from the full solution is given by (hereafter referred to as the full QSSA model):

$$K_{full} = k_2 \Delta t C_b = k_2 \Delta t \ \frac{h + m\bar{E} + \bar{T} - \sqrt{(h + m\bar{E} + \bar{T})^2 - 4m\bar{E}\bar{T}}}{2} \ , \tag{2.21}$$

where C_b is the total number of synapses, $\bar{E}$ and $\bar{T}$ are the total number of cognate CTLs and target cells respectively, k_2 is the killing rate of target cells, h is the Michaelis constant defined as $\dfrac{k_2 + k_{-1}}{k_1}$, and m is the number of binding sites per CTL.

Using a Padé approximation, the resulting equation for the total number of cells killed over a period Δt becomes

$$K_{Padé} = \frac{m k_2 \Delta t \bar{E} \bar{T}}{K_m + m\bar{E} + \bar{T}} \ , \tag{2.22}$$

where $K_m = (k_2 + k_{-1})/k_1$ is the Michaelis constant. Similar to the joint killing scenario, the above equation can be rearranged into a DS model with two different saturation constants:

$$K_{DS} = \frac{k' \Delta t \bar{E} \bar{T}}{1 + \bar{E}/h_E + \bar{T}/h_T} \ , \tag{2.23}$$

where $k' = mk_2/K_m$, $h_E = K_m/m$, and $h_T = K_m$. This functional response implies an earlier onset of saturation of killing with CTL densities than with target cell densities, which is consistent with our simultaneous killing simulations and converse to Merrill's model. The ratio of the two saturation constants reflects the number of binding sites, m, on a CTL.

Fitting the DS model of Eq. (2.23) to the data from our CPM simulations, we find that the DS model describes the data quite well (Fig. 2.4B). Similar to the fits of the monogamous regime, the fit using the full solution is even better (not shown). As expected, the ratio h_T/h_E provides a good estimate for the number of binding sites on a CTL (i.e., maximum number of synapses per CTL; see Figs. S2 and S3).

2.3.5 Mixed killing

Finally, we performed simulations (see Movie S4 and Fig. S4) for the mixed killing regime in which a CTL can kill multiple target cells in the same conjugate and target cells can be killed by multiple CTLs. In these simulations, we find that CTL killing saturates approximately at the same target cell and CTL densities (Fig. 2.5: symbols). When compared to the saturation levels in the monogamous killing regime (Fig. 2.3), the saturation occurs at much higher CTL and target cell densities in the mixed killing regime. This shift in the onset of saturation is because targets and CTLs that are sequestered in complexes, can still interact further with other cells. As a result, the time to find a next target cell decreases. Thus, the formation of multi-cellular conjugates results in an increase in the effective killing capacity of CTLs, and saturation occurs at high cell densities. Similar to the joint killing scenario, we cannot derive an analytical functional response following Merrill's analysis. Nevertheless, as the saturation is symmetric with CTL and target cell densities, it turns out that the phenomenological DS model of Eq. (2.6) with one saturation constant, can fit the data well at all densities examined (Fig. 2.5; see Table 2.3 for parameter estimates).

2.4 Mechanistic insights

Since we cannot mechanistically derive the DS model for the joint and mixed killing regimes, we examine the interpretation of its parameters. The generalised DS model with two different saturation constants is given by

$$f(\bar{E},\bar{T}) = \frac{k'\bar{E}\bar{T}}{1+\bar{E}/h_E+\bar{T}/h_T}. \tag{2.24}$$

When $\bar{E} \to 0$ and $\bar{T} \to \infty$ (i.e., $\bar{E}/h_E \ll \bar{T}/h_T$), this reduces to $k'h_T\bar{E}$, which is the maximum total CTL killing rate. When $\bar{E} \to \infty$ and $\bar{T} \to 0$ (i.e., $\bar{E}/h_E \gg \bar{T}/h_T$), Eq. 2.24 reduces to $k'h_E\bar{T}$, which is the maximum rate at which target cells can be killed. At low CTL and target cell numbers, i.e., $\bar{E} \to 0$ and $\bar{T} \to 0$, the per CTL killing rate becomes $k'\bar{E}\bar{T}$. Thus, k' in the DS model (Eq. 2.24) can be interpreted as a mass-action killing rate. Therefore, even though the DS model cannot be mechanistically derived for all killing regimes, the parameters can be interpreted biologically.

Taken together, our analysis shows that the DS model can be used to interpret the mechanisms of CTL and target cell interactions that underlie cytotoxicity data. If $hE{\approx}h_T$, the data point to either monogamous or mixed killing regimes. The asymmetric cases $h_E > h_T$ or $h_E < h_T$, respectively, suggest that joint or simultaneous killing regimes occur.

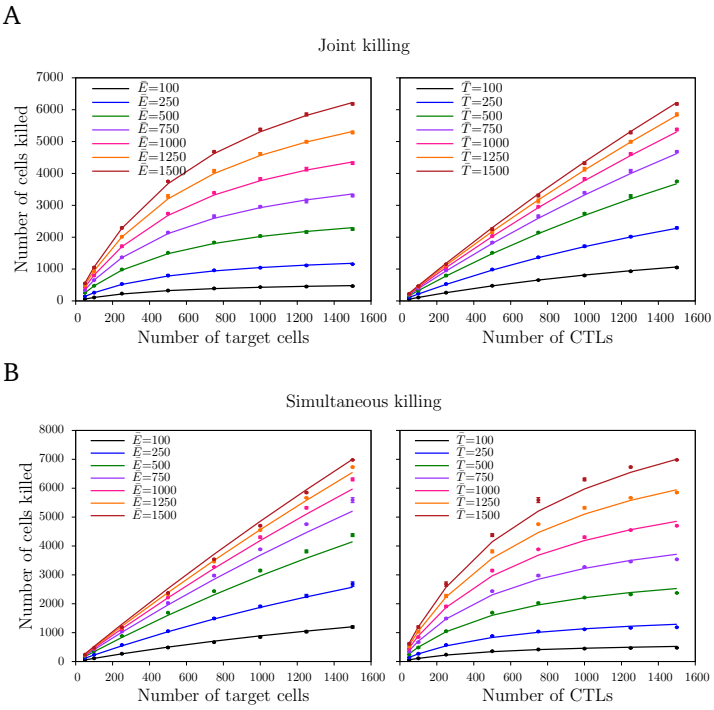

Figure 2.4. The total number of cells killed over 75 mins of simulation as a function of target cell (left panels) and CTL (right panels) densities for joint (A) and simultaneous (B) killing. Markers indicate the mean of the total number of cells killed over 6 independent runs, error bars indicate the standard deviation, and solid lines represent the predictions of the DS model Eq. (2.23) with best fit parameters (see Table 2.3).

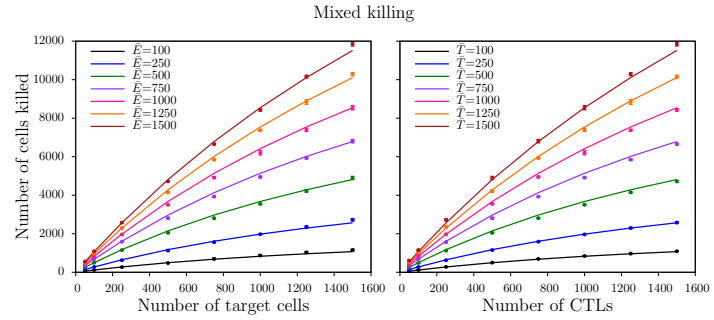

Figure 2.5. The total number of cells killed over 75 mins of simulation as a function of target cell (left panel) and CTL (right panel) densities for mixed killing. As indicated earlier, markers represent the mean of the total number of cells killed over 6 independent runs, error bars indicate the standard deviation, and solid lines represent the predictions of the DS model with best fit parameters (see Table 2.3).

2.5 Discussion

Our aim with this study was to derive a general functional response for target cell killing, which is valid for a wide range of killer and target cell densities. Therefore, we only consider fixed densities, and vary these widely between simulations. Similarly, in the ordinary differential equations (ODEs) we derive the functional response mechanistically by using constant CTL and target cell densities. Thus, our functional response predicts the killing rate at any given density of targets and killers. If in an experimental system these densities change over time (by e.g., target cell proliferation), one would have to add that to the ODEs that are used to describe the data. If the additional dynamics are fast, this could invalidate the QSSA, and one would have to study the full dynamics of CTL-target interactions.

By simulating CTL killing in an *in silico* environment resembling T cell areas of lymphoid tissues, we have shown that the number of target cells that is killed per unit of time is expected to approach a maximum value, i.e., saturates when the density of target cells or that of CTLs becomes large. In asymmetric killing regimes - where either one CTL kills many targets, or where one target is killed by many CTLs - the saturation is also asymmetric (see Table 2.3). We have generalized a mechanistic function with just one saturation constant into a semi-mechanistic functional response with two saturation constants, one for the CTLs and another for the target cells.

Whether or not a CTL can jointly kill multiple target cells, and how this affects the time to kill target cells in such multi-cellular conjugates is not known, and probably depends on factors such as the kind of target cell, its peptide-MHC density, and its presentation of co-stimulatory molecules. We have studied the simplest cases where one CTL can kill multiple target cells, or a target cell is killed by multiple CTLs in the most efficient way. Since our goal is to use the artificial data for the fitting of mathematical models rather than to give detailed predictions, we here used two-dimensional instead of three-dimensional simulations. The number of CTLs and target cells binding to their counterparts and the search efficiency of CTLs are expected to vary between 3D and 2D fields. These differences should only result in different absolute values of the saturation constants. However, the nature of the saturation is expected to remain the same, because our mechanistic ODE models confirm this result and do not depend on the dimensionality of the space.

There are some differences between the conditions of our CPM simulations and our derivation of functional responses. First, following Merrill's model [33], functional responses are derived for binding-limited conditions, whereas killing in our simulations is expected to be diffusion-limited at low cell densities, and binding-limited at either high CTL or high target cell densities. However, we find that our DS model still describes the simulation data well, because the target cell killing observed in simulations with either many CTLs or many targets largely determine the saturation constants. Finally, in our simulations we use a fixed kill time t_D of 15 mins, whereas this time period is assumed to be exponentially distributed while mathematically deriving the functional responses.

Therefore, this suggests that our main conclusions are insensitive to the exact underlying distribution of the killing time t_D. This is important because the precise distribution of killing times *in vivo* is unknown.

The good fits of the DS model to the simulated data implies that it is robust for the above-mentioned differences. Thus, fitting this simple function to experimental data allows one to estimate both the maximum number of targets a CTL can kill per day, i.e., the maximal killing rate, and the relative sizes of its two saturation constants, which reveals information about the interactions between CTLs and target cells. Because the cellular interactions during the killing of target cells are typically unknown, it seems a good approach to fit experimental data with the general DS model with two different saturation constants in order to determine the interactions underlying the killing. Interestingly, it was recently found that neutrophil killing of bacteria is also well described by a double saturation model, with a stronger saturation in the neutrophil density than that in the bacterial density [54]. Our results therefore suggest that single neutrophils are killing several bacteria at the same time (i.e., our simultaneous killing regime) could be the underlying mechanism in these neutrophil killing assays [54].

Our results reconcile conflicting findings of several recent studies. We have shown that the simulation results of Graw and Regoes [15] with saturation only in the CTL density can be understood from their specific killing regime. We showed that the functional response they found can be mechanistically derived. In an another study, Ganusov *et al.* [10] analyzed *in vivo* cytotoxicity data in spleens of mice [23] and found that a mass-action model describes the CTL mediated killing best, i.e., there was no evidence for saturation in killing efficiency. Our results for a realistic killing time of $t_D = 15$ min [26, 36] suggest a saturation constant at a cell frequency of about 10% of all cells for monogamous killing, and at a frequency of about 40% for mixed killing. Because the highest CTL frequency in these *in vivo* data is about 10% [23], there may indeed be very little saturation in the above-mentioned circumstances. Finally, as Ganusov *et al.* [10] noted, some of the target cells may have encountered a CTL *in vivo*, but may actually be killed *ex vivo* after the spleen had been taken out to count cells. In that case their rapid estimated killing rate reflects the search time rather than the true killing time in the spleen, and search times are not expected to saturate. Taken together, we propose the DS model as a generic model to describe and quantify killer-target cell dynamics. The relative values of the saturation constants can be used to identify the underlying CTL and target cell interactions in cytotoxicity assays.

Acknowledgements

The authors thank Renske Vroomans, Jorg Calis, Paola Carrillo-Bustamante, Chris van Dorp, and Ioana Niculescu for critical reading of the manuscript, and technical assistance relating to the CPM and Padé approximation. This study is supported by NWO grant 819.03.009 (to RJdB) and by NWO grants 916.86.080 and 864.12.013 (to JBB). This study is also supported by the "Virgo consortium," funded by the Dutch government

[project number FES0908] and by the “Netherlands Genomics Initiative (NGI)” [project number 050-060-452]. The authors declared that they have no competing interests.

Supplementary Information

Merrill's model for modified joint killing

Surprisingly, Merrill's equation can be deduced if we assume that target cells in conjugates E_nT are killed at the same rate as that of targets in conjugates ET. The dynamics of conjugates and are then given by

$$\begin{aligned}
\frac{dC_1}{dt} &= nk_1(\bar{E}-\sum_{i=1}^{n} iC_i)(\bar{T}-\sum_{i=1}^{n} C_i) - (k_2+k_{-1})C_1 - (n-1)k_1C_1(\bar{E}-\sum_{i=1}^{n} iC_i) \\
&\quad +2k_{-1}C_2 \ , \\
\frac{dC_2}{dt} &= (n-1)k_1C_1(\bar{E}-\sum_{i=1}^{n} iC_i) - k_2C_2 - 2k_{-1}C_2 - (n-2)k_1C_2(\bar{E}-\sum_{i=1}^{n} iC_i) \\
&\quad +3k_{-1}C_3 \ , \\
&\vdots \quad \vdots \\
\frac{dC_n}{dt} &= k_1C_{n-1}(\bar{E}-\sum_{i=1}^{n} iC_i) - k_2C_n - nk_{-1}C_n \ ,
\end{aligned} \tag{S.1}$$

where C_1, C_2, and C_n represent the number of conjugates ET, E_2T, and E_nT, respectively, and $\bar{E}$ and $\bar{T}$ are the total number of CTLs and target cells, respectively. Note that, contrary to the case considered in Eq. 2.11 in the main text, the target cells in all the conjugates are considered to be killed at the same rate k_2 while writing the above equations.

The total number of synapses $C_b = \sum_{i=1}^{n} iC_i$. Therefore, the dynamics of synapses is given by

$$\begin{aligned}
\frac{dC_b}{dt} &= nk_1(\bar{E}-\sum_{i=1}^{n} iC_i)(\bar{T}-\sum_{i=1}^{n} C_n) - (k_2+k_{-1})C_1 - (n-1)k_1C_1(\bar{E}-\sum_{i=1}^{n} iC_i) \\
&\quad +2k_{-1}C_2 + 2\Big((n-1)k_1C_1(\bar{E}-\sum_{i=1}^{n} iC_i) - k_2C_2 - 2k_{-1}C_2 \\
&\quad -(n-2)k_1C_2(\bar{E}-\sum_{i=1}^{n} iC_i) + 3k_{-1}C_3\Big) + \dots \\
&\quad +n\Big(k_1C_{n-1}\bar{E}-\sum_{i=1}^{n} iC_i) - k_2C_n - nk_{-1}C_n\Big) \ .
\end{aligned} \tag{S.2}$$

Replacing $\sum_{i=1}^{n} iC_i$ with C_b and rearranging, we get

$$\frac{dC_b}{dt} = k_1(\bar{E}-C_b)(n\bar{T}-C_b) - (k_2+k_{-1})C_b \ , \tag{S.3}$$

which is identical to Eq. 2.8, which Merrill proposed for the joint killing regime.

Migration properties

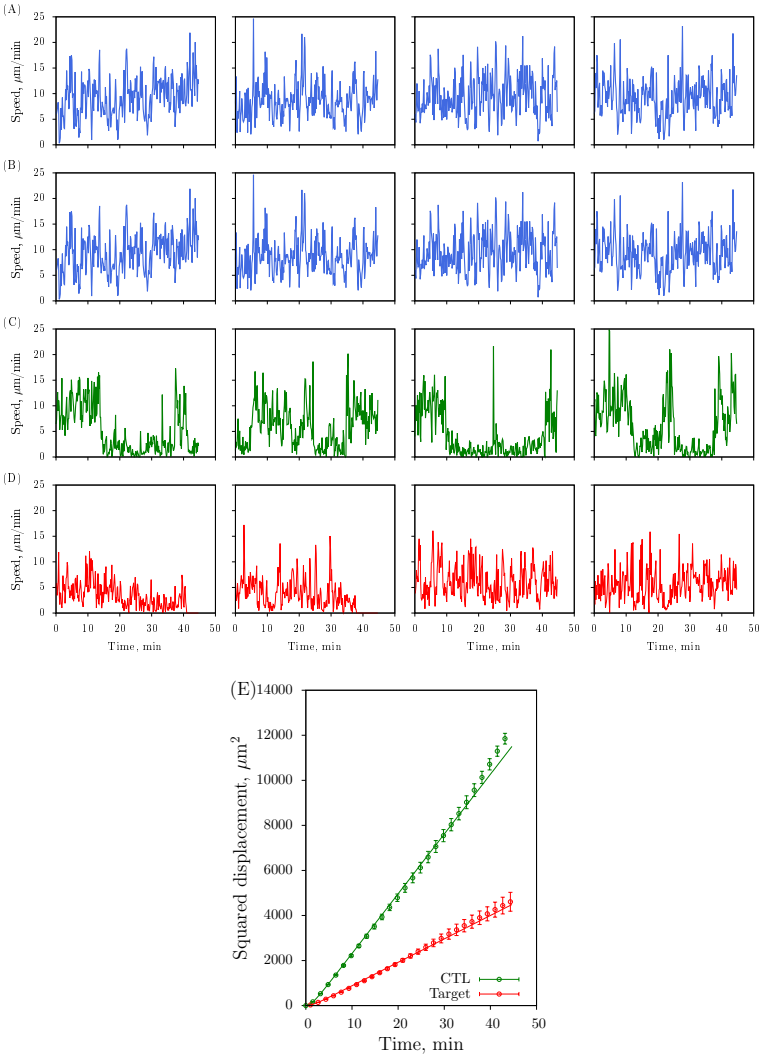

Figure S1. Migration properties during CPM simulations. Panels show representative plots of a 2-dimensional simulation: (A) speed of four representative simulated CTLs in the absence of killing (mean speed: 9.5μm/min), (B) speed of four simulated target cells in the absence of killing (mean speed: 5.6 μm/min), (C) speed of four simulated CTLs in the presence of killing, and (D) speed of four simulated targets in the presence of killing. (E) Mean square displacement ($msdp$) plot in the absence of killing. Markers indicate average over 100 cells from 6 independent simulations, and the error bars indicate the corresponding standard deviation. Lines indicate the predictions of Fuerth's equation: $msdp = 4M\{(t - P(1 - e^{-t/P})\}$ [49], where M is the motility coefficient, and P is the persistence time.

Distributions of synapses

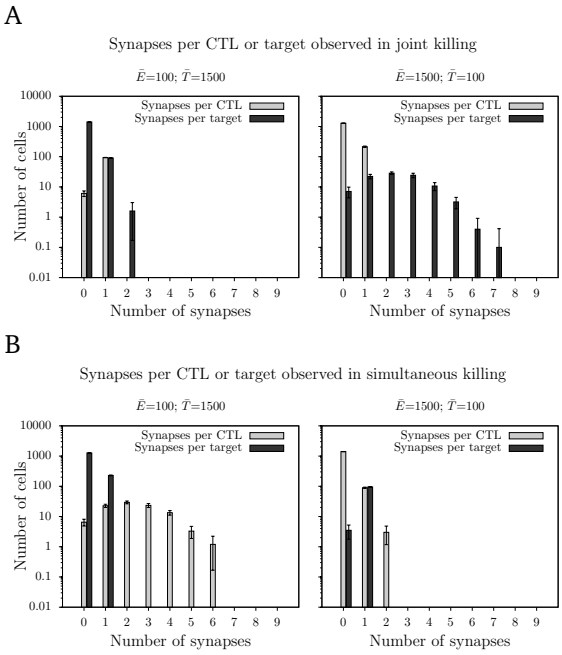

Figure S2. Number of synapses per CTL or target cell observed in (A) joint and (B) simultaneous killing regimes, calculated every 50 mins in a simulation. The left and right panels show results from simulations with $\bar{E}$=100, $\bar{T}$=1500 and $\bar{E}$=1500, $\bar{T}$=100 respectively. Bars indicate the average of 10 measurements in a simulation, and the error bars indicate the standard deviation in the measured occupied sites.

Predictions of number of binding sites

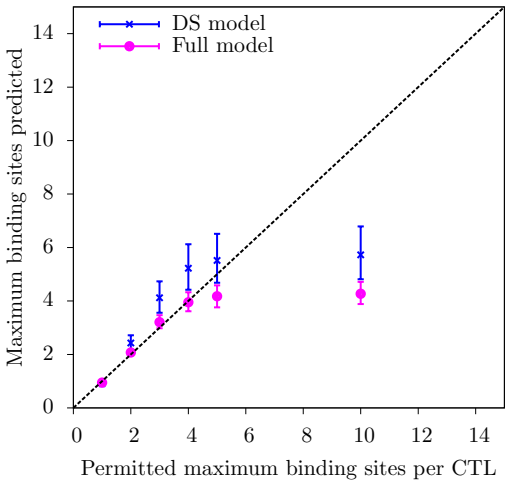

Figure S3. In the main text we showed that the double saturation functional response can be mechanistically derived for the simultaneous killing regime. Therefore the ratio of the saturation constants h_T/h_E should be predictive for the number of binding sites on CTLs. The number of binding sites represents the maximum number of synapses per cell. We tested this prediction by performing simultaneous killing regime simulations in which we restricted the number of binding sites per CTL (i.e., contrary to the simulations with unrestricted binding sites described in the main text). We obtained the number of cells killed as a function of CTL and target cell densities for up to 10 binding sites allowed. Next, we fitted both the full model of Eq. (2.21) and the DS model of Eq. (2.23) to compare the predicted maximum number of binding sites predicted by using m of the full model and the h_T/h_E ratio of the DS model to the actual maximum. Whereas the DS model predictions slightly overpredicted the number of binding sites, the full model predictions are accurate until approximately four binding sites allowed. For more than four permitted binding sites, the actual maximum attained no longer increases due to the finite surface area of CTLs.

CPM simulation algorithms

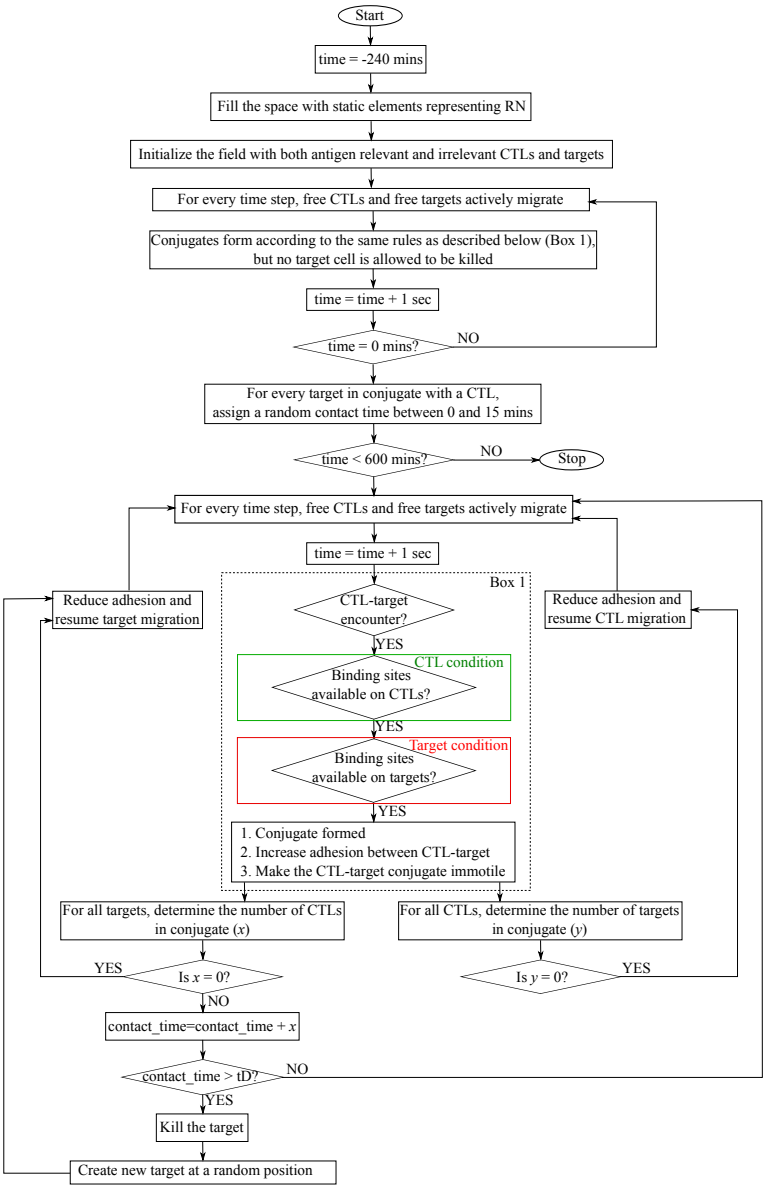

Figure S4. Schematic description of CPM simulations of target cell killing by CTLs. CTLs and targets are considered 'free' if they are not part of any conjugate. Box 1 gives the set of instructions for conjugate formation. For simulations with unrestricted number of binding sites, the 'CTL condition' is performed only for the monogamous and joint killing regimes, whereas the 'Target condition' is performed only for the monogamous and simultaneous regimes.

Representative movies of simulations

Representative movies of the monogamous (Movie S1), joint (Movie S2), simultaneous (Movie S3), and mixed (Movie S4) killing simulations (with $\bar{E} = \bar{T} = 750$ cells) can be found at `http://www.sciencedirect.com/science/article/pii/S0006349514002185`.

Chapter 3

Influence of Multi-Stage Killing on the Functional Response of Cytotoxic T Lymphocyte-Mediated Killing

Saikrishna Gadhamsetty, Athanasius F.M. Marée, Joost B. Beltman, and Rob J. de Boer

In Preparation

Abstract

Cytotoxic T lymphocyte (CTL)-mediated killing involves forming a stable contact with the target cells, followed by delivery of perforin and granzymes (often referred to as a 'lethal hit'). Previously, we have determined the general functional response of CTL killing, assuming that a single lethal hit is sufficient to induce target cell death. However, killing may involve transition through multiple stages. For example, about 50% of motile HIV-infected $CD4^+$ T cells were killed after multiple successive engagements with CTLs. In this study, we determine how the functional response is affected for a scenario in which a target cell transits multiple stages before being killed, compared to single-stage killing. Using spatial simulations of CTL-mediated killing, we show that the functional response resulting from multi-stage killing is qualitatively similar as from single-stage killing, i.e., a double saturation function. However, the saturation in killing occurs at a higher CTL and target cell frequencies.

3.1 Introduction

Cytotoxic T lymphocyte (CTL) killing of tumor and virus-infected cells generally involves four steps: localization of the target cell; formation of a specialized junction with the target (called a cytotoxic synapse); delivery of effector molecules, such as perforin and granzymes; and detachment from the dying target, followed by resumption of the search for new targets. The functional response of CTL-mediated killing is defined as the rate at which single CTLs kill target cells as a function of CTL and target cell frequencies resulting from such CTL-target interactions, and has been studied using mathematical models that are analogous to enzyme-substrate kinetics [16, 17, 33, 55]. All the models so far consider CTLs and targets to form conjugates (mimicking the synapse), which subsequently either dissociate resulting in a naïve target cell, or lead to the death of the target [16, 33, 55], i.e., targets are killed following a single 'lethal hit'. However, using two-photon microscopy, antigen-pulsed B cells *in vivo* were shown to break their synapse with CTLs and were killed in the subsequent conjugation with CTLs [26]. Moreover, in recent *in vitro* collagen gel experiments, it was found that about 50% of the motile HIV-infected $CD4^+$ T cells break the synapses with $CD8^+$ cells [1]. Although these observations do not directly show that multiple stages of killing indeed occur, it also poses no evidence against it.

Here, we investigate how such multi-stage killing affects the functional response of CTL killing. Therefore, we adapt our previous cellular potts model (CPM) simulations [55] to determine the functional response of CTL-mediated killing resulting from multiple, independent hits. Specifically, we simulate short-lived synapses between CTLs and target cells, yet by having target cells remember the accumulated synapse durations we mimic multiple hits (or multi-stage killing). The resulting functional response remains qualitatively similar as in our earlier study [55], i.e., killing rates saturate with both an increase in CTL and target cell densities. However, the onset of saturation in killing is delayed

for multi-stage killing compared to single-stage killing. Furthermore, if targets conjugate with only a single CTL at a time, an analytical expression for the functional response of multi-stage killing can be derived by extending the mathematical enzyme-substrate analogy. Besides confirming the simulation results, the derived functional response shows that the saturation constant increases with an increase in the number of stages. Nevertheless, the maximum CTL killing rate depends only on the cumulative contact time required for CTLs to induce target cell death.

3.2 Results and Discussion

To determine the functional response of CTL-mediated killing resulting from multi-stage killing, we perform 2-dimensional cellular potts model (CPM) simulations similar to our earlier study [55] (see Methods). Briefly, each cell in the CPM is a collection of multiple lattice sites, with surface energies and tensions on the edges of a cell determining its interactions. We consider a torus of $500\text{pixels} \times 500\text{pixels}$, where a pixel corresponds to 1 μm, and is composed of static elements representing the reticular network, CTLs, B cells as targets, and extra-cellular matrix. Each CTL and B cell is assigned a preferred direction of migration, which is updated once in every 3 mins based on its recent direction of migration.

Upon an encounter between a CTL and a target cell, whether a conjugate forms depends on the interaction rules of the four possible killing regimes: monogamous, joint, simultaneous, and mixed killing (see Fig. 1 in Chapter 2). In monogamous and joint regimes of killing, a CTL can maximally conjugate with one target at a time, whereas CTLs can conjugate with many targets in simultaneous and mixed regimes. Targets are allowed to conjugate with at most one CTL at a time in monogamous and simultaneous regimes, but they can conjugate with multiple CTLs at the same time in joint and mixed killing regimes.

In our earlier study [55], we mimicked single-stage killing by aiming for stable conjugates through adhesion increase and through stopping the active migration of cells in conjugates. To simulate multi-stage killing, cells in a conjugate no longer preferentially adhere to each other and continue to migrate, which results in conjugates of short duration. Target cells 'remember' the accumulated duration in conjugates after they dissociate from a conjugate, and accrue upon this existing signal when conjugated later, thus mimicking multi-stage killing. Note that we do not specify the number of stages or their duration. Because we record conjugates once in every 10s, this restricts the shortest conjugate durations observed in our simulations. In all our simulations, we used a fixed 'kill time' $t_D = 15$ mins, i.e., the total time required for a CTL to induce target cell death. Targets accumulate the killing signal independently from all their attached CTLs (depending on the regime), and CTLs can contribute killing signal to all the targets in a conjugate. When the killed target disappears from the field, a new target cell is introduced at a random location in the field to maintain the same target cell numbers within a simulation. Furthermore, the number of CTLs remains constant within a simulation,

thus preventing confounding effects due to changing cell numbers.

3.2.1 Monogamous killing regime

In monogamous simulations, only conjugates of one CTL and one target are allowed to form. Multi-stage killing in this case implies that targets are killed by multiple CTLs in a sequential manner. We vary the number of 'antigen-specific' CTLs and the cognate targets between simulations. Each simulation corresponds to 240 mins, and to ensure that killing is at steady state, we measure the number of target cells killed over the last 75 mins. The number of cells killed saturates to the same extent either with an increase in CTL or target cell densities (Fig. 3.1, symbols), which is qualitatively consistent with the earlier proposed double saturation functional response for single-stage monogamous killing [16, 55].

By assuming that conjugates either dissociate to naïve target cells or lead to dying target cells, Borghans *et al.* [16] derived the functional response for monogamous killing from the reaction scheme

$$E + T \underset{k_{-1}}{\overset{k_1}{\rightleftharpoons}} [ET] \xrightarrow{k_2} E + T^* \ . \tag{3.1}$$

In this scheme, E, T, T^*, and $[ET]$ represent the free cognate CTLs, naïve target cells, dead targets, and conjugates, respectively; k_1 and k_{-1} are the rates of conjugate formation and dissociation, respectively; and k_2 is the killing rate. Using the so-called total quasi-steady approximation, they found the following quadratic equation in the number of conjugates $[ET]$, C:

$$C^2 - (h + \bar{E} + \bar{T})C + \bar{E}\bar{T} = 0 \ , \tag{3.2}$$

where $\bar{E}$ and $\bar{T}$ are, respectively, the total number of CTLs and targets, and h is the Michaelis-Menten saturation constant, defined as $(k_2 + k_{-1})/k_1$. From the above equation, the number of cells killed over a period of Δt is given by

$$K_{\mathit{full}} = \frac{k_2 \Delta t}{2} \left(h + \bar{E} + \bar{T} - \sqrt{(h + \bar{E} + \bar{T})^2 - 4\bar{E}\bar{T}} \right) \ , \tag{3.3}$$

The full solution can be further simplified into a double saturation (DS) model, using a Padé approximation:

$$K_{DS} = \frac{k \Delta t \bar{E} \bar{T}}{1 + \bar{E}/h + \bar{T}/h} \ , \tag{3.4}$$

where k is the mass-action killing rate [55], which for monogamous killing is defined as k_2/h.

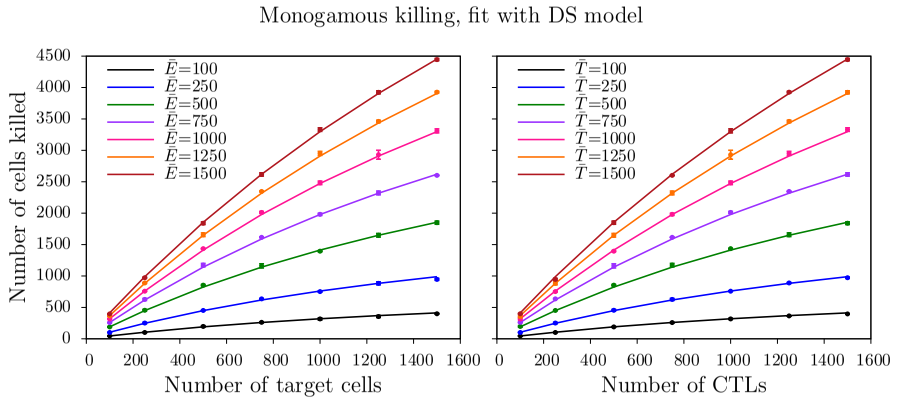

Figure 3.1. Number of target cells killed during multi-stage monogamous killing. The number of cells killed over 75 mins of simulation as a function of CTL and target cell numbers. The mean number of cells killed from 3 independent simulations are shown in markers, and error bars represent the standard deviations. The best-fit DS model predictions are depicted in solid lines (see Table 3.1 for the best fit parameters).

Table 3.1. Summary of best-fit parameters of the DS model. The best-fit parameters for single-stage killing are taken from our previous study [55] (and Chapter 2).

	Single-stage			Multi-stage		
Regime	k' (cells^{-1} min^{-1})	h_E (cells)	h_T (cells)	k' (cells^{-1} min^{-1})	h_E (cells)	h_T (cells)
Monogamous	1.8×10^{-4}	$h_E = h_T = 571$		6.6×10^{-5}	$h_E = h_T = 2004$	
Simultaneous	1.8×10^{-4}	523	2979	6.6×10^{-5}	1928	∞
Joint	1.8×10^{-4}	2051	458	6.8×10^{-5}	22455	1640
Mixed	1.7×10^{-4}	$h_E = h_T = 1945$		6.3×10^{-5}	$h_E = h_T \to \infty$	

To quantify the saturation in killing, we fit the DS model of Eq. 3.4 to the CPM simulation data, and find that the DS model describes the data well (Fig. 3.1, symbols). Although this is qualitatively consistent with our earlier simulations in which conjugates are relatively stable [55], the best-fit parameters (Table 3.1) demonstrate that the saturation in multi-stage killing sets in at much higher cell densities compared to 'single-stage' killing. Furthermore, as expected we find a lower killing rate, k, in multi-stage than in single-stage killing.

From the definition of the saturation constant, h, we expect that an increase in either the conjugate dissociation rate, k_{-1}, or the killing rate of target cells, k_2, results in a higher saturation constant, and that an increase in the conjugate formation rate, k_1 has the opposite effect. In the multi-stage killing simulations, conjugates break up more frequently than for single-stage killing. However, this is not equivalent to a higher dissociation rate because we consider targets to proceed to a next killing stage rather than to fall back to the previous stage upon breakup.

Mechanistic derivation of the functional response for monogamous killing

To better understand why multi-stage killing results in a saturation at higher cell frequencies than single-stage killing, we next attempt to derive the functional response of CTL-mediated killing by extending the Borghans *et al.* [16] model (see also chapter 2) with multi-stage killing. For this purpose, we consider targets to transit sequential stages of conjugate before being killed, and for simplicity, we here limit the number of stages to two,

$$\begin{aligned} E + T &\underset{k_{-1}}{\overset{k_1}{\rightleftharpoons}} [ET] \xrightarrow{k_2'} E + T_1 \ , \\ E + T_1 &\underset{k_{-1}}{\overset{k_1}{\rightleftharpoons}} [ET_1] \xrightarrow{k_2'} E + T^* \ , \end{aligned} \tag{3.5}$$

where E, T, T_1, and T^* represent, respectively, free cognate CTLs, naïve target cells, partially lysed targets, and dead targets; $[ET]$ and $[ET_1]$ represent the conjugates in first and second stages of killing, respectively; k_1 and k_{-1} are the rates of conjugate formation and dissociation, respectively; k_2' is the rate at which targets transit each stage. The dynamics of conjugates and partially lysed targets, T_1, are given by

$$\begin{aligned} \frac{dC_1}{dt} &= k_1 ET - (k_2' + k_{-1}) C_1 \ , \\ \frac{dC_2}{dt} &= k_1 ET_1 - (k_2' + k_{-1}) C_2 \ , \\ \frac{dT_1}{dt} &= k_2' C_1 - k_1 ET_1 \ , \end{aligned} \tag{3.6}$$

where C_1 and C_2 represent, respectively, the number of $[ET]$ and $[ET_1]$ conjugates. The conservation equations for effectors and targets are given by

$$\begin{aligned} \bar{E} &= E + C_1 + C_2, \\ \bar{T} &= T + T_1 + C_1 + C_2, \end{aligned} \tag{3.7}$$

where $\bar{E}$ and $\bar{T}$ are the total CTL and target cell numbers, which are maintained at a constant level within a simulation.

Similar to earlier studies [16, 55], we can rewrite the dynamics in terms of total cell numbers as

$$\begin{aligned} \frac{dC_1}{dt} &= k_1 \overbrace{(\bar{E} - C_1 - C_2)}^{\text{free CTLs}} \overbrace{(\bar{T} - T_1 - C_1 - C_2)}^{\text{naïve targets}} - (k_2' + k_{-1})C_1, \\ \frac{dC_2}{dt} &= k_1 \overbrace{(\bar{E} - C_1 - C_2)}^{\text{free CTLs}} \overbrace{(\bar{T} - T - C_1 - C_2)}^{\text{partially lysed targets}} - (k_2' + k_{-1})C_2, \end{aligned} \tag{3.8}$$

By making a quasi-steady state (QSS) assumption for C_1 and C_2 (i.e, $\frac{dC_1}{dt} = \frac{dC_2}{dt} = 0$), and summing the resulting equations, we obtain the following quadratic equation in terms of the total number of conjugates, $C = C_1 + C_2$:

$$C^2 - (h' + \bar{E} + \bar{T})C + \bar{E}\bar{T} = 0, \tag{3.9}$$

where $h' = (k_2' + k_{-1})/k_1$ is the Michaelis-Menten constant. Except for the difference in the definition of C and h', the above quadratic equation is identical to that for single stage killing (see Eq.(3.2)) [16, 55]. Therefore, we can obtain the expression for C as the full QSSA solution, or simplify further by a Padé approximation. According to the full solution, the density of the conjugates, $C = C_1 + C_2$, at steady state is given by

$$C = C_1 + C_2 = \frac{1}{2}(h + \bar{E} + \bar{T} - \sqrt{(h' + \bar{E} + \bar{T})^2 - 4\bar{E}\bar{T}}) \,, \tag{3.10}$$

which can be further simplified using a Padé approximation, into

$$C = C_1 + C_2 = \frac{\bar{E}\bar{T}}{h' + \bar{E} + \bar{T}} \,. \tag{3.11}$$

From the quasi-steady state equations for partially lysed targets, T_1, and conjugates at the second stage, C_2 (Eq. 3.6), we find that $C_1 = \frac{k_2' + k_{-1}}{k_2'} C_2$ at steady state. Therefore, the total number of conjugates is given by

$$C = C_1 + C_2 = \frac{k_2' + k_{-1}}{k_2'} C_2 + C_2 = \frac{2k_2' + k_{-1}}{k_2'} C_2 \,, \tag{3.12}$$

and the rate at which the target cells are killed is given by

$$\frac{dT^*}{dt} = k_2' C_2 = \frac{k_2' k_2'}{2k_2' + k_{-1}} C \,. \tag{3.13}$$

When synapses break in our CPM simulations, target cells remember the elapsed duration in conjugates. Thus, a high frequency of conjugate breakup implies a high k_2' and the rate of dissociation to naïve targets $k_{-1} \to 0$. The rate at which target cells are killed then reduces to

$$\frac{dT^*}{dt} = \frac{k_2'}{2} C \ . \tag{3.14}$$

Therefore, the number of target cells killed over a time Δt, resulting from two-stage CTL-mediated killing is

$$\begin{aligned} K_{full} &= k_2' \Delta t C_2 = \frac{k_2' \Delta t}{2} \left(h' + \bar{E} + \bar{T} - \sqrt{(h' + \bar{E} + \bar{T})^2 - 4\bar{E}\bar{T}} \right) \ , \\ K_{Padé} &= k_2' \Delta t C_2 = \frac{1}{2} \frac{k_2' \Delta t \bar{E} \bar{T}}{h' + \bar{E} + \bar{T}} \ . \end{aligned} \tag{3.15}$$

These functional responses are similar to that obtained for single-stage killing (Eqs. (3.3) and (3.4)) [55]. To quantify the influence of multi-stage killing, let us consider the same average time a target should be in conjugate to be killed, irrespective of the number of stages. To make the kill time t_D the same between single- and multi-stage killing scenarios, we set $k_2' = 2k_2$, and obtain the following functional responses for multi-stage killing:

$$\begin{aligned} K_{full} &= \frac{k_2 \Delta t}{2} (h' + \bar{E} + \bar{T} - \sqrt{(h' + \bar{E} + \bar{T})^2 - 4\bar{E}\bar{T}}) \ , \\ K_{Padé} &= \frac{k_2 \bar{E} \bar{T} \Delta t}{h' + \bar{E} + \bar{T}} \ , \end{aligned} \tag{3.16}$$

where the Michaelis-Menten saturation constant is $h' = k_2'/k_1 = 2k_2/k_1$ (because $k_{-1} = 0$). Therefore, the resulting functional response qualitatively remains the same but multi-stage killing results in a higher saturation constant, which is consistent with our simulations (Fig. 3.1). The maximum killing rate in multi-stage killing is the same as in single-stage killing (i.e., k_2). Furthermore, from the definition of $h = (k_2 + k_{-1})/k_1$, the saturation also occurs at higher CTL and target cell frequencies when the dissociation rate to naïve targets, k_{-1}, is increased. Taken together, these results show that increasing the number of stages for target cells to be killed, or increasing the dissociation rate of conjugates k_{-1}, both result killing rate saturation at higher CTL and target cell frequencies, without altering the maximum killing rate.

3.2.2 Non-monogamous killing regimes

Next we examined whether the above findings can be generalized to non-monogamous regimes. We performed similar multi-stage killing simulations for simultaneous, joint, and mixed killing regimes, and find that CTL killing generally saturates both in CTL and target cell densities. Furthermore, consistent with our previous study [55], the onset of saturation is asymmetric in simultaneous and joint killing regimes (Fig. 3.2). In the mixed killing regime, the number of cells killed increases almost linearly with an

increase in CTL or target cell numbers, i.e., there is no evidence for saturation at these densities. This lack of saturation is also consistent with our earlier single-stage mixed killing simulations [55], and is now even weaker due to multi-stage killing.

To quantify the saturation in killing, we fit the DS model of Eq. 3.17 to the data from non-monogamous killing simulations and find that the saturation constants are indeed higher than the corresponding single-stage killing (Table 3.1). Taken together, these results demonstrate that the influence of multi-stage killing can be generalized, and that the double saturation model is a good approximation even if multiple hits are required to induce target cell death.

Our results show that, for a given kill time an increased number of stages (or multiple hits) to kill a target cell results in saturation at higher CTL and target cell frequencies, without altering the maximum possible killing rates. Throughout this study, we considered targets to remember the durations they spent in conjugates when they break the synapse, i.e., targets advance a killing stage. Although there is no experimental evidence supporting or denying this, such a 'memory' represents an ideal case for efficient CTL killing. Still, compared to single-stage killing, multi-stage killing or a high dissociation rate generally results in inefficient killing, except at very high cell densities when maximum killing rates are attained. Consistent with this, it was recently shown that CXCR3$^{-/-}$ T cells have less stable interactions with virus-infected target cells than wild-type T cells, resulting in reduced control of the virus [56].

3.3 Methods

3.3.1 Cellular potts model simulations

The simulations performed in this study are similar to our earlier study [55], and differ only in the stability of conjugates (see Chapter 2 for full details of the simulation protocol). Briefly, we achieve multi-stage killing by continuing CTL and target cell migration despite being in a conjugate. Moreover, there is no preferential adhesion between these cell types, thus preventing their sticking together during migration. Together, this results in short-lived conjugates. We keep track of the time spent in conjugates by the targets at a temporal resolution of 10 sec. When a conjugate dissociates, the target cell remembers the duration it spent in a conjugate, and accumulates on top of the elapsed contact duration when subsequent conjugates with the same or different CTLs are formed. A target cell is killed when the cumulative conjugate duration reaches $t_D = 15$ mins, and the killed target vanishes in a few seconds. When it has fully disappeared, a new target cell is introduced at a randomly chosen position in the field. To ensure that we measure CTL-mediated killing at steady state, we perform each simulation for 240 minutes, but count the number of cells killed only during the last 75 mins.

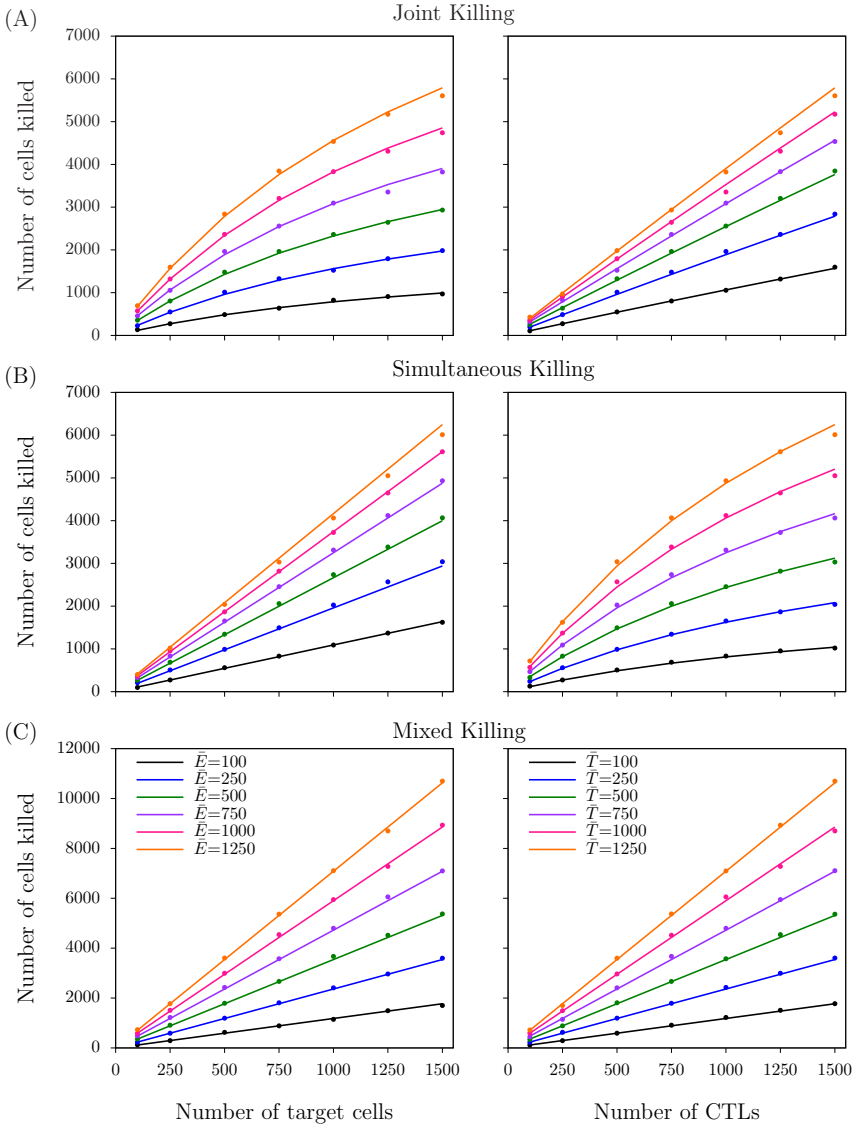

Figure 3.2. Number of cells killed during non-monogamous killing regimes: joint (A), simultaneous (B), and mixed (C). The mean number of cells killed obtained from 3 independent simulations are shown in markers, and error bars represent the standard deviations. The best-fit DS model predictions are depicted in solid lines.

3.3.2 Mathematical models

According to the general double saturation (DS) model [55], the number of cells killed over a period Δt is given by

$$K_{\mathrm{DS}} = \frac{k\Delta t\bar{E}\bar{T}}{1+\bar{E}/h_E+\bar{T}/h_T}\ , \tag{3.17}$$

where k is the 'mass-action' killing rate (see below); h_E and h_T are saturation constants in CTL and target cells, respectively; and $\bar{E}$ and $\bar{T}$ are the number of CTLs and targets, respectively. At low densities of CTLs and target cells, or when saturation constants are very large ($h_E = h_T = \infty$), the total killing rate approaches the mass-action term, $k\bar{E}\bar{T}$, showing that the killing rate k has the same interpretation as a mass-action killing rate. Whenever a fitting procedure leads to parameter estimates where $h_E \to \infty$ and $h_T \to \infty$ one should conclude that the data are well described by a mass-action process. If $h_E \to \infty$, the DS model reduces to

$$K_{\mathrm{DS}|\mathrm{h_E}\to\infty} = \frac{k\Delta t\bar{E}\bar{T}}{1+\bar{T}/h_T}\ , \tag{3.18}$$

which results from a conventional Holling's type II functional response with saturation in target cells, T, and if $h_T \to \infty$, the DS model reduces to

$$K_{\mathrm{DS}|\mathrm{h_T}\to\infty} = \frac{k\Delta t\bar{E}\bar{T}}{1+\bar{E}/h_E}\ . \tag{3.19}$$

3.3.3 Non-linear regression

For all the regression analyses of models to the data, we used the function *nlinfit*, which uses the Levenberg-Marquardt algorithm, in Matlab (The MathWorks Inc., Natick, MA). To prevent skewing of the fit to large number of cells killed, we log-transformed the data prior to fitting.

Chapter 4

Tissue Dimensionality Influences the Functional Response of Cytotoxic T Lymphocyte Mediated Killing

Saikrishna Gadhamsetty, Athanasius F.M. Marée, Joost B. Beltman and Rob J. de Boer

In Preparation

Abstract

Cytotoxic T lymphocyte (CTL)-mediated killing of virus infections and tumors occurs over a wide range of conditions. The spatial environments in which CTLs encounter target cells vary from narrow vessels, to two-dimensional epithelial tissues, to densely populated 3-dimensional (3D) T cell areas within lymphoid tissues. How such spatial environments alter the functional response of CTL-mediated killing is unclear. In this study, we perform cellular Potts model simulations in different spatial configurations to investigate how the dimensionality of the space affects the functional response of CTL-mediated killing. We show that saturation in a fully 3D environment is stronger than in a 'flat' 3D environment, which is largely due to accompanying differences in CTL-target encounter rates. Irrespective of the spatial configuration, the double saturation function that we previously proposed can in all cases describe the CTL-mediated killing, demonstrating its generality.

4.1 Introduction

Cytotoxic T lymphocytes (CTLs) continuously search for and kill virus-infected cells. For example, CTLs specific to HIV co-localize with infected cells in the sub-capsular sinuses of lymph nodes [57], whereas CTL interactions with peptide pulsed B cells predominantly occur in T cell areas in the cortex of lymph nodes [26]. Furthermore, tissue-resident memory T cells continuously patrol the skin epidermis to find targets [3, 20], and tumor-infiltrating CTLs navigate through spatially complex environments [2, 19]. Therefore, it is important to understand how spatial environments influence the CTL-mediated killing rates of target cells.

As in ecology, the functional response of CTL-mediated killing is defined as the rate at which a single CTL kills targets, as a function of the CTL and the target cell densities. The total killing rate at which target cells are killed is given by the product of CTL density and the functional response. Theoretical studies hitherto have studied the functional responses of CTL-mediated killing in 2D or 3D environments [15, 55]. In an earlier study [55], we performed 2D cellular Potts model (CPM) [43, 44] simulations of CTL-mediated killing in a densely packed cellular environment mimicking T cell areas of a lymph node, and found that a double saturation (DS) model (with two different saturation constants) describes the CTL-mediated killing well, regardless of the number of cells allowed in CTL-target cell conjugates. Additionally, we could analytically derive this DS model for cases where target cells are killed by a single CTL. For other cases, the double saturation model still provides a semi-mechanistic description, having three parameters with a sound biological meaning [55]. Thus, the DS model is a general functional response of CTL-mediated killing, expected to apply across a wide range of conditions. However, the quantitative effects of tissue dimensionality on the functional response are still unknown.

In this study, we investigate how dimensionality of the tissue influences the functional response. To this end, we perform 3D CPM simulations of CTL killing in two spatial configurations. As expected from our previous study [55], the DS model appears valid for different types of CTL-target interactions, irrespective of the dimensionality of the simulation field. Moreover, we find that the tissue dimensionality affects the onset of saturation in killing, predominantly due to differences in CTL-target encounter rates. Taken together, our results demonstrates that the double saturation model is a generic functional response, and that spatial dimensionality plays a hitherto unrecognized role in determining the extent of saturation of CTL-mediated killing.

4.2 Results

4.2.1 Cellular Potts model simulations of CTL-mediated killing

The CPM is a lattice-based model [43, 44], in which each cell is composed of multiple lattice sites. Previously, we performed 2D CPM simulations to determine the general functional response of CTL-mediated killing [55]. Here, we investigate the quantitative differences of the CTL-mediated killing functional response between 2D and 3D environments.

The parameters in our previous 2D CPM simulations [55] were chosen such that the motility properties of *in silico* cells mimic those observed *in vivo* [2, 26]. To achieve a similar motility in 3D simulations, we require a different set of CPM parameters, confounding a direct comparison of killing rates observed in 2D and 3D simulations. Therefore to rigorously compare the functional responses of CTL-mediated killing in different spatial environments, we consider two 3-dimensional fields of equal volume: a slab and a cube, with dimensions of $107 \times 107 \times 107$ and $350 \times 350 \times 10 \mu\text{m}^3$, respectively (Fig. 4.1). The slab configuration resembles a 2D space as its height is close to the diameter of a CTL [7] or a target cell in our simulations, and hence it mostly consists of cells in a mono-layer. To restrict the migration of cells in the z-direction, we made the boundaries of both cube and slab fields in the z- direction impermeable to cells (i.e., a fixed boundary condition in the z-direction alone; see Fig. 4.2A-D for representative snapshots of the simulations). Thus, the slab closely resembles a 2D space, and the cube a 3D space.

The simulation protocol used in this study is same as in our previous study (see Methods and Chapter 2 for details). Briefly, we consider a finite 3D space (wrapped in x- and y-directions), filled with static rods representing the fibroblastic reticular network (RN), CTLs, and B cells as target cells; the empty voxels represent extracellular matrix (Fig. 4.2A-D). The two configurations differ only in the dimensionality of the space; the rest of the parameters, including the volume of the field, total number of cells and RN density, remain the same. CTLs and target cells perform a persistent random walk in this space according to well-defined migration rules (for details see [45, 46, 55]). The simulation parameters are chosen such that we approximate the migration properties

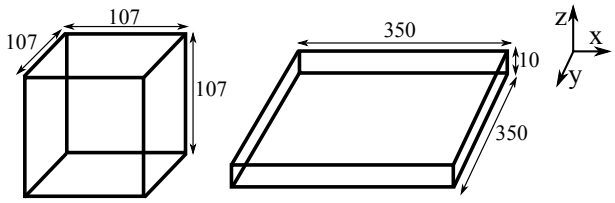

Figure 4.1. Schematic of the fields. The cube (left) and slab (right) are of equal volume, and the numbers on the edges indicate the dimensions of the environments.

of T cells observed in imaging studies [26]. The migration speeds of CTLs and targets are similar between slab and cube. However, despite the same simulation parameters between slab and cube simulations, cells in the two configurations exhibit different motility coefficients (Table 4.1). This could be due to the fact that cells in a cube have the additional freedom to migrate in the z-direction, resulting in a lower motility coefficient in a cube simulation. Note that for the estimation of the motility coefficient by Fuerth's equation [51], it is unclear whether a slab should be considered as a 2D or 3D space. Nevertheless, these motility coefficients between slab and cube are significantly different, irrespective of the space dimensionality (n) used in the equation (Table 4.1).

Table 4.1. Summary of the migration properties of CTLs and targets observed in the two configurations. Motility coefficients, M, and persistence times, p, are obtained by fitting Fuerth's equation to the mean square displacement (msd) of cells: $msd = 2nM\{(t - p(1 - e^{-t/p})\}$, where t is the time from the beginning of the observation and n is the dimensionality of the space (see Fig. S1 in the appendix). Numbers in parentheses indicate the 95% confidence intervals of the parameters.

	Motility coefficient (μm^2/min)		Persistence time (min)		Speed (μm/min)	
	CTL	Target	CTL	Target	CTL	Target
Cube	29.9($\pm$0.03)	17.4($\pm$0.1)	3.4($\pm$0.1)	3.3($\pm$0.1)	5.0	3.9
Slab (with $n = 3$)	34.4($\pm$0.2)	21.1($\pm$0.1)	3.9($\pm$0.1)	3.8($\pm$0.05)	5.0	3.9
Slab (with $n = 2$)	51.6($\pm$0.3)	31.7($\pm$0.1)	3.9($\pm$0.1)	3.8($\pm$0.03)	5.0	3.9

To quantitatively compare the functional response of CTL-mediated killing in slabs and cubes, we perform simulations with different numbers of antigen-expressing target cells, $\bar{T}$, and their cognate CTLs, $\bar{E}$, for four different killing scenarios: monogamous, joint, simultaneous, and mixed killing (Fig. 4.2E). In the monogamous scenario, a CTL can only kill a single target cell at a time, and a target cell can only be killed by a single CTL. The mixed killing scenario is opposite to monogamous, i.e., conjugates of multiple CTLs and multiple targets are allowed to form, in which each CTL can induce death of multiple target cells simultaneously, and a target cell can be killed by multiple CTLs. Joint and simultaneous killing regimes are intermediates between monogamous and mixed

regimes (Fig. 4.2E). In joint killing, a CTL can kill a single target cell at a time, but a target cell can be killed by many CTLs acting together at the same time; whereas in the simultaneous regime a CTL can induce death of multiple target cells simultaneously, and a target cell can only be killed by a single CTL. Unless otherwise specified, we do not restrict the number of synapses that cells can form (for simplicity referred to as 'binding sites' hereafter) in the non-monogamous regimes of killing, and use a time required for a CTL to kill a target cell, t_D, of 15 mins. When multiple CTLs are bound to a target, they independently induce its death (i.e., the time required to kill a target cell is inversely related to the number of CTLs in the conjugate). Similarly, single CTLs bound to multiple targets can kill all of them within the same kill time, i.e., killing of individual targets remains the same irrespective of how many targets a CTL is conjugated with. To precisely determine the CTL killing rates at a particular CTL and target cell density, we maintain constant target cell numbers throughout the simulations, by immediately replacing every killed target cell with a new target cell at a random position in the field. CTLs in our simulations neither die nor divide.

In the simulations we record the number of cells killed and the total number of synapses over intervals of 1 min. Both measures approach a steady state value soon after the start of the simulation (Fig. 4.3). Because conjugated cells can form additional synapses with other cells in mixed killing, we observe more synapses than in the monogamous scenario (compare Fig. 4.3A with 4.3B). We consistently found a higher number of synapses in cube than in slab simulations (compare solid and dashed lines in Fig. 4.3). Because killing takes 15 mins, and because the number of cells killed is counted over intervals of 1 min at any given time, the number of cells killed is about 1/15 of the total number of synapses (Fig. 4.3). We perform simulations corresponding to 150 mins in real time, and count the number of cells killed during the last 75 mins, i.e., when the system has approached a steady state. The 3D simulations are computationally expensive, with each simulation requiring about 8 days of CPU time on a single Intel Xeon processor, 3.33 GHz, with 48 GB of memory. For this reason, we limited our analysis to a single run for each CTL and target cell frequency.

4.2.2 Conjugates break frequently in 3D simulations

We allow conjugate formation by a strong adhesion between CTL-target pairs upon their encounter, and making the cells in a conjugate immotile (i.e., by setting $\mu = 0$; referred to as the 'stopping-rule' henceforth). Despite the enhanced adhesion and stopping-rule, we find that the conjugates in both cube and slab simulations are relatively unstable, which can be seen from the 'killing signal' distribution: for monogamous simulations with an excess of targets (e.g., $\bar{E} = 100$, $\bar{T} = 1500$), the number of targets accumulating killing signal would be similar to the number of CTLs if the conjugates were stable. Instead we observe that 10-fold more targets accumulate killing signal than there are CTLs present in the field (Fig. S2), implying that conjugates are not very stable.

Targets 'remember' the accumulated killing signal when a conjugate breaks, and upon renewed contact with the same, or another CTL, the kill signal accrues on the existing sig-

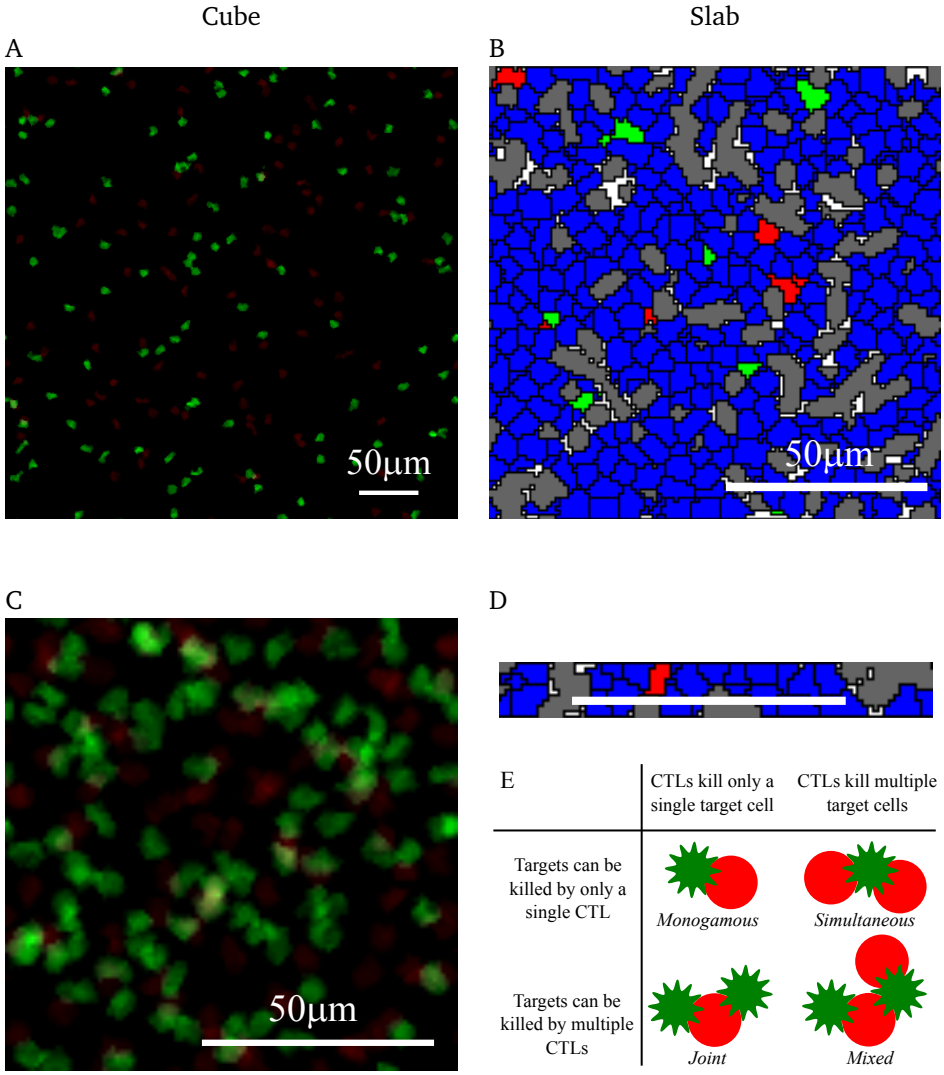

Figure 4.2. Representative snapshots of the simulations in cube and slab. (A, C) Representative mean-intensity projections of the cube (A) and slab (C). (B, D) Cross-section views of cube (B) and slab (D) simulations. (E) Illustration of the scenarios of killing. In all images, CTLs and target cells are shown in green and red, respectively, and the reticular network is shown in grey. Non-specific target cells and CTLs are shown in blue. These snapshots were taken from simulations with $\bar{E} = 100$ CTLs and $\bar{T} = 100$ targets. The scale bar indicates 50 μm.

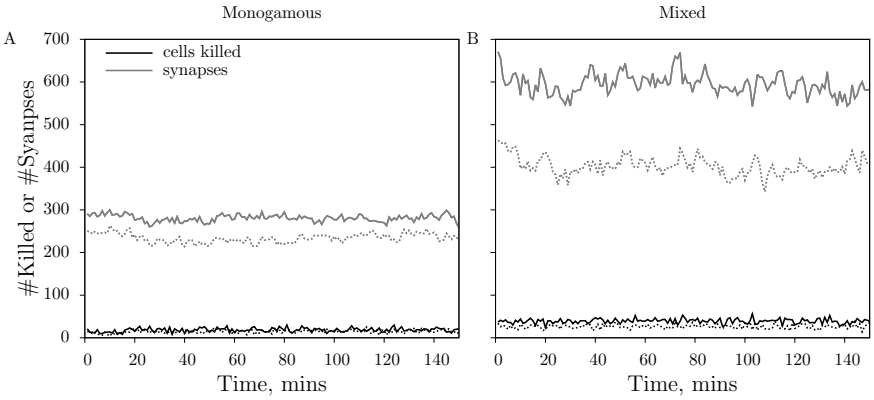

Figure 4.3. The number of cells killed (black lines) and the total number of synapses (gray lines) over 1-min intervals during a simulation with $\bar{E} = 500$ CTLs and $\bar{T} = 500$ targets for monogamous (A) and mixed killing (B). The measurements from the cube simulations are depicted as solid lines, and those from the slab as dashed lines. We measure the number of cells killed is counted over the last 75 mins of the simulations to ensure that killing is at steady state.

nal. Since the targets remember the 'killing signal', these relatively unstable conjugates mimic a multi-stage killing scenario. Such multi-stage killing results in higher saturation constants in both CTL and target cell densities compared to single-stage killing (Chapter 3). Thus, we expect generally higher saturation constants in these 3D simulations relative to our earlier 2D simulations (Chapter 2). Because the killing signal distributions are similar between slab and cube configurations ($P = 0.8$, $\chi^2 = 5.6$; Fig. S2), our approach to assess the influence of dimensionality on the functional response with these configurations is valid.

4.2.3 Monogamous killing

In the monogamous killing regime, conjugates of just one CTL and one target cell are allowed to form (Fig. 4.2E). As expected [16, 55], also in the 3D simulations the number of cells killed saturates symmetrically with an increase in CTL and target cell frequencies, both in slab and cube configurations (Fig. 4.4). The saturation in killing is expected from the handling time (which in our case is $t_D = 15$ mins) [16, 33] and its symmetric nature is due to the monogamous CTL-target interactions [16, 33, 55]. The full QSSA and DS functional responses for monogamous killing can be derived by applying an enzyme-substrate analogy [16], and are given by

$$\begin{aligned} K_{\text{full}} &= k_2 \Delta t \, \frac{h + \bar{E} + \bar{T} - \sqrt{(h + \bar{E} + \bar{T})^2 - 4\bar{E}\bar{T}}}{2} \,, \\ K_{\text{DS}} &= \frac{k' \Delta t \bar{E} \bar{T}}{1 + \bar{E}/h + \bar{T}/h} \,, \end{aligned} \tag{4.1}$$

where $\bar{E}$ and $\bar{T}$ are the total number of cognate CTLs and target cells, respectively; k_2 is the killing rate of target cells; h is the Michaelis-Menten constant, defined as $\frac{k_2 + k_{-1}}{k_1}$; k_1 and k_{-1} are the rates at which conjugates form and dissociate, respectively; and k' in the DS model is the maximum killing rate, defined as k_2/h. Fitting the Padé and full QSSA models to the simulated data from the two spatial configurations, we find that the full QSSA model describes the data (Fig. S3) better than the Padé model (Fig. 4.4), particularly when the frequencies of CTLs and targets together are larger than 40% of the total cells in the field. These results are consistent with our earlier 2D simulations [55]. Interestingly, the saturation in killing sets in at higher CTL and target cell densities in the slab configuration, compared to the cube (i.e., the saturation constant is almost 2-fold lower in cube). Thus, the spatial configuration affects the functional response of CTL-mediated killing.

The differences in the saturation constants between slab and cube could either result from altered migration properties or from altered CTL-target encounter rates, both emerging due to differences in the spatial organization). As the migration speeds are similar between the two configurations (Table 4.1), we hypothesized that the higher killing in cube simulations is due to a faster detection of target cells, i.e., a higher rate of conjugate formation, k_1. Since the diameter of the CTLs and targets is comparable to the height of the slab, CTLs in the slab are expected to scan fewer cells compared to CTLs in the cube configuration. Indeed, the number of targets that are in contact with each CTL in simulations with an excess of target cells, i.e., $\bar{E} = 100, \bar{T} = 1500$ cells, is higher in a cube than in a slab configuration (Fig. S6; $P < 0.01$, $\chi^2 = 95$). Similarly, the number of neighboring CTLs per target is also highest in cube simulations (not shown). Taken together, the CTL-target encounter rates are highest in cube simulations, and result in an increased rate of conjugate formation, k_1, and a higher number of synapses in cube simulations (Fig. 4.3). As a result, fewer CTLs are sufficient to achieve the maximum killing in a cube, and killing saturates at lower cell densities than in a slab configuration ($h = (k_2 + k_{-1})/k_1$).

4.2.4 Simultaneous killing

In the simultaneous killing regime, a CTL can kill multiple target cells simultaneously, but a target cell can only be killed by a single CTL (Fig. 4.2E). The resulting functional response can be analytically derived [55] and is given by:

$$K_{QSSA} = \frac{k_2 \Delta t}{2} \left(m\bar{E} + h + \bar{T} - \sqrt{(m\bar{E} + h + \bar{T})^2 - 4m\bar{E}\bar{T}} \right), \tag{4.2}$$

where k_2 is the killing rate, m is the maximum number of targets bound to a CTL (i.e., binding sites on a CTL), Δt is the time period during which killing is measured, and h is the Michaelis-Menten-like saturation constant, defined as $(k_2 + k_{-1})/k_1$ [55]. This can be simplified using a Padé approximation to a double saturation (DS) model with two

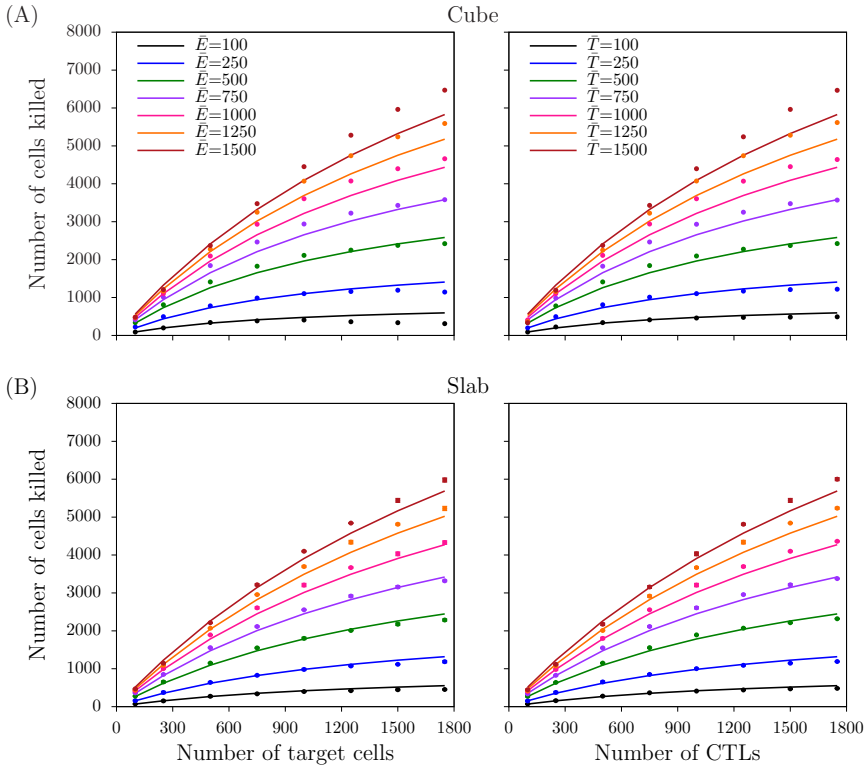

Figure 4.4. Number of target cells killed for monogamous killing. The total number of cells killed over 75 mins as a function of target cell (left panels) and CTL (right panels) densities, obtained from simulations in cube (A) and in slab (B) configurations. Markers depict the measurements from the simulations, and solid lines represent the DS model predictions with the best-fit parameters (Table 4.2).

Table 4.2. Best fit parameters and 95% confidence ranges of the double saturation (DS) model for the different killing regimes in slab (A) and in cube (B) configurations.

(A) Slab	k' (cells^{-1} min^{-1})	h_E (cells)	h_T (cells)
Monogamous	$1.07(\pm0.07)\times10^{-4}$	$h_E = h_T = 1202(\pm137)$	
Joint	$1.18(\pm0.07)\times10^{-4}$	∞	$740(\pm88)$
Simultaneous	$1.18(\pm0.04)\times10^{-4}$	$889(\pm73)$	∞
Mixed	$1.08(\pm0.01)\times10^{-4}$	$h_E = h_T \to \infty$	
(B) Cube	k' (cells^{-1} min^{-1})	h_E (cells)	h_T (cells)
Monogamous	$1.54(\pm0.29)\times10^{-4}$	$h_E = h_T = 772(\pm216)$	
Joint	$1.71(\pm0.12)\times10^{-4}$	∞	$446(\pm49)$
Simultaneous	$1.86(\pm0.08)\times10^{-4}$	$482(\pm35)$	∞
Mixed	$1.61(\pm0.02)\times10^{-4}$	$h_E = h_T = 3.8(\pm0.95)\times10^4$	

different saturation constants—one for CTL and another for target cell densities:

$$K_{DS} = \frac{mk_2\bar{E}\bar{T}\Delta t}{h + m\bar{E} + \bar{T}} = \frac{k'\bar{E}\bar{T}\Delta t}{1 + \bar{E}/h_E + \bar{T}/h_T}, \tag{4.3}$$

where k' is the mass-action killing rate, defined as mk_2/h, and $h_E = h/m$ and $h_T = h$ are the saturation constants in CTLs and target cells, respectively. These derivations show that the number of cells killed is expected to saturate at lower CTL frequencies than target cell frequencies, i.e., asymmetric saturation, which is confirmed by both cube (Fig. 4.5A) and slab configurations (Fig. S4A).

Fitting the DS model of Eq. 4.3 to the data from cube and slab simulations, the saturation constant in target cells, h_T, approaches infinity ($P = 0.08$, $F_{1,61} = 3.09$ (cube); $P = 0.08$, $F_{1,61} = 3.09$ (slab); Table 4.2), thereby suggesting a lack of saturation in this range of target cell densities. As occurred for monogamous killing, the saturation sets in at lower CTL densities in cube than in slab simulations. This likely again results from differences in scanned region by CTLs, leading to faster target detection (i.e., increasing k_1 in Eqs. (4.2) and (4.3)). Consistent with the higher CTL-target encounter rates in cube, we find that the average number of targets in conjugate with a CTL is higher than the slab simulations (not shown; $P = 10^{-12}$ for a simulation with $\bar{E} = 100$, $\bar{T} = 1500$ cells).

4.2.5 Joint killing

In joint killing simulations (Fig. 4.2E), conjugates of multiple CTLs attached to a single target can form, and all the conjugated CTLs independently kill the target cell (i.e., the average time required to kill a target cell is t_D/n, where n is the number of CTLs bound

to a target). In both slab and cube configurations, the number of cells killed saturates in target cell frequencies, but increases linearly with CTL frequencies (Figs. 4.5B and S4B). Joint killing is a converse scenario to simultaneous killing, compared to which the onset of saturation in the CTL and target cell densities is reversed, in both the slab and cube configurations. This asymmetric saturation is consistent with our earlier study [55].

For joint killing, we have previously been unable to derive the functional response analytically. Nevertheless, the DS model with two different saturation constants in CTLs and targets provides a semi-mechanistic description of joint killing [55]. Consistent with this, we find that the DS model of Eq. 4.5 provides a good description of the data from both cube (Fig. 4.5B, solid lines) and slab simulations (Fig. S4B, solid lines). Setting $h_E \to \infty$ of Eq. 4.7 describes both the cube and slab simulation data equally well ($P = 1$, $F_{1,61} = 0$), suggesting that the killing rate does not saturate with an increase in target cell densities within the range of densities examined. While the results are qualitatively similar between slab and cube configurations, the saturation constant h_T differs between the two configurations (Table 4.2). As was the case for monogamous and simultaneous killing, the fitted saturation constant was lower for cube simulations than for slab simulations. Again, the difference in the saturation constants between the two configurations can be explained by differences in the CTL-target encounter rates k_1.

4.2.6 Mixed killing

Next, we performed simulations for the mixed killing scenario in which CTLs can induce killing of multiple target cells simultaneously, and target cells can be killed jointly by multiple CTLs (Fig. 4.2E). Both in the slab and cube configurations, the number of cells killed increases almost linearly with target cell and CTL densities (Figs. 4.5C and S4C). Fitting DS and mass-action ($h_E = h_T \to \infty$; see Methods) models to the data from mixed killing, we indeed find no evidence for saturation in the slab configuration ($P = 1$, $F_{1,62} = 0$), but a small significant saturation in cube configurations ($P < 10^{-11}$, $F_{1,62} = 71$). Thus, the low level of saturation in our published 2D simulations [55] is further lowered in the cube and completely absent in the slab configuration. Furthermore, synapses were breaking at a similar frequency in the cube and slab simulations, which is evident by the killing signal distribution of the targets (not shown). Thus, as in other killing scenarios, the differences in the saturation between the two configurations are due to the higher CTL-target encounter rates in cube simulations.

Two factors may explain the lack of or low saturation in the 3D mixed killing simulations. First, conjugates are less stable in 3D than in 2D, despite the high adhesion and 'stopping rule' and the associated breaking of conjugates is expected to delay the onset of saturation (see Chapter 3). Second, compared to 2D simulations [55], we expect a higher number of maximum possible binding sites on cells in 3D, which could delay the onset of saturation [55]. Indeed, when we restricted the maximum number of cells in a conjugate, saturation is more pronounced and occurred to a similar extent in CTL and target cell frequencies (Fig. S5). In summary, the altered saturation in 3D is due to a combination of a high number of binding sites and short-lived conjugates.

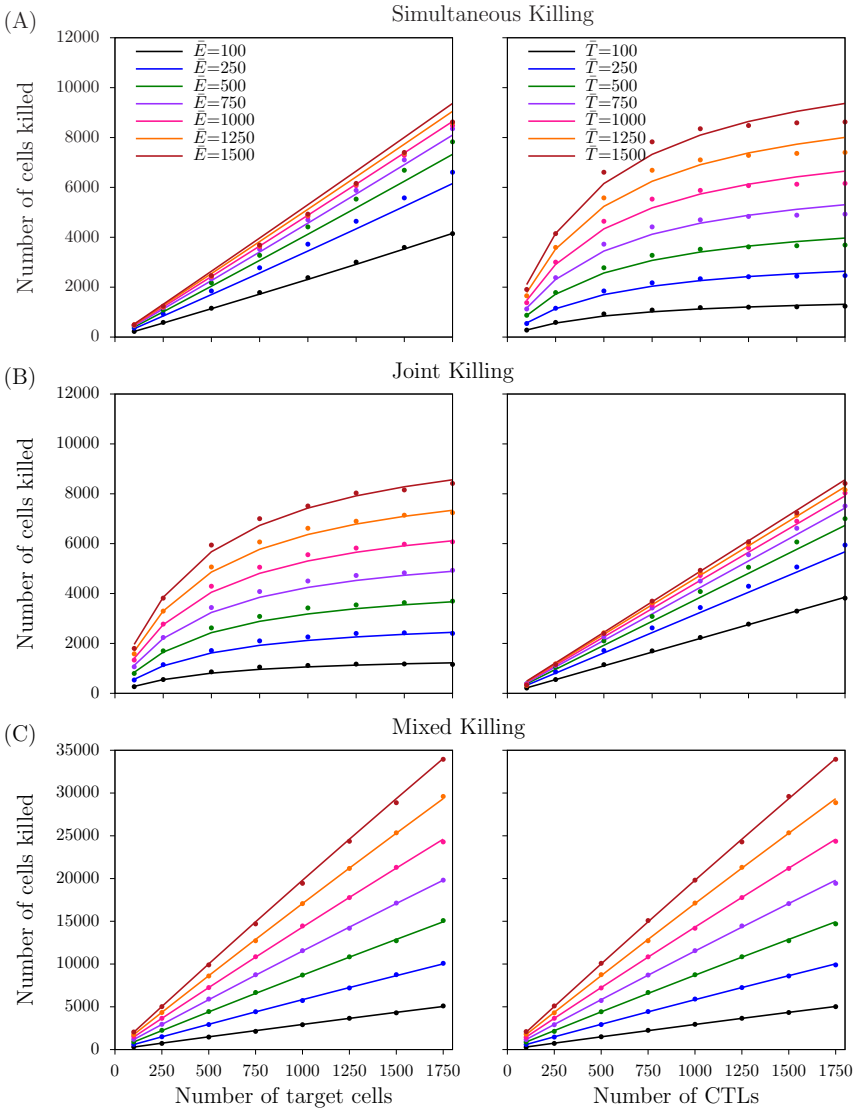

Figure 4.5. Number of target cells killed for non-monogamous killing regimes in the cube configuration. The number of cells killed as a function of CTL and target cell densities for simultaneous (A), joint (B), and mixed (C) killing regimes in cube simulations. Markers indicate the mean of the total number of cells killed over 75 mins, and solid lines represent the predictions of the DS model with the best-fit parameters (Table 4.2). Functional responses observed in the slab simulations are shown in Fig. S4

Taken together, our results suggest that the DS model is robust over a wide range of conditions, including variation in spatial factors, and that dimensionality of the space plays a role in determining the onset of saturation.

4.3 Discussion

By simulating CTL killing in two distinct 3D configurations, we have shown that the total number of target cells killed per day saturates when either the density of target cells or that of CTLs becomes large. Consistent with our previous 2D simulations [55], in asymmetric killing scenarios (joint and simultaneous regimes), the saturation is most pronounced for either CTLs or targets. Similarly, killing saturates symmetrically with CTL and target cell frequencies if their interactions are symmetric (i.e., monogamous and mixed regimes). We conclude that the double saturation (DS) function remains a robust functional response describing CTL-mediated killing, also in different spatial configurations.

The CPM is one of the most sophisticated spatial modeling formalisms available to model cellular interactions, and it has been used to answer a variety of questions on topics such as cell migration [45], morphogenesis [58], and tissue development [59]. However, one of the limitations in these 3D CPM simulations is that the conjugate stability was difficult to achieve. For a given diameter of a cell, the number of neighbors that a cell can have in 3D spaces is greater than in 2D spaces. As a result of the pressure of many migratory neighboring cells the cells in a conjugate can be pushed apart, resulting in a reduced stability of the conjugates in 3D compared to 2D. In chapter 3, we showed that the onset of saturation in killing is delayed when targets dissociate from CTLs frequently, but 'remember' the previously developed killing signal. Therefore, the high saturation constants observed in the 3D simulations is primarily due to the relatively unstable conjugates.

Recent *in vitro* experiments also suggest that the synapses break frequently if the CTLs and targets are both migrating [1]. Since the killing signals that the targets accumulated were similar between slab and cube simulations, the comparison of the functional response between the two configurations remains unaffected by the relatively short-lived synapses. Further, as we only vary the spatial dimensions of the fields between the two configurations, our results suggest that the differences in the functional response of killing arise from the different search efficiencies that arise between the two configurations, thereby highlighting the importance of tissue dimensionality. Earlier saturation in cube simulations implies that the maximum killing rate is attained with fewer CTLs, thus implying that CTLs in a cube kill more efficiently.

Our results predict variation in the killing efficiency in different environments. For instance, CTLs specific to human immunodeficiency virus co-localize with infected cells in the sub-capsular sinus of lymph nodes (LNs) [57]. Since sinuses of LNs are narrow spaces, they roughly resemble our slab configuration. Even when all other conditions are similar, our findings suggest that the CTL-mediated killing of HIV-infected cells in

this narrow spatial environment is less efficient than the killing of peptide-pulsed B cells, which predominantly occurs in 3D-like T cell areas [26].

In summary, our results suggest that the spatial configuration of the field may play a role in determining the extent of saturation in CTL-mediated killing. Analyzing the functional response of CTL-mediated killing in different spatial configurations, we find that DS model describes the data well, unless the CTL and target cell frequencies are extremely high. Thus, the double saturation model is a reliable general functional response of CTL-mediated killing, that is able to capture different spatial environments.

4.4 Methods

4.4.1 Model description

We simulate a region of a spleen or a lymph-node using the CPM formalism, in which each biological cell consists of multiple connected lattice sites. We consider a field composed of fibroblastic reticular cells forming a reticular network (RN; $\approx 24\%$ of the field), 2500 B cells (37%), and 2500 CTLs (37%), and extracellular matrix (≈3%). Changes in the cell configuration and movements of the cells occur due to minimization of the surface energy of the cells. Within each time step, all voxels are considered for extension into a random neighboring site, and the change in surface energy due to an extension is calculated by the difference in Hamiltonians H of two configurations. The Hamiltonian is given by

$$H = \sum_{ijk} \sum_{i'j'k'} J_{\tau(\sigma_{ijk}),\tau(\sigma_{i'j'k'})} \left(1 - \delta_{\sigma_{ijk},\sigma_{i'j'k'}}\right) + \sum_{\sigma} \lambda(v_\sigma - V_{\tau(\sigma)})^2, \tag{4.4}$$

where $J_{\tau(\sigma_{ijk}),\tau(\sigma_{i'j'k'})}$ is the surface energy associated with the neighboring lattice sites, and δ is the Kronecker delta. The first term in the above equation represents the sum of all surface energies, and the second term is a volume constraint applied to maintain the size of the cells close to their target volume, $V_{\tau(\sigma)}$; $\tau(\sigma)$ is the cell type of the cell, σ; and λ is the inelasticity. The probability that a lattice site is copied into the neighboring site is one if $\Delta H < 0$, and $e^{-\Delta H/\theta}$ otherwise, where θ represents the membrane fluctuation amplitude of cells. The details of the simulation protocol, including the migration and killing algorithms, are described in full detail elsewhere [55]. The entire model is implemented in the C programming language.

4.4.2 Default model parameters

We use the following parameters described, unless otherwise specified. We consider two 3D fields of similar volume $107 \times 107 \times 107$ and $350 \times 350 \times 10 \mu\text{m}^3$, where the length of each voxel equals 1 μm. Parameters are chosen such that one time step in the simulation

Table 4.3. Default surface energies, J, and surface tensions, γ, used in the simulations of both the configurations.

	ECM	RN	CTL	Tgt
ECM	$J_{ECM,ECM} = 0$	$\gamma_{ECM,RN} = 0$	$\gamma_{ECM,CTL} = 0$	$\gamma_{ECM,Tgt} = 0$
RN	$J_{RN,ECM} = 0$	$J_{RN,RN} = 0$	$\gamma_{RN,CTL} = 175$	$\gamma_{RN,Tgt} = 175$
CTL	$J_{CTL,ECM} = 350$	$J_{CTL,RN} = 350$	$J_{CTL,CTL} = 350$	$\gamma_{CTL,Tgt} = 0$
Tgt	$J_{Tgt,ECM} = 350$	$J_{Tgt,RN} = 350$	$J_{Tgt,CTL} = 350$	$J_{Tgt,Tgt} = 350$

(i.e., attempting to update all the lattice sites) corresponds to 1 second in real time. To maintain similar migration properties at different frequencies of CTLs and target cells, we vary the number of antigen-expressing target cells, $\bar{T}$, and their cognate CTLs, $\bar{E}$, while keeping the total number of CTLs and target cells constant in the field to 5000 cells. Following the initialization of the RN, both target cells and CTLs are initialized at empty random positions as a cube of 27 μm^3, which subsequently grow to their target volume of 180 μm^3, corresponding to a diameter of about 7.7 μm [60]. We use a kill time (i.e., the time required for a CTL to induce a target cell death), t_D of 15 mins [26].

We choose the surface energies J and the surface tensions γ such that the interactions between any pair of cells (including the RN) present in the simulation box are neutral, i.e., there is no preferential adhesion. The default surface energy values and the adhesion strengths used in the simulations are shown in Table 4.3. Other default parameters used in the both configurations: directional propensity, $\mu = 1150$ for CTLs, $\mu = 850$ for target cells; inelasticity of cells, $\lambda = 350$, and membrane fluctuation amplitude, $\theta = 0$. To restrict abrupt changes in migration direction, the actual μ value of a cell is adjusted according to its recent direction of displacement: $\mu_{actual} = \mu e^{-\rho(1-cos\beta)}$, where β is the angle between displacement and the target direction, and ρ scales how rapidly directional propensity decreases with a turn in the cell migration; $\rho = 1$ is used in our simulations.

4.4.3 Mathematical models

According to the double saturation (DS) model, the number of cells killed over a period, Δt is given by

$$K_{\mathrm{DS}} = \frac{k' \Delta \bar{E} \bar{T}}{1 + \bar{E}/h_E + \bar{T}/h_T} \,, \tag{4.5}$$

where k' is the mass-action killing rate; h_E and h_T are saturation constants in CTL and target cells, respectively; and $\bar{E}$ and $\bar{T}$ are the number of CTLs and targets, respectively. At low densities of CTL and target cells, the total killing rate approaches the mass-action term, $k' \bar{E} \bar{T}$, showing that the killing rate $k' = k/h$ has the same interpretation as a mass-action killing rate. Whenever a fitting procedure leads to parameter estimates where $h_E \to \infty$ and $h_T \to \infty$ one should conclude that the data are well described by a mass-

action process. If $h_E \to \infty$, the DS model reduces to

$$K_{\mathrm{DS|h_E}\to\infty} = \frac{k'\Delta\bar{E}\bar{T}}{1+\bar{T}/h_T} \ . \tag{4.6}$$

which results from a conventional Holling's type II functional response with saturation in target cells, T, and if $h_T \to \infty$, the DS model reduces to

$$K_{\mathrm{DS|h_T}\to\infty} = \frac{k'\Delta\bar{E}\bar{T}}{1+\bar{E}/h_E} \ . \tag{4.7}$$

4.4.4 Non-linear regression (or fit) to the data

All the regression analyses of models to the data from simulations are performed using the function *nlinfit* in matlab (The MathWorks, USA), which uses the Levenberg-Marquardt algorithm. To prevent the fit to skew towards high number of cells killed, log-transformed numbers of cells killed were used for all the regressions.

Acknowledgements

The authors thank Johannes Textor, Rutger Hermsen, Lidija Berke, and Paola Carrillo-Bustamante for helpful discussions during the design of the simulations and during the preparation of the manuscript. This study is supported by NWO grants 819.03.009 (to RJdB) and 864.12.013 (to JBB), by the "Virgo consortium," funded by the Dutch government [project number FES0908] and by the "Netherlands Genomics Initiative (NGI)" [project number 050-060-452]. The authors declared that they have no competing interests.

Supplementary figures

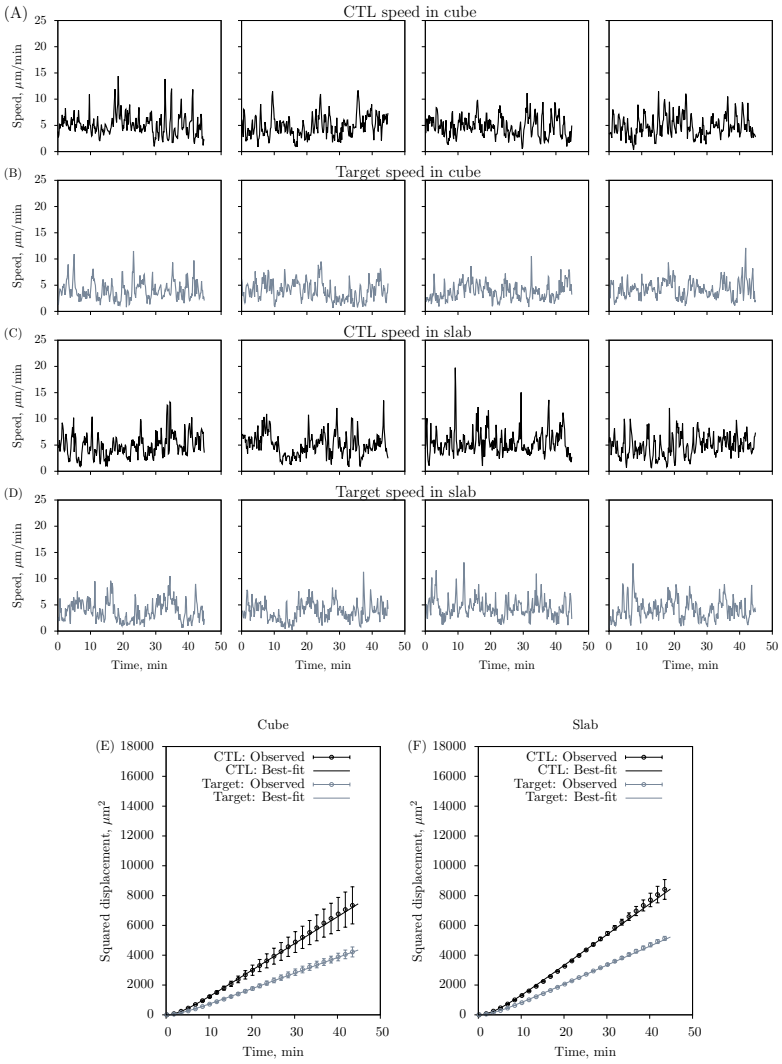

Figure S1. Migration properties of individual CTLs and targets in the simulations. Panels (A-D) show representative plots of migration speeds over time in cube (A-B) and slab (C-D) simulations (in the absence of killing): (A and C) four representative simulated CTLs, (B and D) four representative simulated target cells. Mean square displacement, msd, plots (in the absence of killing) for 3-dimensional simulations of (E) cube and (F) slab. Markers indicate the mean over four independent simulations, and solid lines depict the best-fit predictions of Fuerth's equation: $msd = 2nM\{(t - p(1 - e^{-t/p})\}$, where t is the time from the beginning of the observation, and n is the dimensionality of the field. The migration properties of CTLs are depicted in black lines, and of targets in gray lines.

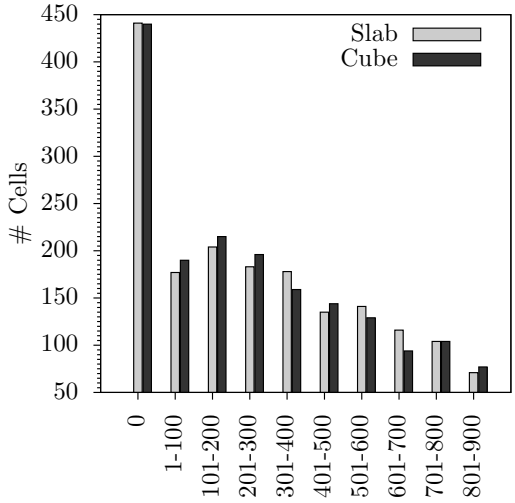

Figure S2. Distributions of cumulative conjugate durations (killing signal) for all targets in monogamous simulations ($\bar{E} = 100$, $\bar{T} = 1500$ cells). The killing signal distributions in the slab (grey bars) and in the cube (black bars) are categorized into bins, and are not significantly different ($P = 0.7$, $\chi^2 = 5.6$). Target cells are killed when their accumulated killing signal reaches 900 s (i.e., $t_D = 15$ mins).

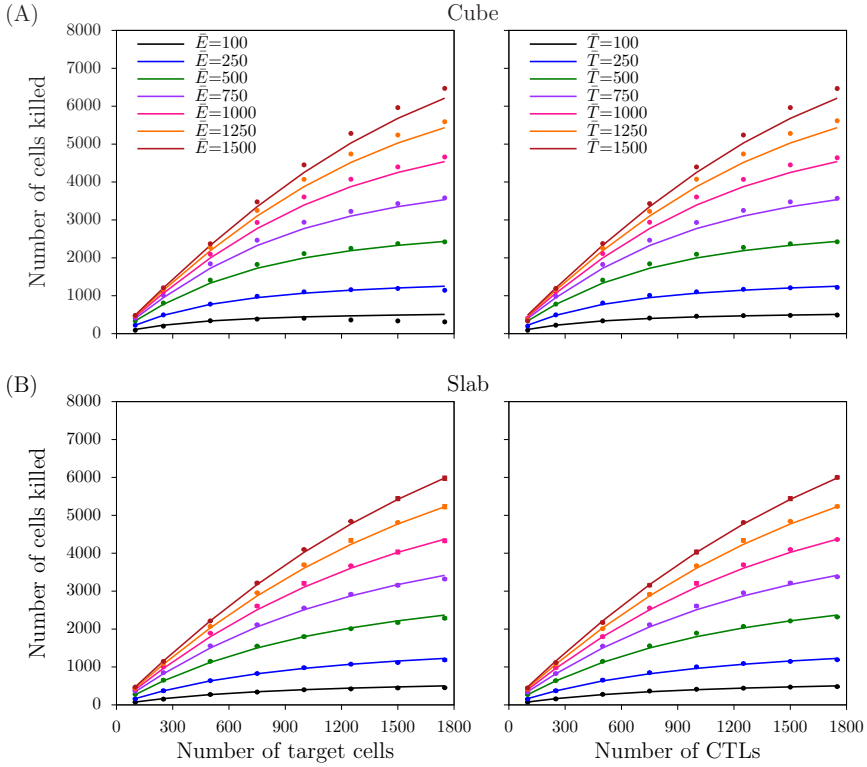

Figure S3. Number of target cells killed for monogamous killing. The total number of cells killed over 75 min of simulation as a function of target cell (left panels) and CTL (right panels) densities, obtained from simulations in a cube (A) and in a slab (B). Markers depict the measurements from the simulations, and solid lines represent the full QSSA model predictions with the best-fit parameters, slab: $k_2 = 9.8 \times 10^{-2}$ min^{-1}, $h_E = h_T = 792$ cells; cube: $k_2 = 8.3 \times 10^{-2}$ min^{-1}, $h_E = h_T = 381$ cells.

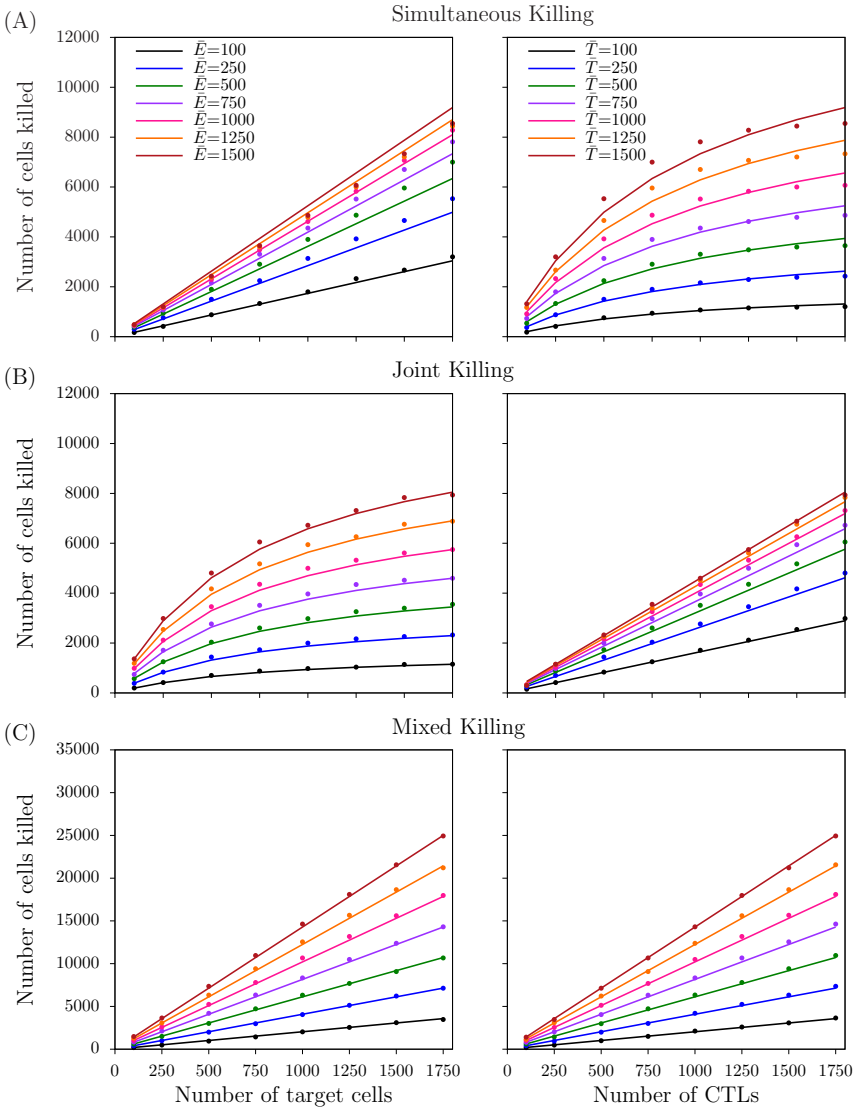

Figure S4. Number of target cells killed for non-monogamous killing regimes in slab simulations. The number of cells killed as a function of CTL and target cell densities for simultaneous (A), joint (B), and mixed (C) killing regimes. Markers indicate the mean of the total number of cells killed over 75 mins, and solid lines represent the prediction of the DS model with the best-fit parameters (Table 4.2).

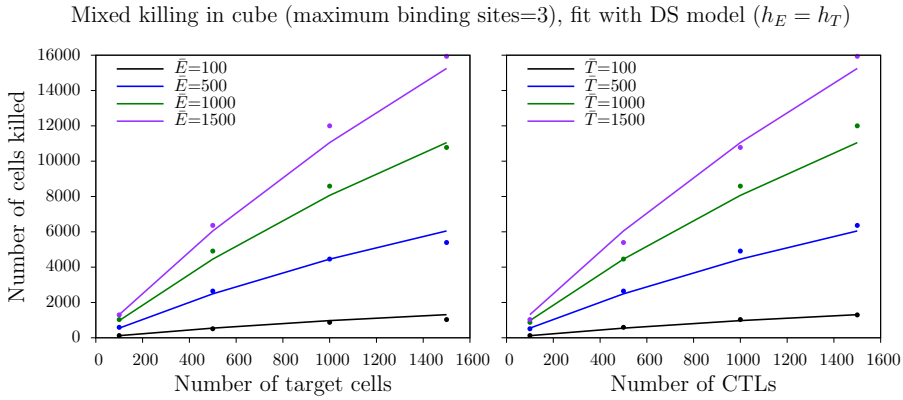

Figure S5. Number of cells killed for mixed killing (in cube) with the maximum number of binding sites restricted to three. Markers depict the measurements from the simulations, and solid lines represent the DS model predictions with the best-fit parameters: $k' = 1.73 \times 10^{-4}$ cells^{-1} min^{-1}, $h_E = h_T = 3.27 \times 10^3$ cells.

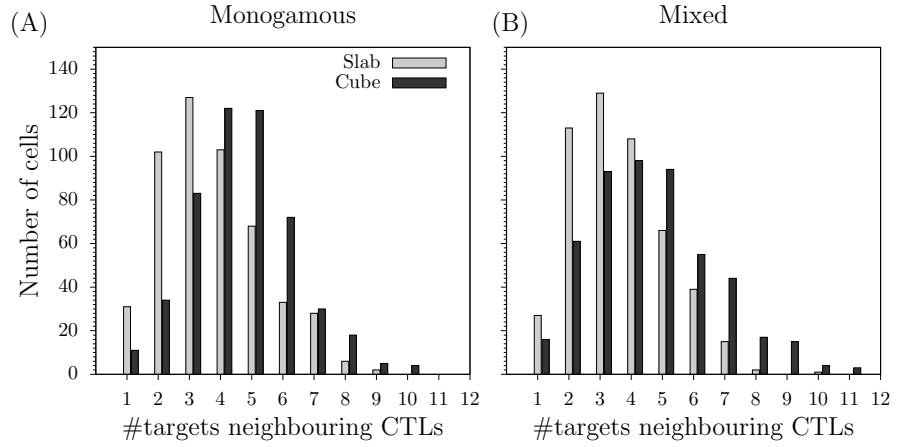

Figure S6. Distributions of CTLs with different numbers of contacting targets. The number of neighboring targets observed during monogamous killing simulation with $\bar{E} = 100$ and $\bar{T} = 2450$ in monogamous (A) and mixed (B) killing. Black bars indicate the number of neighboring targets observed in cube simulations, and gray bars in slab simulations. The difference between slab and cube simulations are significant ($P < 0.01$, $\chi^2 = 95$).

Chapter 5

Cytotoxic T Lymphocyte Mediated Killing of Melanoma in Collagen Gels

Saikrishna Gadhamsetty, Vitaly V. Ganusov, Sadna Budhu, Samuel C. Silverstein, Joost B. Beltman and Rob J. de Boer

In Preparation

Abstract

Cytotoxicity assays are widely used to quantify the rate at which cytotoxic T lymphocytes (CTLs) kill tumor and virus-infected cells. Collagen-fibrin gel assays provide a tissue-like environment for the migration of CTLs, making it an ideal system to study the cytotoxicity *in vitro*. In this study, we reanalyze published data of CTL mediated killing of B16 melanoma cells in collagen-fibrin gels. We find that the killing efficiency of a CTL decreases with an increase in the CTL density, i.e., a ten-fold increase in CTL density implies a less-than ten-fold increase in the total killing rate. Specifically, both a mechanistic saturation model and a phenomenological square root function describe the experimental data significantly better than a mass-action model. Although the phenomenological model statistically outperforms the mechanistic model, it remains puzzling why the killing rate would increase less than linearly at very low CTL densities, where killing can only be limited by the search efficiency of CTLs. We compared how well the models describe various aspects of the experiments. For example, among the two studied models, the saturation model best describes the 'critical T cell density' (at which killing and growth are balanced), whereas the square root function describes the data better than the saturation model at low CTL densities (where the killing rates are quite variable). Summarizing, we show that the killing saturates with an increase in CTL density, and the saturation model is currently the best mechanistic descriptor of the CTL-mediated killing of B16 melanoma cells in these gels.

5.1 Introduction

Cytotoxic T lymphocytes (CTLs) are crucial in providing protection to viral infections and tumors. CTL mediated killing is a multi-step process: migration of CTLs to the tumor site, recognition of tumor-associated antigen, formation of a cytotoxic synapse, and induction of apoptosis of tumor cells by the secreted effector molecules (e.g., perforin and granzymes). To reliably estimate the CTL killing efficiency *in vitro*, assays should closely recapitulate these *in vivo* processes. Recently, three-dimensional cytotoxicity assays [7, 21] have employed collagen-fibrin gels as a model system for extra-cellular matrix (ECM) *in vitro*. These collagen-fibrin gels support the migration of CTLs and provide an important platform to study the mechanisms of CTL-target interactions [21, 61].

Previous studies have shown that various mathematical models can describe the CTL-mediated killing of target cells [10, 15, 55]. Ganusov *et al.* [10] show that the CTL mediated killing in the spleen follows mass-action kinetics, whereas Graw and Regoes [15] concluded that the killing saturates with the CTL density. We recently found, using computer simulations, that the CTL mediated killing is generally expected to saturate with an increase of CTL or target cell densities [55], i.e., double saturation. Moreover, the amount of saturation depends on factors like the types of conjugates [55], the stability of conjugates (Chapter 3) and the dimensionality of the space (Chapter 4). Thus, the double saturation model helps to reconcile previously reported models.

In this study we reanalyze published data from a cytotoxicity assay of B16 melanoma cells in collagen-fibrin gels, to better understand the interactions and mechanisms of tumor cell killing by CTLs. We examined how well various models describe these data and find that a mechanistic saturation model and a phenomenological square root function describe them better than a mass-action model. Because these experiments were performed at low densities, the killing should be limited by the CTL search efficiency rather than the time required to kill B16 cells. At these low densities we already find saturation in killing efficiency, which is surprising because it cannot be explained by the competition between CTLs or by target cell limitation. We compared how well these two models describe various aspects of the experiments and found that the square root function does not predict the critical T cell concentration (at which killing balances growth) very well. However, it describes the highly variable data at low CTL densities better than the saturation model. We conclude that the saturation model is currently the best mechanistic descriptor of the OT-I killing of B16 melanoma cells in these assays.

5.2 Results

Budhu *et al.* [7] performed cytotoxicity assays in collagen-fibrin gels by co-incubating SIINFEKL-pulsed B16 melanoma cells and OT-I $CD8^+$ cells, with maximal CTL and target cell densities of 10^7 cells/mL and 10^6 cells/mL, respectively (see Methods and [7] for experimental details). After 24 hours of co-incubation, the collagen gels are lysed to

determine the number of surviving B16 cells using clonogenic assays [7, 62]. Therefore, the initial (T_0) and surviving (T_{24}) target cell numbers after 24 hour co-incubation with (or without) OT-I cells cannot be determined both from the same experiment.

Since each experiment is performed in duplicate, we use the mean initial target cell number (T_0) from the two duplicate measurements of one experiment as the general initial condition, to predict the surviving target cell number (T_{24}) in all other experimental conditions. Similarly using means from the duplicate measurements of the initial (T_0) and surviving targets after 24 h (T_{24}) in the absence of CTLs, we estimate a B16 cell proliferation rate of $g = 0.017 \pm 0.006$ h^{-1}, from an exponential growth model: $T_{24}|_{E=0} = T_0 e^{24g}$. In these experiments, the number of CTLs remained fairly unchanged over 72 h [7], and thus in all our analysis we let the total number of OT-I CTLs be constant.

5.2.1 Killing saturates in CTL densities

The B16 melanoma cells proliferate at a rate g and are killed by OT-I cells; the dynamics of B16 cells are given by

$$\frac{dT}{dt} = gT - K(E,T)T \ , \tag{5.1}$$

where g is the proliferation rate of B16 melanoma cells and $K(E,T)$ is the CTL-mediated death rate of B16 cells (hereafter referred to simply as death rate), defined as a function of the OT-I density, E, and the B16 cell density, T. The exact definition of this death rate function depends on the chosen model.

To identify the model that describes CTL mediated killing of B16 melanoma cells, we first fit the mass-action model to the surviving B16 cells data at various B16 and OT-I densities. According to the mass-action model, the death rate of B16 cells increases proportionally with the CTL density and independent of the target cell density:

$$K(E,T) = kE \ , \tag{5.2}$$

where k is the killing rate, and E is the OT-I density. Fitting Eq. 5.1 after substitution with Eq. 5.2 to the number of surviving targets after 24h of co-incubation, we find that the mass-action overestimates the survival of B16 cells at intermediate CTL densities of 10^5 and 10^6 cells/mL (Fig. 5.1; see Table 5.1 for best fit parameters).

Recently, using computer simulations we have shown that a double saturation (DS) model with two different saturation constants, describes the CTL killing of target cells for various scenarios of CTL and target cell interactions [55]. This function can be derived mechanistically when target cells are killed by single CTLs under quasi-steady state conditions, whereas for other scenarios it is a semi-mechanistic model and describes the killing well (see [55] and Chapters 2-4). According to the DS model, the death rate is given by

$$K(E,T) = \frac{kE}{1 + E/h_E + T/h_T} \ , \tag{5.3}$$

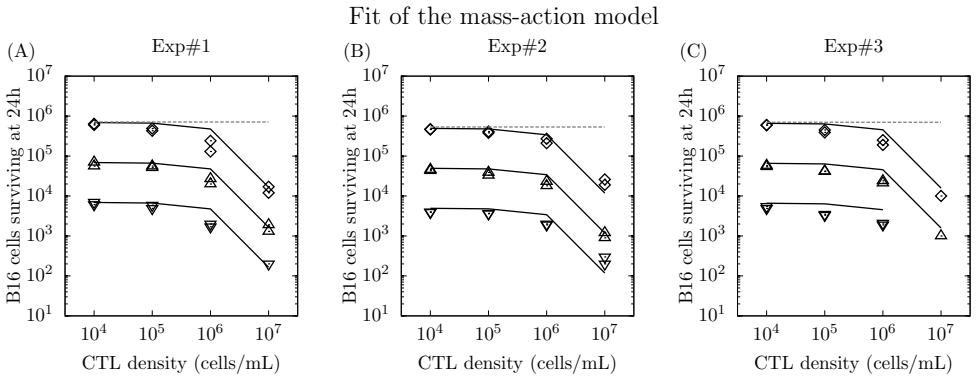

Figure 5.1. Mass-action model predictions of the number of B16 cells surviving after 24 hours of co-incubation. Each panel depicts the data from two duplicates of each experiment. The solid black lines indicate the mass-action model predictions with the best fit parameters; the dashed gray lines indicate the number of surviving B16 cells T_{24} at the end of 24 hours in the experiments without OT-I cells (shown only for $T_0 = 10^6$ cells/mL); and the markers $\triangledown$, $\triangle$, and $\diamond$, respectively, indicate the experimental observations for initial B16 densities of $T_0 = 10^4$, 10^5, and 10^6 cells/mL. The experiments aimed at initial B16 cell densities of $T_0 = 10^4$, 10^5, and 10^6; we depict the realized densities in the clonogenic assays.

where h_E and h_T are the saturation constants in CTLs and target cells respectively, and k, E, and T are the mass-action like killing rate, CTL, and target cell densities, respectively. Fitting Eq. 5.1 after substitution with Eq. 5.3 to the 24 h assay data, we find that the DS model improves the description of the data over the mass-action model ($F_{2,64} = 61.4$, $P < 10^{-10}$; see Fig. 5.2 and Table 5.1). Because the saturation constant for the target cells is much larger than the highest B16 density used, i.e., $h_T \gg 10^6$, it is reasonable to only consider saturation with an increase in CTL density in these assays. The DS model therefore reduces to the following (hereafter referred to as saturation model):

$$K(E,T) = \frac{kE}{(1 + E/h_E)} \,. \tag{5.4}$$

Fitting Eq. 5.1 after substitution with Eq. 5.4 to the 24 h assay data, we confirm that the quality of the fit remained the same as the DS model fit ($F_{1,64} = 0$, $P = 1$). Since this provides a reasonable description of the data, one could argue that the killing rate saturates at relatively high CTL densities, i.e., when $E > h_E$, when target cells tend to be encountered by more than one CTL.

5.2.2 Square root function further improves the fit quality

To study whether saturation is the best model, we also examine how well a general Hill model with a free exponent describes the data. Since there is no evidence for a saturation of killing in the target cell density, we only consider saturation in the CTL density. The

Table 5.1. Best fit parameters of the models (95% confidence intervals shown in the parentheses).

Model	k (cells^{-1} min^{-1})	h_E (cells/mL)
Mass-action	$1.55(\pm 0.11) \times 10^{-8}$	-
Saturation	$6.09(\pm 1.04) \times 10^{-8}$	3.29×10^6 $(2.50 \times 10^6, 4.09 \times 10^6)$
Square root	$3.76(\pm 0.17) \times 10^{-5}$	-

death rate according to this model is given by

$$K(E,T) = \frac{kE^n}{1 + (E/h_E)^n} \ , \tag{5.5}$$

where k is the killing rate, n is a constant, and h_E remains the saturation constant in CTLs. The Hill model is an excellent general model as all of the above models can be deduced as specific cases of the Hill model: setting $n = 1$, delivers the saturation model; letting $h_E \to \infty$ and $n = 1$, gives the mass-action model; and $h_E \to \infty$ and $n \neq 1$, gives the power model (described below). If the saturation model is the best model, we indeed should find the best-fit n to be around 1.

Interestingly, we find that the Hill model with an exponent $n \approx 0.5$ describes the data statistically better than the saturation model ($F_{1,64} = 18.39$, $P = 0$; Fig. 5.2). Both the Hill and saturation models visually describe the data with similar quality (compare the dashed and solid lines in Fig. 5.2). However, statistically the Hill model with an estimated exponent $n \approx 0.5$ outperforms the saturation model, which is due to an even better fit at intermediate OT-I densities (Fig. 5.2). The best-fit exponent is found to be $n \neq 1$, suggesting that the best-fit of the Hill model is a different solution from the saturation model. Since the saturation constant estimated by the Hill model is about 1000-fold higher than the highest CTL density employed in these assays, the Hill model can be approximated by a simple $K(E,T) = kE^n$ (with $n = 0.5$); and fitting a square root function, $K(E,T) = k\sqrt{E}$, corroborates that it is indeed indistinguishable from a Hill model ($P = 0.8$, $F_{2,64} = 0.2$; Table 5.1).

5.2.3 Which model describes all data best?

To identify which of the above models describe the data best, we compare (1) the 'critical T cell density', (2) the death rates expected from the migration properties of CTLs, and (3) the robustness of the CTL-mediated death rates to the initial conditions.

Critical T cell concentration

One easy test is to compare the critical T cell concentration (CTC), i.e., the T cell density required to exactly balance the B16 cell proliferation, predicted by all models to

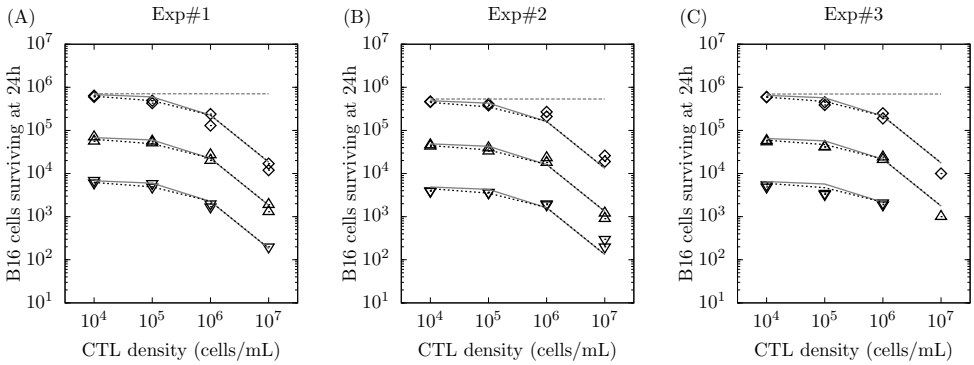

Figure 5.2. Comparison of the saturation and Hill model predictions. The number of B16 cells surviving predicted by saturation (gray solid lines) and Hill (black dashed lines) models using their respective best fit parameters. The solid gray lines indicate the saturation model predictions with the best fit parameters; the dotted black lines indicate the Hill model predictions; the dashed gray lines indicate the number of surviving B16 cells ($T_0 = 10^6$ cells/mL) at the end of 24 hours in the experiments without the OT-I cells; and the markers $\triangledown$, $\triangle$, and $\diamond$, respectively, indicate the experimental observations for initial B16 densities of $T_0 = 10^4$, 10^5, and 10^6 cells/mL.

the one determined experimentally. Budhu *et al.* [7] determined that a CTC of approximately 3.5×10^5 OT-I/mL was required to arrest the proliferation of B16 cells in their experiments. The square root function and the saturation model predict a CTC of about 1.43×10^5 and 3.23×10^5 OT-I/mL, respectively. Thus, the saturation model predicts a CTC close to that was found in the experiments.

Saturation already occurs at low CTL densities

Budhu *et al.* [7] performed experiments with maximal CTL and target cell densities of 10^7 cells/mL and 10^6 cells/mL respectively, in wells containing about 0.1 mL. Assuming CTLs and target cells as perfect spheres of radii 4μm [60] and 8.7μm [7] respectively, the cells together constitute only 0.54% of the entire volume of a well at the maximum CTL and target cell densities. This low occupancy of the gel suggests that in the experiments CTLs and target cells are typically far apart, and that the killing observed in these experiments is likely to be limited by the search efficiency of the CTLs, especially at the lowest CTL densities. Indeed, at the lowest target (4×10^3) and CTL (10^4) densities, we estimate that only about 500 target cells are killed in 24h (calculated as the difference between T_{24} in the presence and the absence of CTLs), suggesting that at most only 5% of the CTLs actually killed a target. At these target cell densities, the other CTLs apparently failed to kill a target because they were unable to find one.

To obtain an intuition on the scanning ability of CTLs in the gel, consider for simplicity a CTL moving along perfectly straight trajectories. Let the width of the path be approx-

imately equal to the sum of the radii of targets r_{tgt} and CTLs r_{ctl} (considering cells as perfect spheres; see Fig. 5.3A), and let the length of the path be $s_{ctl}\times$t (where s_{ctl} is the mean speed of CTL in μm/min and t is time in min). The scanned volume of a CTL is then approximately $s_{ctl}\times t\times\pi\times(r_{ctl}+r_{tgt})^2$ (see Fig. 5.3A). In reality, this could be somewhat lower because cells performing a persistent random walk can return on their path (although this effect is limited in a 3-dimensional space). Taking the estimated radii for CTLs and targets [60], and a speed of 11 μm/min in collagen gels [63], this leads to a scanned volume of approximately $8\times10^6\mu\text{m}^3$ (or a fraction $p=8\times10^{-6}$ of the gel) in 24h for a single CTL. The fraction of the gel scanned by all the CTLs together is given by $1-(1-p)^E\approx1-e^{-pE}$, where E is CTL density. Note that this expression takes into account overlap in CTL scan volumes. If we assume that the targets are killed by CTLs if their centers are within the scan volume, the fractions of volume scanned and cells killed are equivalent. For 10^4 CTLs/mL, the fraction of volume scanned (or target cells killed) is about 7.7% (Fig. 5.3B), which is close to the 13% of the target cells being killed at this CTL density. This confirms that at the lowest CTL and target densities most CTLs do not kill because they cannot find a target.

According to the same scanning model, 10-fold more target cells should be killed when the number of target cells is increased by 10-fold. For a 10-fold increase in target cell density, 10-fold more target cells are expected to be in the volume scanned by all the CTLs, and the number of target cells killed should increase proportionally to the increase in target cell density. Indeed, the number of cells killed in the experiments increases about 10-fold for any 10-fold increase in target cell density [7], confirming that the killing is limited by the CTL search efficiency. Our calculations suggest that at the highest target density of 4×10^5 cells/mL, almost 4×10^4 cells (10%) are killed by 10^4 CTLs. Thus, in that setting each CTL on an average kills 4 targets in 24 hours, which is feasible given that killing time estimates from *in vivo* microscopy are on the order of one hour [26, 64].

A similar calculation suggests that the predicted number of cells killed should increase from 7.7% to 55.1%, i.e., about 7-fold, when CTL densities increase from 10^4 to 10^5 CTLs/mL (Fig. 5.3B). However, the experimental data suggests an increase of only about 3-fold. Additionally, we computed the expected cells killed with different CTL migration speeds and find that the observed cells killed at 10^5 and 10^6 CTLs/mL cannot be explained with one migration speed. Summarizing, the gels are sparsely populated at the cell densities employed experimentally, and the observed 3-fold increase in cells killed for a 10-fold increase in CTL density cannot be explained by the overlap in the CTL scan volumes.

The square root function is not consistent with the 'scanning volume' predictions for any particular migration speed (compare Figs. 5.3B and C), but it is consistent with the experimental data. In contrast, the saturation model predictions are consistent with the 'scan volume' calculations, albeit at a low CTL migration speed of about 15% of published migration speeds within collagen gels (Figs. 5.3B, C). Two factors might explain why the saturation model is consistent with low migration speeds. First, migration speeds of the CTLs may be low in the collagen-fibrin gels used in these experiments, for instance because of a dependence on the collagen density [65]. Second, target cells are consid-

ered to die instantly in the scanning volume calculations, whereas the saturation model assumes a finite killing time upon conjugate formation.

Robustness to initial condition

A potential source of variability in the measurements of surviving B16 cells is due to 'unlinked' experiments, i.e., T_0 and T_{24} are measured in separate experiments. For instance, in some measurements Budhu *et al.* [7] find the same number of surviving B16 cells in the presence and absence of CTLs.

Next, we examined the robustness of the square root dependence of the killing rate to the uncertainty in the T_0 measurements. To this end, we treat each measurement of T_0 and T_{24} as independent, and compute the CTL-mediated death rates (the number of cells killed by all CTLs per day) for a given T_0 and T_{24} from all four possible combinations of T_0 and T_{24}. This approach allows us to capture the possible variation in the death rate due to the uncertainty in the measurements. At the lowest CTL density, the resulting death rates vary up to about 100-fold, and include negative death rates at two instances (Fig. 5.4, markers). The death rates computed from the means of the duplicates for T_0 and T_{24}, are within those computed from the 'shuffled' T_0 (not shown). Comparing the death rates predicted by the models with the reshuffled data, we find that in most cases the predicted death rates by the square root function fall within the experimentally measured death rates, whereas the saturation model predictions fall within the experimental measurements in almost half of the instances.

In summary, the phenomenological square root function appears to describe the CTL-mediated killing better than the saturation model at low CTL densities, whereas the saturation model predicts the CTC best and can be derived mechanistically. We conclude that the saturation model is currently the best mechanistic descriptor of the B16 melanoma cells killing in these experiments.

5.3 Discussion

Cytotoxicity assays in collagen gels provide a 3-dimensional tissue-like environment for CTLs to migrate in. Using experimental data from such collagen-gel assays, we have here identified two competing functional forms that improve the fit quality over the mass-action model (square root and saturation), and that the square root function describes the data better than the saturation model. Budhu *et al.* [7] also performed experiments of longer duration than 24 h (Fig. 5 in [7]). Since they used only two CTL densities in those experiments, they do not allow distinguishing between the models. The saturation model can be mechanistically derived (or at least provides a semi-mechanistic description) [55], whereas the square root function is phenomenological.

We performed extensive tests of comparisons of model predictions with the experiments

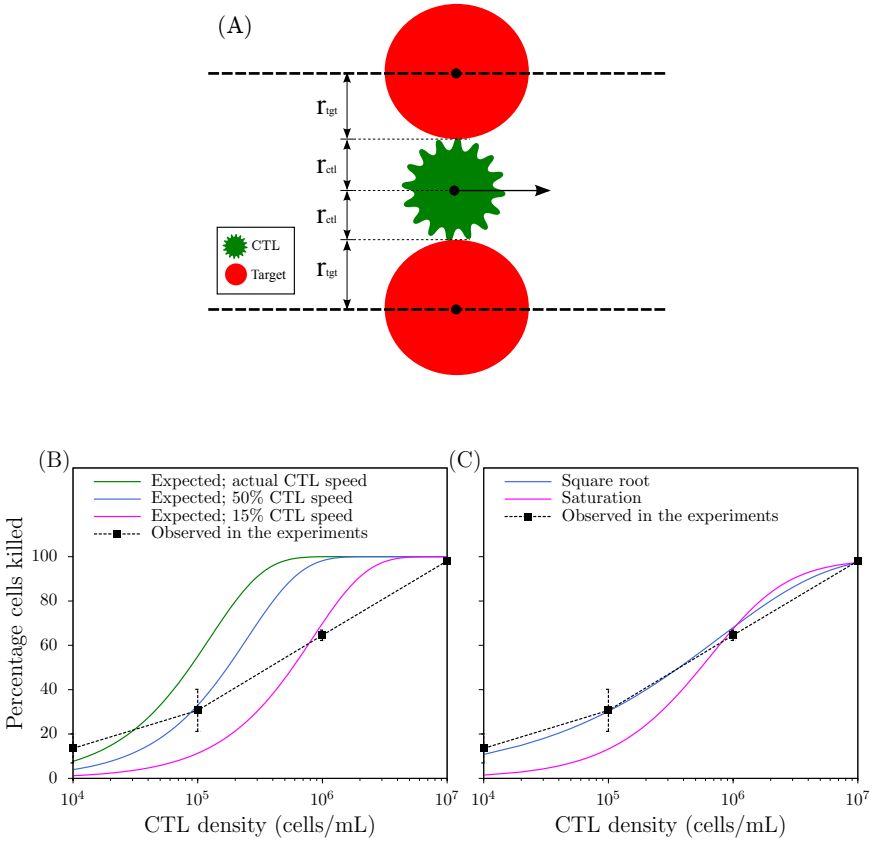

Figure 5.3. Comparison of observed fraction of cells killed and expected fraction based on scanning by CTLs. Panel (A) shows the schematic on which our calculation of the volume scanned by CTLs is based. Panel (B) depicts the percentages of cells killed, which is given by $100(1-(1-p)^E)$; E and p are the CTL density and the fraction of volume scanned by a single CTL, respectively. The solid lines indicate the expected percentages of cells killed obtained using 15% (magenta), 50% (blue), and 100% (green) of the baseline CTL speed. Panel (C) depicts the percentages of cells killed predicted by the saturation model (magenta; using the best-fit parameters in Table 5.1) and the square root function (blue). The black dashed lines in panels (B) and (C) indicate the percentage of cells killed observed in the experimental data, computed as $100\dfrac{T_{24}|_{E=0} - T_{24}|_{E>0}}{T_{24}|_{E=0}}$, and error bars indicate the standard deviations of the three independent experiments.

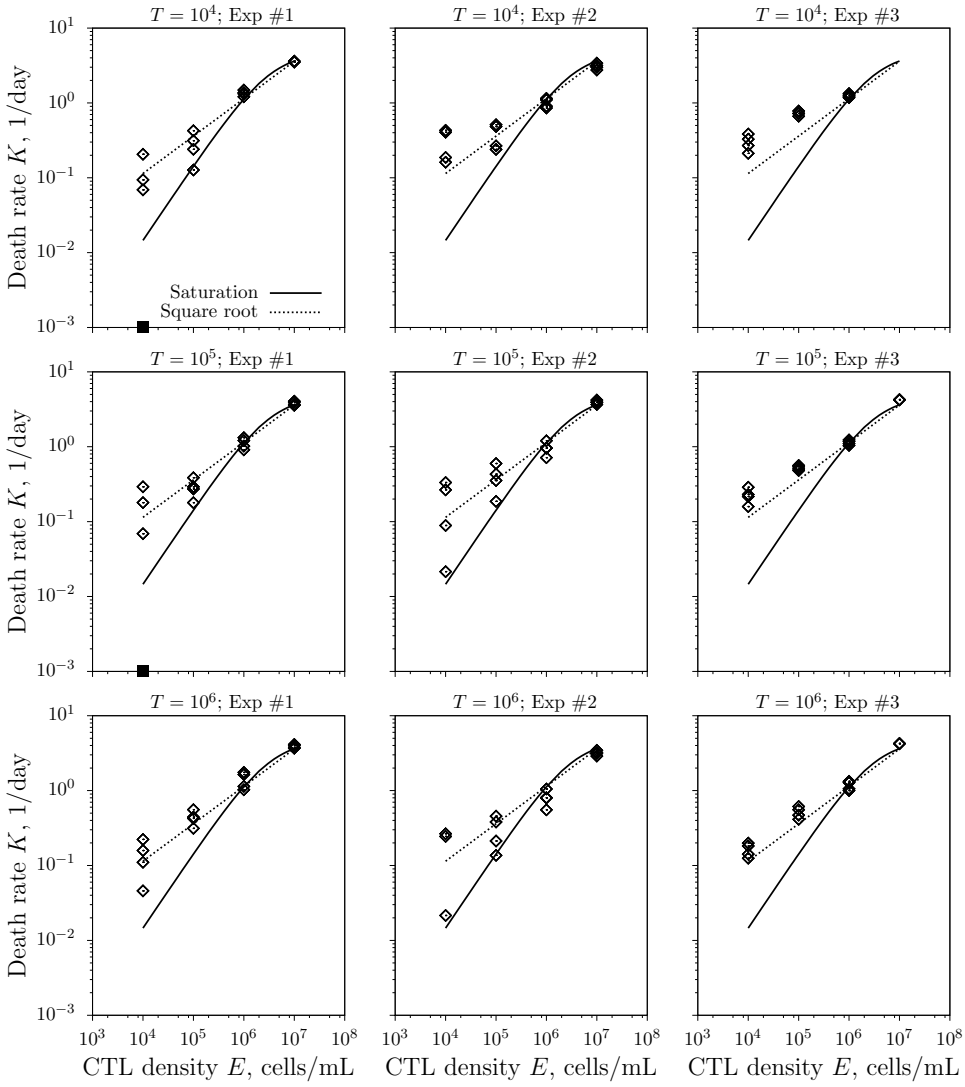

Figure 5.4. The death rates observed in the experiments and those predicted by the models. Markers indicate the death rates obtained by permutating all T_0 and T_{24} measurements. Negative killing rates are found at two instances, which are shown as square markers at the horizontal axis. The predictions of the saturation model is depicted in solid black lines, and square root function predictions in dashed black lines.

and find that the saturation model describes most experimental measurements approximately as well as the square root function, except at very low CTL densities. However, the death rates observed in these experiments were quite variable at low CTL densities. In addition, although the square root function gives a good description of the percentages of cells killed for different CTL densities, we showed that the square root dependence of CTL-mediated killing is not supported by a simple CTL scanning volume calculation. Finally, the CTC is better described by the saturation model than by the square root function. Taken together, without an explanatory mechanism for the square root function, we conclude that the saturation model currently provides the best mechanistic description of the CTL-mediated killing of B16 melanoma cells in these gels.

Since the CTL-mediated killing of B16 melanoma cells saturates at much lower CTL than target cell densities, this suggests that the 'simultaneous killing' could be the underlying mode of CTL-target interactions in these gels, i.e., CTLs binding and killing multiple melanoma cells at the same time [15, 55] (see also Chapters 2-4). However, at the end of these experiments, B16 cells predominantly existed as single cells, and only around 3 days post-incubation spheroids composed of many more cells were observed [7]. Indeed, the estimated growth rate of B16 cells suggests that about 30% of cells undergo division by the end of 24 hours. It therefore seems unlikely that such a large difference in the saturation constants in CTLs and target cells can be explained by simultaneous killing in these experiments. In our analysis of another independent data set from collagen-gel assays (similar to [21]), we also find that CTL-mediated killing saturates at lower CTL than target cell densities, but the difference in saturation constant is in that case only about 2.5-fold (see Chapter 6). However, when we simulated these assays, the CTL-mediated killing saturated at much lower target cell than CTL densities, irrespective of the mode of CTL-target cell interactions. This is in large part due to only a small fraction of CTLs arriving close to the target cells in that experimental set-up. Therefore, the mechanisms that result in more pronounced saturation in CTL densities within these experiments must be very strong (see Chapter 6 for more details).

Without additional experiments to thoroughly examine this, we can only speculate as to why CTL-mediated killing rates strongly saturate with CTL densities. While determining the general functional response, we considered that a target cell is killed when its cumulative duration in a conjugate (killing signal) reaches the threshold (i.e., the kill time). However, when synapses break frequently (i.e., CTLs form kinapses [66]), a more pronounced saturation in CTL densities may occur if target cells accumulate killing signal more efficiently than by just summing all short-lasting kinapse signals. For example, this could occur by target cells continuing to accrue killing signal between consecutive kinapses. An increase in CTL density would then likely result in a less than linear increase in the killing rate. An increase in target cell density, on the other hand, would still result in more CTL contacts (or kinapses) and hence more killing. Thus, such a mechanism could explain the much more pronounced saturation in CTL than in target cell densities.

Alternatively, the saturation (or square root) dependence in CTL densities could be related to the measurement of the surviving B16 cells. The clonogenic assays were performed following a 10-1000 fold dilution of the lysed gel depending on the initial target

cell density [7], to have a similar number of colonies irrespective of the target cell density. However, the final number of colonies varies with the OT-I density used. As a result, the density of the colonies on the plate is relatively sparse at 10^7 OT-I cells/mL compared to lower CTL densities. Thus, the likelihood of overlap of the colonies at CTL densities of 0 or 10^4 CTLs/mL is higher than at 10^7 CTLs/mL, and the measurement accuracy is also low at high OT-I densities.

Considering all the above points, we conclude that the saturation model is currently the best mechanistic descriptor of the killing in these experiments as it describes well several aspects of these experiments. More experimental data and a closer examination of the collagen-fibrin gels are needed in order to determine whether one of the aforementioned mechanisms is at play in these assays.

5.4 Methods

5.4.1 Collagen-fibrin gel assays

The details of collagen gel experiments are described in detail elsewhere [7]. Briefly, collagen-fibrin gels are prepared by incubating 5μL PBS containing 0.1U thrombin, 100μL PBS containing 1 mg/mL of human fibrinogen, 1mg/mL of rat tail collagen I, and 10% FBS for 15mins at 37°C in 95% air/5% CO_2. Cytotoxic assays are performed by incubating ovalbumin derived peptide SIINFEKL-pulsed B16 melanoma cells with or without OT-I cells together with 0.5mL OT-I growth medium. At indicated times, the gels were digested with 100μL PBS containing 2.5mg/mL collagenase type-IA for 20mins at 37°C, followed by 100μL containing 2.5mg/mL trypsin for 20mins at 37°C. The resulting solution is diluted, and the number of surviving B16 cells are analyzed by clonogenic assays [62].

In these experiments, the number of cells killed cannot be measured directly, as the gels have to be lysed for every measurement. As a surrogate measure of the number of cells killed, we calculate the difference of the surviving target numbers in the absence and presence of CTLs. This allows a comparison of the number of cells killed as observed experimentally and as predicted by the models. Note that the surrogate measure is an overestimate of the actual number of cells killed, especially at the highest CTL densities. Nevertheless, for our purpose it is a good metric because we apply the same rule of computation to the experimental data and to the model predictions.

All the models are fit to the log-transformed data of the surviving B16 melanoma cells 24h post co-incubation, which prevents skewing of the fit towards high numbers of surviving targets. To take the variation in the target cell densities between experiments into account, we use the mean number of B16 cells (computed from the experimental duplicates) in our model regression to the data. The regression analyses are performed using the function *nlinfit* in MATLAB (The Mathworks, Natick, MA).

Acknowledgements

The authors thank Sophia Scheper for help with analysis of the models, and Jorg Calis for helpful discussions. This study is supported by NWO grants 819.03.009 (to RJdB) and 864.12.013 (to JBB). This study is also supported by the "Virgo consortium," funded by the Dutch government [project number FES0908] and by the "Netherlands Genomics Initiative (NGI)" [project number 050-060-452]. The authors declared that they have no competing interests.

Chapter 6

Inferring the Interactions from Cytotoxic T Lymphocyte Mediated Killing of Tumor Cells in Collagen Gels

Saikrishna Gadhamsetty*, Cindy Dieteren*, Athanasius F.M. Marée, Peter Friedl, Joost B. Beltman and Rob J. de Boer

In Preparation

---

* These authors have equally contributed to this work. CD performed the cytotoxicity assay experiments and responsible for the data; SG analyzed the data and wrote the chapter.

Abstract

Cytotoxic T lymphocytes (CTLs) kill virus-infected and tumor cells with high specificity and are critical for protection against pathogens and tumors. The collagen gel assay provides a tissue-like environment for the migration of CTLs, which makes it an ideal system to study cytotoxicity *in vitro*. In this study, we determine the rate of CTL-mediated killing of tumor cells in such gels at various CTL and target cell densities, and find that a standard double saturation model with different saturation constants for target cell and CTL densities describes the data well. The CTL-mediated killing rate (number of target cells killed per unit time) saturates more rapidly with an increase in the CTL density than with an increase in target cell density. Previous results suggest that this more pronounced saturation in CTL density can be due to a CTL killing multiple target cells simultaneously. To test whether the more pronounced saturation of killing with CTL density is indeed due to CTLs simultaneously killing multiple target cells, we performed cellular Potts model simulations specifically tailored to these experiments, and in contrast to the experiments we always found that CTL-mediated killing rate always saturates strongly with increases in target cell densities in the model—irrespective of the mode of CTL-target cell interactions. We conclude that the mode of interaction cannot be inferred from the saturation constants alone, and discuss several other potential mechanisms that may explain this discrepancy.

6.1 Introduction

Cytotoxic T lymphocytes (CTLs) are critical to contain and eliminate viral infections and tumors. Adoptive transfer of *in vitro* activated CTLs have been shown to induce tumor regression successfully in mice [2, 38, 39] and humans [40]. Cytotoxicity assays in collagen gels provide a tissue-like 3-dimensional environment supporting T cell migration [21], making them suitable systems to determine CTL mediated killing rates *in vitro* and how they vary with CTL and target cell densities. Knowledge of the CTL killing efficiency is important to estimate the critical CTL density that can induce sterilizing immunity to tumors and viral infections [7, 9].

In this study, we perform recently developed cytotoxicity assays in collagen gels [21] starting with different effector, $\bar{E}$, and target cell, $\bar{T}$, densities to determine how the CTL-mediated killing rate (total number of cells killed per unit time) changes as a function of $\bar{E}$ and $\bar{T}$. We find that a standard double saturation (DS) model [55] with different saturation constants for target cell and CTL densities describes the experimental data well. The CTL-mediated killing rate saturates more strongly with an increase in CTL density than in target cell density. Previous simulation results demonstrated that the extent of saturation in CTLs and target cells depends on whether a CTL can kill multiple target cells, whether a target cell can be killed by multiple CTLs at the same time [55], and on how the duration of target cell death varies with number of CTLs and targets in a conjugate [15, 55]. The more pronounced saturation in CTLs in the current experiments

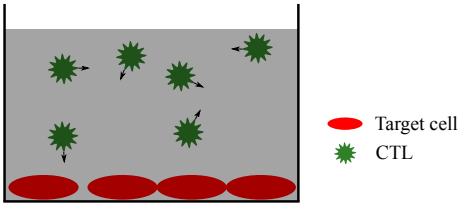

Figure 6.1. Schematic of the collagen gel assay setup. A monolayer of target cells (red) was overlaid with collagen gel containing CTLs (green). The region shaded with grey represents the collagen gel matrix, and the arrows represent CTL migration.

suggests that a CTL can induce death of multiple target cells simultaneously [55]. However, in these gels the restricted localization of target cells to the bottom mono-layer and the free migration of CTLs in the gel might confound the inference of the underlying CTL-target cell interactions from the relative extent of saturation of killing in CTL and target cell densities.

To test whether we can distinguish between different modes of CTL-target cell interactions, we performed cellular Potts model simulations that mimic these cytotoxicity assays. For parameters that are largely consistent with the observed migration properties and our collagen gel experiments in this study, we always found that CTL-mediated killing saturates strongly in target cell densities. This is in strong contrast with the saturation constants found in the analysis of the experimental data. Further analysis suggests that the fact that only a fraction of total CTLs is present in the target cell mono-layer and that the killing rate is not at steady state, can together explain why we find stronger saturation with increases in target cell densities in these simulations. Thus, spatial effects and non-equilibrium dynamics can confound the inference of underlying CTL-target cell interactions in killing assays. Finally, our results imply that to explain the observed strong saturation of killing efficiency in CTL densities additional mechanisms must be at play.

6.2 Results

Cytotoxicity assays were performed in collagen gels, in which target cells (BOK tumor cells pulsed with ovalbumin-derived SIINFEKL peptide) are adherent to the bottom of the well (Fig. 6.1). Such 'monolayer' gels for instance mimic the process of localization of CTLs to the site of a tumor or a viral infection in peripheral tissues like the skin. After 24 hours of incubation, collagen-fibrin gels containing SIINFEKL-specific OT-I CTLs are laid on top of them (see Methods and [21] for more details). At 30 hours post-coincubation, propidium iodide is added and the surviving target cells are determined by imaging a section (about 10%) of the target cell mono-layer using bright field imaging. These experiments are repeated with different starting CTL ($\bar{E}$) and target cell ($\bar{T}$) densities.

6.2.1 Mass-action and Michaelis-Menten models

The BOK cells proliferate at a rate $g = 0.0433$/hour and are killed by CTLs; the dynamics of B16 cells are given by

$$\frac{dT}{dt} = gT - K(E,T)T \ , \tag{6.1}$$

where $K(E,T)$ is the CTL-mediated death rate of BOK cells, defined as a function of the OT-I density, E, and the B16 cell density, T. We consider that the CTL density remains constant over the duration of the experiment.

To determine the variation of the CTL mediated killing rate of target cells with CTL and target cell densities, we fit the mass-action model (see below) and the double saturation (DS) model to the data. According to the mass-action model, the CTL-mediated death rate of target cells (hereafter referred to simply as death rate) increases proportionally with the CTL density and independent of the target cell density:

$$K(E,T) = kE \ , \tag{6.2}$$

where k is the killing rate, and E is the OT-I density. On the other hand, the death rate according to the DS model is given by

$$K(E,T) = \frac{kE}{1 + E/h_E + T/h_T} \ , \tag{6.3}$$

where h_E and h_T are the saturation constants in CTLs and target cells respectively, and k, E, and T are the mass-action like killing rate, CTL, and target cell densities, respectively.

We find that the DS model describes the CTL mediated killing better than the mass-action model (Fig. 6.2; see Table 6.1 for best fit parameters). The predictions of the mass-action model with the best fit parameters deviate from the data at several instances. For the DS model, we find that the saturation of killing of target cells is more pronounced with an increase in CTL than in target cell density (i.e., $h_E = 55.5$ cells and $h_T = 100.6$ cells). A possible explanation for this pronounced saturation in CTL density is the occurrence of simultaneous killing in these gels, i.e., when CTLs kill multiple target cells simultaneously, but a target cell can only be killed by a single CTL [15, 55].

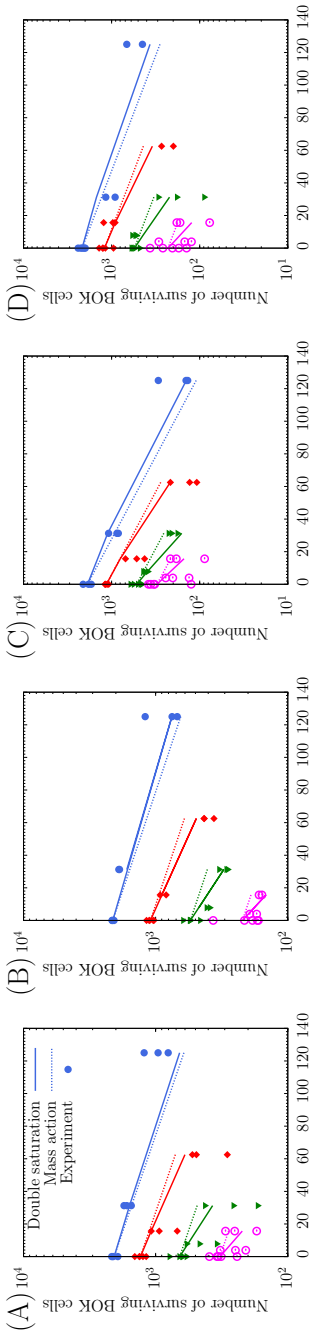

Figure 6.2. Comparison of the DS model (solid lines) and the mass action model (dashed lines) predictions and the experimental data of surviving BOK cells found at the end of 30 hours in the gels at various target cell and CTL densities. Note that the mass-action model predictions (dashed lines) run parallel to each other in every panel. Panels show the data from experiments (symbols) performed on different days; different colors represent the number of surviving cells found with different initial target cell numbers.

Model	k (cells^{-1} hour^{-1})	h_E	h_T
Mass-action	$2.2(\pm 0.14) \times 10^{-4}$	-	-
Double saturation model	$3.4(\pm 1.44) \times 10^{-3}$	$55.5(\pm 25)$	$100.6(\pm 54)$

Table 6.1. Best fit parameters of the models that describe the experimental data (95% confidence intervals shown in parentheses).

A factor not taken into account in the model is that CTLs are initially absent from the bottom layer where the target cells reside, and that they gradually accumulate in the bottom mono-layer as the experiment progresses. Indeed, only a fraction of the CTLs is present in the bottom 'layer' of the gel at the end of 30 h (see supplementary videos in [21]), but the precise number of CTLs in the bottom layer was unknown in these experiments. If only few CTLs are present in the bottom layer, it is unlikely that multiple CTLs are in conjugate with a single target cell. Thus, it might be difficult to distinguish simultaneous killing from mixed killing, in which conjugates of any number of target cells and CTLs can occur. Other factors that could have an impact on the saturation constants estimated with the DS model are the occurrence of non-equilibrium dynamics and of cluster formation amongst the targets in the mono-layer.

6.3 Simulations to verify CTL-target interactions

To examine whether we can distinguish between different scenarios in this experimental setup, we perform cellular Potts model simulations tailored to these experiments. In addition to the simultaneous killing regime, we consider three other interaction scenarios: monogamous, joint, and mixed, as defined in Chapters 2-4 (see Fig. 1 in Chapter 2). In monogamous and joint killing regimes CTLs can only kill a single target cell at a time. Moreover, targets can only be killed by a single CTL at a time in monogamous killing, whereas they can be jointly killed by multiple CTLs in the joint killing regime. For mixed killing, there are no restrictions on the number of cells in conjugates, and all interactions contribute to killing. CTLs can induce death of all the targets in a conjugate equally well irrespective of the number of target cells in a conjugate. Target cells accumulate the duration in a conjugate (hereafter referred to as 'killing signal') independently from all the CTLs in a conjugate. A target cell is killed when the cumulative conjugate duration reaches $t_D = 8.3$ hours, and the killed target vanishes in a few seconds.

We consider a 2-dimensional field filled with clusters of targets, representing the target cell mono-layer at the bottom surface of the gel (see Fig. 6.3). Unless otherwise mentioned, we introduce target cells with normally-distributed cluster sizes (with a mean of 5 cells and standard deviation of 5×10^{-3}). To mimic CTL entry from the gel into the target cell mono-layer, we introduce CTLs into the bottom layer at a constant probability of 10^{-5} per CTL in the gel (at every simulation time step). The CTLs in the mono-layer are removed at a constant probability of 10^{-4} per CTL per time step, which mimics CTL

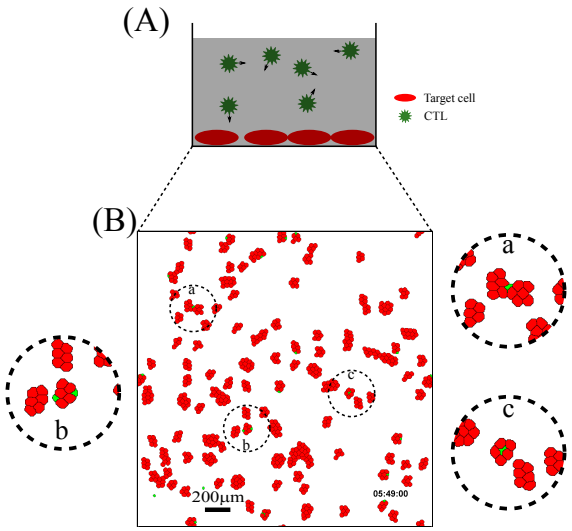

Figure 6.3. Schematic of the simulation field. Panel (A) shows schematic of the collagen gel assay, and panel (B) shows the simulation field of the mono layer. Insets a, b, and c highlight the some of the instances in which single CTLs killing multiple targets. In both the panels, target cells are depicted in red and CTLs in green. Scale bar represents 200μm.

migration into the bulk of the gel. Attempting to update all the lattice sites constitutes one time step in the simulation, which corresponds to 7.5 s in real-time. Consistent with the assays, each simulation corresponds to an experiment duration of 30 hours. In the mono-layer of the gel, CTLs perform a persistent random walk according to a set of well-defined rules (see Chapter 2 for the details of the migration algorithm).

In Chapters 2-4, we showed that in a high cell density environment (with a network of fibroblastic reticular cells) these migration rules for the CTLs result in a directional persistence over short time scales of minutes, but no directional preference over long time scales. In the current low cellular density simulations, the same set of rules also results in a persistent random walk—even without the reticular network. For the default parameters (see Methods), CTLs migrated at about 2-3μm/min. The motility coefficient and persistence of CTLs are 19.6μm^2/min and 6.7 min, respectively, as estimated by fitting Fuerth's equation [45, 51] to the mean square displacement.

Although these migration properties are on the low side of the experimental observations, all the simulation parameters (including those related to migration speeds, killing time, and the probability of CTL entry into the mono-layer) are chosen such that we find about 10-20% surviving target cells at the end of the simulations for the lowest target cell numbers, i.e., similar as in the experiments. Upon CTL-target cell encounter, we upregulate the adhesion between the cells to allow the formation of synapses, but as shown in the movies, CTLs in clusters continue to migrate and form many short lived 'kinapses' [66] with several targets in their cluster. The CTLs were programmed to have

a preference to adhere to the target cells (see Methods), and consequently they tend to stay in a cluster until all the target cells in the cluster are killed.

The maximum numbers of CTLs and target cells employed in these simulations are chosen such that they are comparable to those used in the collagen gel experiments, i.e., we model the part of the gel that was imaged to count surviving target cells. Like in the experiments we measure the number of surviving target cells at the end of simulation, and perform such simulations for different initial target and CTL densities and for several modes of CTL-target cell interactions. Consistent with the experiments, the total number of CTLs in the gel, E, remains constant in the simulation. However, note that there are no CTLs in the bottom layer at the onset of simulation or experiment, and that they slowly accumulate over time (see Movie S1 for a representative simulation of simultaneous killing with $\bar{E} = \bar{T} = 720$ cells; located at `http://tbb.bio.uu.nl/sai/movies/chapter6/`). Since we have no measurements on the speed of CTL entry in the experiments, we (1) fit the data with the total CTL density in the gel, and (2) we chose the simulation parameters such that 80-90% of the target cells have been killed at the lowest target and the highest CTL densities. For simplicity, we consider that target cells do not proliferate ($g = 0$), and we write for the dynamics of surviving target cells:

$$\frac{dT}{dt} = -\frac{kET}{1 + E/h_E + T/h_T} , \tag{6.4}$$

where T and E represent the total numbers of targets and CTLs in the gel.

6.3.1 Killing saturates at much lower target cell densities in all the scenarios

Fitting the DS model of Eq. 6.4 to the number of surviving target cells at the end of the simulations, we find that it provides an excellent description of the simulation data for all killing regimes (Fig. 6.4). For all the four killing regimes the killing rate (i.e., number of target cells killed per unit time) saturates both with CTL and target cell densities (and the mass-action model consistently overestimates the surviving target cells; not shown). However, the killing rate in these simulations saturates at low target cell densities and high CTL densities ($h_T \ll h_E$; see Table 6.2 for parameter estimates). This is surprising in two regards. First, the asymmetry in the saturation constants is not expected for the monogamous and mixed regimes, and is expected to be reversed ($h_T > h_E$) in the simultaneous regime [55]. Second, in the experimental data $h_T \approx 100 > h_E \approx 55$, whereas in the simulations (only in the mixed and simultaneous) h_T is similar whereas h_E is about 10–50 fold larger than h_T.

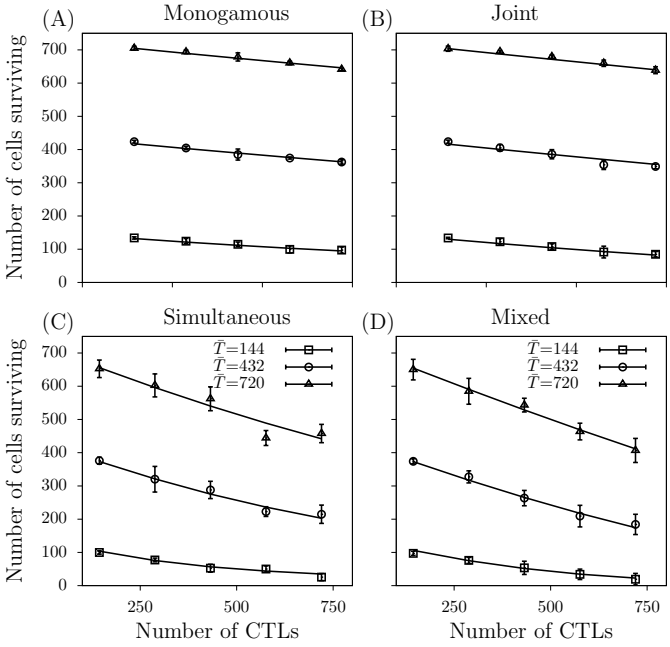

Figure 6.4. Comparison between the DS model predictions of the surviving target cells and that observed in the simulations: monogamous (A), joint (B), simultaneous (C), and mixed (D) regimes. Markers indicate the average over 4 independent runs with starting target cell numbers of $\bar{T} = 144$ (□), 432 (○), and 720 (△); error bars indicate the standard deviations over the runs; and the solid lines indicate the predictions obtained by fitting the DS model with the best fit parameters (Table 6.2).

Table 6.2. Best fit parameters of the double saturation (DS) model for different simulated killing regimes.

Regime	k (cells^{-1} hour^{-1})	h_E (cells)	h_T (cells)	Ratio, h_E/h_T
Monogamous	7.89×10^{-5}	1073	48	22
Joint	1.51×10^{-4}	1233	26	47
Simultaneous	2.08×10^{-4}	579	82	7
Mixed	1.97×10^{-4}	1194	90	13

6.4 What explains the pronounced saturation of killing in target cell densities in the simulations?

Since it is puzzling that we find hardly any saturation of killing in CTL densities for all modes of CTL-target cell interactions, we examine whether the differences between our earlier simulations [55] —that were idealized to derive the functional response— and the current simulations —that were designed to mimic the experiments— could explain the weak saturation in CTL densities.

6.4.1 Only a fraction of CTLs reaches the target cell mono-layer

First, we realized that in the simulations only a fraction of the CTLs reaches the bottom target cell mono-layer, and that the saturation constant, h_E, is estimated for the total number of CTLs in the gel (both in the data and the simulations). If only a fraction α of CTLs is present, we require a higher CTL density in the gel to achieve the maximum killing rate—i.e, in the monogamous regime h_E is expected to be larger than h_T. This intuitive reasoning is confirmed by an analytical derivation using the Michaelis-Menten kinetics analogy [16, 55] (see Methods): in the monogamous regime we obtain $h_E = h_T/\alpha$.

At the end of our simulations, we find that a fraction of about 0.13 of the CTLs are present in the bottom layer, which would average to about $\alpha \simeq 0.065$ over the entire simulation. Since this $\alpha \simeq 0.065$ is in agreement with the ratios $h_E/h_T \simeq 1/\alpha$ observed in the simultaneous and mixed regimes (Table 6.2), we think that the unexpected large asymmetry, $h_E \gg h_T$, in the saturation constants is largely due to the fact that most CTLs in the simulations reside in the gel and never arrive in the bottom layer. The reversed asymmetry, $h_E > h_T$, in the experimental data therefore suggests (1) that the interactions are even more "simultaneous" than they are in our simulations, and/or (2) that a much larger fraction of the CTLs arrives at the bottom layer of the gel.

6.4.2 Transients partly explain the saturation in target cell densities

In our previous functional response simulations [55] (and Chapters 3-4), we allowed for a "burn-in" time to allow the distribution of conjugate times to approach steady state before we started quantifying the killing. In the current simulations, in which we aim to mimic the experimental simulations, we start with zero conjugates, and killing cannot occur at times earlier than the killing time t_D. Thus, the distribution of times that target cells have spent in conjugates (hereafter referred to as 'killing signal distribution') is initially far from the steady state uniform distribution. We here study how this initial transient affects the symmetry of the saturation constants.

Consider the initial phase with all targets in the bottom layer and CTLs slowly arriving

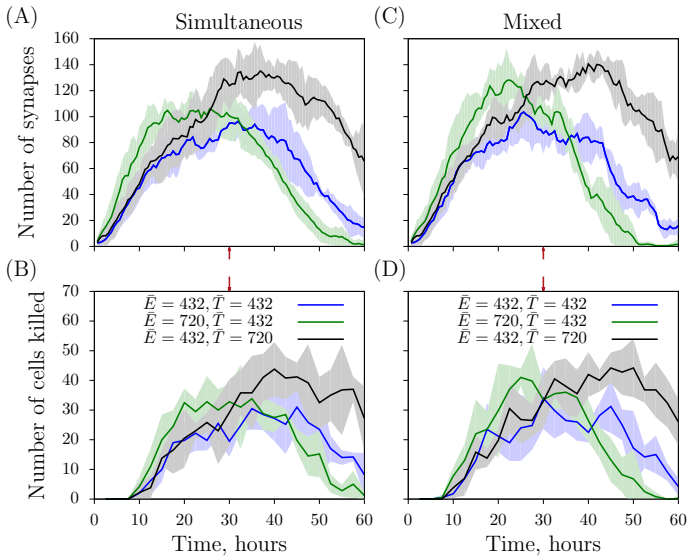

Figure 6.5. The total number of synapses with target cells (A,C) and the number of cells killed (B,D) over 150 min intervals during simulations for the simultaneous (A-B) and mixed (C-D) regimes. Solid lines indicate the average from 4 independent simulations, and the shaded regions indicate standard deviations over these 4 observations. $\bar{E}$ and $\bar{T}$ represent the starting CTL and target cell numbers in the simulations, respectively. Red arrows depict the end of the duration of the experiment.

from the gel. If the arrival time of the CTLs is the limiting factor, the rate at which conjugates are formed is expected to be proportional to the rate at which the CTLs arrive. Moreover, when these CTLs form conjugates with target cells in a particular cluster, target cells in other clusters will not be affected by them, until the target cells in the first cluster die. Thus, increasing the target cell density will only moderately increase the killing rate, whereas the killing rate should initially be more or less proportional to the CTL density in the bottom layer of the gel. Recording the conjugates and the killing rate over time, we indeed find that the number of synapses and number of cells killed during intervals of 150 mins increases more when we increase the CTL density by 67% compared to an increase of the target cell density by the same amount (Fig. 6.5). Further, as expected the first target cells are killed around the kill time t_D. Since at early times the target cell density affects the killing rate less strongly than the CTL density, this helps to explain why we find $h_T < h_E$ when we fit the DS function to the *in silico* data. Moreover, we performed additional simulations in which all the CTLs are introduced in the bottom layer from the beginning of the simulation, and again find that the killing rate saturates at higher CTL than target cell densities (not shown). Therefore, the impact of the transient on the saturation coefficients is independent of the CTL entry into the bottom layer. Note that similar initial transients should play a role in the experimental data, where we nevertheless find the opposite asymmetry.

Finally, since the conjugates dissociate fairly frequently in the data and the simulations (i.e., CTLs form kinapses rather than synapses), an increase in the target cell density is expected to increases the rate at which CTLs move from one target cell to the next one. This "dilutes" the killing signal that target cells receive from CTLs, and the higher the target cell density, the higher this dilution effect. Basically, an increase in the target cell density decreases the probability that a CTL returns to the same targets to finish off their killing. During the initial transient, when targets are slowly accumulating killing signal, higher target cell densities therefore increase the average time required to kill the target cells. On the other hand, an increase in the CTL density increases the probability target cells are visited by CTLs, and increases the killing rate. This would again be reflected in an asymmetry of the saturation constants, i.e., $h_E > h_T$, when the data is fitted with the DS function, and might partly explain why we observe differences (observed in Fig. 6.5) in killing rates and number of conjugates formed for a similar increase in CTL or target cell numbers. Since the synapses formed in the experimental data also tend to be short-lived, similar dilution effects could play a role there. Note that between consecutive short-lasting kinapses in the simulations target cells perfectly retain the killing signal they accumulated over time.

6.5 Discussion

We have shown that the double saturation model [55] suffices to describe data from 3-dimensional cytotoxicity experiments in collagen gels, and that the data suggest a more pronounced saturation in CTLs than in targets (i.e., $h_E < h_T$). Other *in vitro* data were also well described by the DS model, and a similar early saturation in CTL densities was found in Chapter 5, and in assays in which bacteria were killed by neutrophils [54]. Previous results suggested that the saturation in CTL densities found in the current data is expected when CTLs kill target cells simultaneously [15, 33, 55]. However, in our simulation model of the 3D collagen experiments we found a much weaker saturation in CTL than in target cell densities (i.e., $h_E > h_T$), with a similar h_T between experiments and simulations (in the simultaneous and mixed killing regimes). We have identified several confounding factors that can account for this opposite saturation. An important bias is the simple fact that only a fraction of the CTLs is expected to be present in the bottom layer of the gel, whereas the transient to the steady state killing signal distribution is not a bias of these collagen gels, but equally applicable to all cytotoxicity assays.

In our previous functional response simulations the target cell density was kept constant, whereas here they decline with time. At late times the target cell density will therefore become the limiting factor, and this will occur earlier when CTL densities are high. This is confirmed by time courses of the conjugates and the number of cells killed in Fig. 6.5, where in the second half of the simulations the number of conjugates drops markedly because most target cells have died. The fact that the killing drops early at the highest CTL density shows that the saturation constants estimated for this type of data critically depend on the time point at which the number of surviving cells is measured. In both the current experiments and the simulations, we have tried to prevent this by sampling the

data at a time where 10-20% of the target cells survive for the highest CTL and lowest target cells densities used.

The fact that we spotted several mechanisms towards an opposite asymmetry of the saturation constants shows that we do not yet fully understand the cellular interactions in the data. In fact, the unknown mechanisms underlying the saturation in CTL densities in the data have to be strong, as they must exceed the opposite effect of the biases. At this point we can only speculate about the true mechanisms. First, it could be that in reality far more CTLs arrive in the bottom layer. This would decrease the degree of asymmetry predicted by the simulations, but would require even longer killing times than the $t_D = 8.3$ h that we are using now to remain in agreement with the observed survival of targets. Although it was consistently found that the kill time of tumor cells is much longer than that to kill virus-infected cells [19, 26, 37, 67], more than 8.3 h seems unlikely. Second, it could be that the short-lived kinapses kill target cells more efficiently than we are currently assuming. In the simulations the total amount of time spent in kinapses sums up to the total killing time t_D before a target cell dies, and it could be that during the intermittent phases between kinapses target cells continue to accrue death signals, for example because of local production and excretion of IFN-γ by CTLs. This is expected to lead to saturation in CTLs, because having several migrating CTLs in the same cluster and frequently hitting the same target cells, would then hardly increase the killing rate compared to single CTLs in a cluster. Similarly, it could be that the accumulation of killing signal is not strictly additive, and that additional CTLs hitting the same target cell hardly increase its death rate. This would also lead to saturation in CTL densities, as was found in the earlier simulations by Graw Regoes [15]. Consistent with this hypothesis, in experiments where CTLs and targets were allowed to form conjugates before plating them out [18], the death rate of a target cell increased with the number of CTLs conjugated with that target, but only when conjugates involved maximally three CTLs. Having more than three CTLs conjugated with the same target failed to increase the death rate [18].

As yet, we do not known whether a combination of these speculative mechanisms would suffice to explain the saturation observed in the data, given the biases that we identified. In future studies the number of CTLs in the bottom layer of the gel should be recorded, and it would be interesting —but challenging— to estimate the death rates of cells in clusters harboring different numbers of CTL. Finally, it would be interesting to perform more studies varying target and CTL densities *in vivo*, as it has been suggested that killing *in vivo* does not saturate and obeys mass action kinetics [10], whereas several *in vitro* data sets consistently find saturation in CTL densities (see Chapter 5 and [18, 54]).

6.6 Methods

6.6.1 Cytotoxicity assay in collagen gel

The cytotoxicity assay in collagen gels is described in detail elsewhere [21]. Briefly, the cytotoxicity experiments consist of target cells (SIINFEKL-pulsed BOK cells) adherent to the bottom of a well, and CTLs (OT-I T cells) in a polymerized collagen gel laid on top of the target cells at the beginning of the experiment. At the end of 30 hours, propidium iodide (PI) is added to the well, and the number of surviving cells within a part of the well ($\approx$835μm$\times$636μm^2; corresponding to $\approx$10% of the well) is counted. Experiments are performed with different starting CTL and target cell numbers to estimate the killing efficiency as a function of CTL and target cell densities.

BOK cells proliferate at a rate, g=0.0433 hour^{-1} (not shown). Because about 10% of the well is imaged to count the surviving target cells, we took the initial number of target cells T_0 and CTLs to be 10% of the total cells used. We assume that the CTL numbers remain constant, i.e., no CTL proliferation or death. Since the CTL activity can vary across cultures, we use a different killing rate constant k for experiments performed on each day.

6.6.2 Mathematical models

In a mass-action model, killing of a target cell is instantaneous upon contact with a CTL, and the rate of killing of target cells is proportional to the densities of target cells, T, and CTLs, E, present in the gel. Therefore, the dynamics of target cells is then given by

$$\frac{dT}{dt} = gT - kET \ , \tag{6.5}$$

where g is the proliferation rate of the target cells, and k is the CTL mediated killing rate of target cells.

Recently, using computer simulations we have shown that a double saturation (DS) model with two different saturation constants, describes the CTL killing of target cells for various scenarios of CTL and target cell interactions [55]. This function can be derived mechanistically when target cells are killed by single CTLs under quasi-steady state conditions, whereas for other scenarios it is a semi-mechanistic model and describes the killing well (see [55] and Chapters 2-4). The dynamics of surviving target cells is then given by

$$\frac{dT}{dt} = gT - \frac{kET}{1 + E/h_E + T/h_T} \ , \tag{6.6}$$

where h_E and h_T are the saturation constants in CTLs and target cells respectively, and k, E, and T are the mass-action like killing rate, CTL, and target cell densities, respectively. In the cellular Potts model simulations of the experiments (see below), we consider that the target cells do not proliferate, i.e., $g = 0$.

6.6.3 CTL-mediated killing when only a fraction present in the target cell mono-layer

Using the Michaelis-Menten kinetics analogy [16, 55], we here derive how the saturation constants change if only a fraction, α, of the CTLs is present in the bottom mono-layer. Let $\bar{T}$ and $\bar{E}$ be the total number of targets and CTL in the gel. For simplicity, we average over time and assume that a fixed fraction, α, is present within the bottom layer. The effective number of CTLs in the bottom layer is then given by $\alpha\bar{E}$. For monogamous killing, the 'free' CTLs bind 'free' target cells (i.e., those that are not bound in a conjugate) at a rate k_1 to lead to conjugate, $[ET]$, which subsequently can either dissociate at a rate k_{-1} to result in a 'free' CTL and a 'free' target, or lead to the death of the target cell at a rate k_2:

$$E + T \underset{k_{-1}}{\overset{k_1}{\rightleftharpoons}} [ET] \xrightarrow{k_2} E + T^* \,, \tag{6.7}$$

where E, T, ET, and T^* represent free cognate CTLs, free target cells, CTL-target conjugates, and dead targets, in the bottom layer, respectively. The corresponding dynamics of conjugates and the killed target cells are given by

$$\frac{dC}{dt} = k_1 ET - (k_2 + k_{-1})C \,, \quad \frac{dT^*}{dt} = k_2 C \,, \tag{6.8}$$

where C and T^* represent, respectively, the number of conjugates, $[ET]$, and the number of cells killed. The conservation equations for effectors and targets are given by $\alpha\bar{E} = E + C$ and $\bar{T} = T + C$, where $\alpha\bar{E}$ and $\bar{T}$ are the total CTL and target cell numbers in the mono-layer. Following Borghans *et al.* [16], we perform the "total quasi-steady state" approximation and rewrite the dynamics of conjugates in terms of total cell numbers, i.e.,

$$C^2 - (h + \alpha\bar{E} + \bar{T})C + \alpha\bar{E}\bar{T} = 0, \tag{6.9}$$

where $h = (k_2 + k_{-1})/k_1$ is the Michaelis-Menten constant. Solving this quadratic equation by a Padé approximation we obtain the conventional

$$C = \frac{\alpha\bar{E}\bar{T}}{h + \alpha\bar{E} + \bar{T}} \,. \tag{6.10}$$

Thus, the dynamics of killed target cells is given by

$$\frac{dT^*}{dt} = \frac{k\bar{E}\bar{T}}{1 + \bar{E}/h_E + \bar{T}/h_T} \,, \tag{6.11}$$

where $k = k_2\alpha/h, h_E = h/\alpha$, and $h_T = h$. Thus, whenever only a fraction of the CTLs is present in the bottom layer, i.e., whenever $\alpha < 1$, we predict that $h_T < h_E$, despite the symmetry expected for monogamous killing [16, 55].

6.6.4 Cellular Potts model simulations

The cellular Potts model (CPM) is a grid based model, in which each cell is represented with connected multiple lattice sites (see Chapter 2 for details of the CPM). We consider a

two-dimensional torus of 1000×1000 pixels (the length of each lattice site equals 1 μm), in which we only consider the bottom layer explicitly. It contains non-motile target cells (of about 16 μm diameter) and CTLs (of about 8 μm diameter) that enter the field at a constant probability per time step (mimicking their continuous migration in the bulk of the gel and appearance in the bottom layer of the gel). Conversely, CTLs also exit from the field at a constant probability to mimic their migration into the top layers of the gel. Surface energy (J) and surface tension (γ) parameters that define interactions between the *in silico* cell types are given in Table 6.3, and are chosen such that CTLs prefer to be adjacent to target cells and targets prefer to adhere to other targets over being surrounded by the medium.

Table 6.3. Default surface energies and surface tensions used in the simulations. Surface energies are represented by J, and γ are the surface tensions in arbitrary units.

	ECM	CTL	Target (tgt)
ECM	$J_{ECM,ECM} = 0$	$\gamma_{ECM,CTL} = 40$	$\gamma_{ECM,tgt} = 150$
CTL	$J_{CTL,ECM} = 190$	$J_{CTL,CTL} = 300$	$\gamma_{CTL,tgt} = -150$
tgt	$J_{tgt,ECM} = 400$	$J_{tgt,CTL} = 250$	$J_{tgt,tgt} = 500$

In the target cell mono-layer, CTLs perform a persistent random walk [26, 45] as long as they are present in the field. As in Chapters 2-4, CTLs follow a set of well defined migration rules. Briefly, a random target direction from a uniform distribution of [$-\pi$,π] is assigned to all the CTLs at the start of the simulation, and thereafter changes every 3 mins based on its direction of recent migration (i.e., self-adjusting motility [45]).

Following our recent experiments [21], we let the CTLs continue migration upon target encounter, i.e., they form kinapses. We record the durations that targets interact with CTLs at every time step. Targets 'remember' the contact duration when the CTL breaks the kinapse, and when the cumulative kinapse duration reaches 8.3 hours the target cell dies. The dying target quickly shrinks in size and disappears from the field. Each time step (i.e., attempting to update all the lattice sites) corresponds to 7.5 s in real time, and each simulation is equivalent to 30 hours of co-incubation. Other parameters are the same as in the simulations of short-lived synapses in Chapter 3.

6.6.5 Non-linear regression (or fit) to the data

All the regression analyses of models to the data from simulations are performed using the function *nlinfit* in MATLAB (The MathWorks Inc., Natick, MA), which uses the Levenberg-Marquardt algorithm. Log-transformed numbers of cells killed were used for all the regressions to prevent skewing of the fit to the killing observed at high CTL and target cell densities.

Acknowledgements

The authors thank Nobuto Takeuchi for helpful discussions. This study is supported by NWO grants 819.03.009 (to RJdB) and 864.12.013 (to JBB). This study is also supported by the “Virgo consortium,” funded by the Dutch government [project number FES0908] and by the “Netherlands Genomics Initiative (NGI)” [project number 050-060-452]. The authors declared that they have no competing interests.

Chapter 7

What Do Mathematical Models Tell Us about Killing Rates During HIV-1 infection?

Saikrishna Gadhamsetty, Joost B. Beltman and Rob J. de Boer

Immunol. Lett. Review in press.

Abstract

Over the past few decades the extent to which cytotoxic T lymphocytes (CTLs) control human immunodeficiency virus (HIV) replication has been studied extensively, yet their role and mode of action remains controversial. In some studies, CTLs were found to kill a large fraction of the productively infected cells relative to the viral cytopathicity, whereas in others CTLs were suggested to kill only a small fraction of infected cells. In this review, we compile published estimates of CTL-mediated death rates, and examine whether these studies permit determining the rate at which CTLs kill HIV-1 infected cells. We highlight potential misinterpretations of the CTL-killing rates from the escape rates of mutants, and from perturbations of the steady state viral load during chronic infection. Our major conclusion is that CTL-mediated killing rates remain unknown. But contrary to current consensus, we argue that killing rates higher than one per day are perfectly consistent with the experimental data, which would imply that the majority of the productively infected cells could still die from CTL-mediated killing rather than from viral cytopathicity.

7.1 Introduction

$CD8^+$ Cytotoxic T lymphocytes (CTLs) are an indispensable arm of the adaptive immune system for protection against tumors, and against viral and bacterial infections. CTLs protect by killing infected cells and by various non-lytic mechanisms, including the secretion of interferon-γ, macrophage inflammatory proteins (MIP)-1α and MIP-1β [68, 69]. The relative contribution of these two mechanisms in controlling infections is poorly understood,and an important parameter determining the extent of CTL protection is the rate at which they kill infected cells. Although $CD4^+$ T cells that have become productively infected with the human immunodeficiency virus type 1 (HIV-1) are known to die rapidly [70, 71], recent studies into the role of CTLs in controlling HIV-1 infection have suggested that their mode of action is largely non-lytic [29, 72–75]. This would imply that the majority of the productively infected cells are not killed, but die rapidly from infection (viral cytopathicity). Here we review these studies to see if they indeed support the minor contribution of the lytic effects of CTLs, and whether they are truly incompatible with rapid CTL killing rates. There are multiple ways to report CTL-mediated killing rates (see [11, 17, 27] for excellent overviews and how to interconvert these rates). In this review, we report published estimates of killing rates as the death rate of productively infected cells induced by all CTLs together.

Several kinetic parameters of HIV-1 and SIV infections are similar. During acute infection in their respective hosts, the two viruses initially replicate at comparable rates of 1.5–2.0/day [76–79], and during anti-retroviral therapy (ART) they exhibit similar viral load decay rates of 1–2/day [72, 73, 80, 81]. One notable difference between HIV-1 and SIV is that HIV-1 immune escape rates were consistently lower than SIV escape rates [82]. Here, we primarily focus on CTL-mediated killing rates during HIV-1-infection and dis-

cuss a few published SIV estimates from studies that can only be performed in monkeys.

7.2 Estimating killing rates from escape rates

HIV and SIV mutate when they infect new target cells. If these mutations occur within CTL epitopes, they can reduce the ability of CTLs to recognize and control infected cells, thereby allowing the virus to escape CTL surveillance. Such escape mutants have a selective advantage over wild type viruses, and hence can out-compete them. The rate at which escape mutant replaces the wild type—defined as the escape rate—provides an indication of the efficiency of the CTL response that was evaded. However, escape mutations are often accompanied by fitness costs of the mutations, which slow down the escape rate [17, 29]. The fitness costs can be estimated *in vitro* by competition assays [83–85] and *in vivo* from the rates at which escape mutants revert back to wild type in HLA-mismatched patients [29, 86, 87]. By accounting for fitness costs, researchers have tried to estimate the *in vivo* CTL-mediated killing rate from the escape rates of mutants (reviewed in [17]).

7.2.1 Early escape rates

Asquith *et al.* [29] examined longitudinal measurements of the frequencies of immune escape mutants and found very slow escape and reversion rates in 12 HIV-1-infected individuals at different stages of infection. Combining the estimated escape and reversion rates, and considering a model where CTLs control by killing infected cells, they estimated a median killing rate by the escaped CTL response of 0.04/day during the acute phase of the infection. Since the total death rate of productively infected $CD4^+$ T cells is about $\delta = 1$/day [80] (see below), they concluded that a CTL response targeting a single epitope is responsible for the death of only a minor fraction of virus-producing cells, i.e., at most 4%. In patients mounting CTL responses to, say, five epitopes, the contribution of CTL killing to the death of productively infected $CD4^+$ T cells would still be just 20%, suggesting that most infected cells die by viral cytopathic effects. Although later studies using the same approach frequently find at least 10-fold faster escapes [88–90] and more rapid reversions [87], other recent studies confirm that both immune escapes and reversions can be slow [91]. One possible explanation for these slow immune escape rates is that CTLs largely control by non-lytic mechanisms [75]. Immune escapes from non-lytic CTLs impose lower selection pressures than escapes from lytic responses because cells infected with escaped virus remain susceptible to non-specific factors secreted by the CTL in their neighborhood [75].

At least two other explanations for slow immune escape rates have been suggested, both implying that the published escape rates underestimate the actual CTL killing rates. First, there are some general issues associated with estimating killing rates from escape rates, i.e., by sequencing the HIV-1 quasi species in a patient at various time points and fitting

simple population genetic models to the time course describing the fraction of mutated sequences within each epitope [92]. One major problem with such models is that the escapes are treated independently, whereas in reality the immune escapes appear more or less sequentially, i.e., subsequent escapes can only evolve after previous immune escapes have become established. This competition is known as "clonal interference" in population genetics [93, 94], and several authors have recently shown that clonal interference can markedly decrease the escape rate inferred independently for each epitope [92, 95–98]. For example, Kessinger *et al.* [96] developed a novel mathematical model combining the escape data from all epitopes, and showed that their estimation procedure markedly increased the most likely set of escape rates. Another major problem with this kind of data is that the time courses are underpowered due to sampling that is fairly infrequent [99] and that is not deep enough to detect the exact arrival time of the escape mutants. By testing clonal interference models on simulated data, it was indeed found that the estimated escape rates are very sensitive to the sampling frequency and to the sequencing depth [96, 98], casting additional doubt on the estimated escape rates [92, 96]. Next generation sequencing (NGS) methods have been used to sequence much deeper [100], but due to their prohibitive costs, the sampling frequency remains limited. An interesting approach is to reconstruct whole genome haplotypes from the NGS data [101], which allows one to observe the clonal interference directly and to estimate the escape rate of all the major haplotypes.

A second line of explanations for slow immune escape that does not involve non-lytic mechanisms is that large fitness costs can explain at least some of the slow escapes observed. Several immune escapes confer severe fitness defects, which can be observed *in vivo* by poor replication of the virus in subsequent HLA-mismatched patients [87] or *in vitro* by viral competition assays [83–85]. Additionally, the reversion rates estimated *in vivo* also suffer from clonal interference, and could hence be markedly underestimated. Finally, several immune escape mutations ultimately become repaired by compensatory mutations increasing the replicative fitness of the virus. Following transmission to an HLA-mismatched patients such a repaired immune escape may have a high fitness, and hence reverts very slowly.

7.2.2 Late escape rates

In Asquith *et al.* [29] study the immune escape rates tended to be even slower in chronically infected patients, i.e., about 0.008/day than in acute stage. They were also found to decrease over time in a study following three HIV-1-infected individuals over one year [89]. Moreover, a recent study following about 120 HIV-1-infected individuals starting at a median of 11 weeks post seroconversion found very few escapes over the subsequent 2–3 years of chronic infection [91]. The apparent decrease in the immune escape rate has been attributed to a lower killing efficiency during chronic infection due to exhaustion of CTLs [11, 29, 92], and due to the decrease in CTL numbers after the acute phase [17].

However, other explanations for the escape rate decrease over time are possible. First,

a trivial explanation could again be the small number of time points in these studies, because the sampling frequency typically decreases over time [98]. Second, similar observations have been made in mathematical models in which the data is "sampled" very frequently [99]. Van Deutekom *et al.* [102] and Ganusov *et al.* [89] demonstrated that escape rates are expected to decrease during chronic infection when the number of CTL responses increases during infection progress. This is because multiple CTL responses can collectively induce rapid death, while the contribution of each individual CTL response remains small. As a result, the selective advantage for the virus to escape just one CTL response decreases [102], leading to slow escape. Consistent with this, a recent study showed that broad Gag responses are associated with few escapes and low viral load in HIV-1-infected individuals [103]. Thus, slow escape rates during chronic infections are to be expected for broad immune responses, and are not indicative of non-lytic or poor control by CTLs.

Summarizing, the current data on the immune escape and reversion rates in HIV-1 infection have been described with over-simplified mathematical models, and are not rich enough for reliably estimating the contribution of CTLs during the acute and chronic phases of HIV-1 infection, let alone the relative contribution of lytic and non-lytic mechanisms. Fortunately, with the current rise of NGS approaches [100, 101], and the novel models taking clonal interference into account [92, 95–98], this is expected to improve once we can afford to sample the viral quasi species very frequently. This is important because immune escape and reversions provide natural *in vivo* experiments providing information on the role of CTLs in HIV-1 infection.

7.3 Estimating killing rates from ART data

During chronic HIV/SIV infection, the plasma viral load remains constant over many years due to the balance between viral replication and clearance mechanisms, i.e., a steady state. In several studies the steady state was perturbed, and the ensuing viral dynamics were analyzed to estimate the kinetic parameters of viral replication and CTL-mediated killing rates. The approaches used to perturb steady state can be classified into three broad categories: treatment with anti-retroviral therapy (ART), depletion of $CD8^+$ cells, or adoptive transfer of $CD8^+$ T cells. In the remainder of this review, we focus on estimates of killing rates during chronic HIV/SIV infection obtained using these three methods.

Ho *et al.* [70] and Wei *et al.* [71] examined the dynamics of HIV-1 following ART with one or two protease inhibitors, and found that the plasma viral load declines very rapidly after treatment. In later studies, the viral load was found to decline in multiple phases [104, 105], and using an even more potent combination of drugs [80], it was found that the initial downslope of the viral load is about $\delta = 1$/day. These downslopes were estimated by fitting a basic model (Fig. 7.1A) to the viral load, in which this initial downslope, δ, reflects the death rate of productively infected $CD4^+$ T cells [70, 71, 80, 104, 105].

A meta-analysis of various clinical data sets showed that δ hardly depends on the CD4$^+$ T cell count or on the pre-treatment viral load [81]. This was surprising because the death rate of productively infected CD4$^+$ T cells represents both "normal death" and CTL killing, i.e., $\delta = d_P + K$, where d_P is the normal death rate (including viral cytopathic effects), and K is the rate at which infected cells are killed. Since δ was so invariant in the meta-analysis, and patients with different viral loads probably have different CTL responses, it was proposed that CTLs hardly affect the death rate of productively infected CD4$^+$ T cells [81]. This is reminiscent of the minor contribution of killing estimated from the escape rates [29] and hence again suggests that CTLs largely control by non-lytic mechanisms.

Recently, Klatt *et al.* [72] and Wong *et al.* [73] independently studied the contribution of CTL-mediated killing, K, during SIV-infection to the death rate of productively infected cells, δ. The viral dynamics were studied following ART in both CD8$^+$ cell-depleted and control rhesus macaques infected chronically with SIV. Note that targeting the CD8 molecule for CTL depletion also depletes other CD8-expressing cells (such as NK cells) [72]. Nevertheless, the rate at which the plasma viral load declined was similar between CD8-depleted and control macaques. By fitting the basic model (see Fig. 7.1A) to the viral load, the authors estimated similar death rates, δ, of virus-producing cells in CD8-depleted (where $\delta = d_P$) and control hosts (where $\delta = d_P + K$). Because this implies that K is very small, this again suggest a negligible role of CTLs in the death of virus-producing cells.

7.3.1 Interpreting ART and CD8-depletion data with two-stage mathematical models

The above studies estimated lifespans of the productively infected cells using the basic model of virus dynamics (Fig 7.1A), which ignores several aspects of viral replication that are relevant to HIV-1 infection. For instance, it does not account for the eclipse phase, i.e., the time period between viral entry and production of viruses [106]. In other words, the basic model assumes that the infected cells start producing virus particles immediately after infection.

Klenerman *et al.* [31] developed an HIV/SIV-specific mathematical model that includes two infected cell stages and a viral production stage for the infected cells (i.e., three-stage viral replication; similar to the two-stage model shown in Fig. 7.1B). They assumed that antigen expression and ensuing recognition by CTLs only occurred in the viral production stage (late-stage killing model). Furthermore, they argued that the rate, γ, at which HIV-infected cells transit to antigen-expressing stage is the slowest timescale of HIV replication. In that case, the observed downslope of the viral load during ART, δ, reflects this slow transition rate. Because the average duration of the eclipse phase, $1/\gamma$, is about one day [106], this is in excellent agreement with a decay rate of $\delta = 1$/day, and with the independence of the viral load and the CD4$^+$ T cell count [80, 81].

Further, when Wick *et al.* [30] performed stochastic simulations similar to the late-stage

killing model with a rapid CTL-mediated killing rate of $K \approx 7$/day, they found approximately equal viral decay rates between CD8-depleted and control hosts when γ was the rate limiting step. Although the Wick *et al.* [30] simulation model differs from the late-stage killing model in several details, analysis of a similar deterministic model (Fig. 7.1B) confirms its consistency with the CD8-depletion experiments (i.e., viral decay rate reflects $\gamma + d_I$; Fig. 7.2A). Therefore, in both the two- and three-stage variants of the late-stage killing model, CTL-mediated killing can be rapid, if it acts only in late stages of infection [30, 31] and thus separates the timescales of viral replication and CTL lysis. However, Klatt *et al.* [72] argue that the time scale of infected cells in the eclipse phase is not necessarily slow, because some HIV epitopes are expressed on infected cells as early as an hour after infection [107]. Thus, infected cells could be susceptible to CTL-mediated killing immediately after infection.

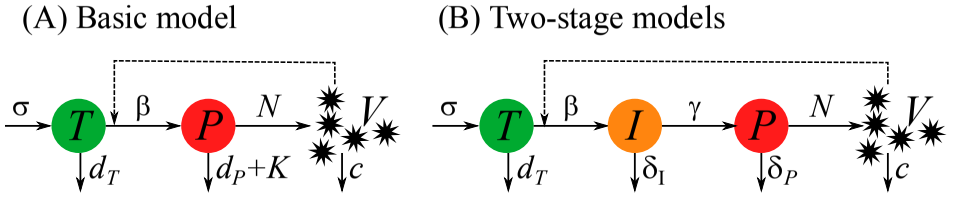

		Predicted viral decay rate, δ	
Model	Model-specific parameters	Control	With CD8-depletion
Basic [71, 108]	-	$\delta = d_P + K$	$\delta = d_P$
Late-stage killing [31, 82]	$\delta_I = d_I$, $\delta_P = d_P + K$	$\delta = \min(\gamma + d_I,\ d_P + K)$	$\delta = \min(\gamma + d_I,\ d_P)$
Early-stage killing [32]	$\delta_I = d_I + K$, $\delta_P = d_P$	$\delta = \min(\gamma + d_I + K,\ d_P)$	$\delta = \min(\gamma + d_I,\ d_P)$

Figure 7.1. Summary of various models used to describe HIV dynamics. The scheme summarizes the three models discussed: (A) basic and (B) two-stage infection models in which CTL-mediated killing acts either during eclipse phase or during virus-production phase. HIV viral particles, V, infect healthy CD4$^+$ T cells, T, at a rate β. Following infection, infected cells, I, transit the eclipse phase at a rate γ to become virus-producing cells, P, which produce new virus particles. Healthy CD4$^+$ T cells are produced at a constant rate, σ, and die at a rate d_T, and free virus particles are cleared at a rate c. Infected cells in the eclipse phase, I, and productively infected cells, P, die normally at a rate d_I and d_P, respectively. Additionally, they can be killed by CTL at a rate K, which, depending on the model increases their total death rates to δ_I and δ_P, respectively. The predicted viral decay rates, δ, are summarized in the accompanying table, where $\min(x, y)$ represents the minimum of x and y. Note that the basic model can be obtaining from the two-stage models by making the eclipse phase very short (i.e., by letting $\gamma \to \infty$).

It is unclear whether the timescale of the eclipse phase is indeed the slowest process in the short life of productively infected cells. Therefore, Althaus *et al.* [32] used the mathematical model of Fig. 7.1B to show that early antigen expression followed by rapid CTL-mediated killing of infected cells at an early stage within the eclipse phase (early-stage killing model), is also consistent with the similar decay rates of viral loads observed in CD8-depleted and control hosts (Fig. 7.2B). Because CTLs in this model only kill infected cells in the eclipse phase, the viral decay rates are independent of CTL activity. These decay rates now represent the death rate of virus-producing cells, which can be large due to viral cytopathicity alone (i.e., $\delta = d_P$; Fig. 7.1).

In conclusion, the viral load dynamics is determined by the timescale of the slowest process, and CTL lysis need not be slow. The two-stage model is a simple extension of the basic model, and underlines how the rate limiting step alters the interpretation of the initial viral decay. More sophisticated models either with multiple cellular compartments [104, 110], or with n stages from infection to viral production [111, 112] have been proposed for a complete description of all three phases of viral decay. Nevertheless, the two-stage model with CTL-mediated killing of infected cells either in the early or late stage can qualitatively explain the results from ART studies (phase I) with or without CD8-depletion. Importantly, this implies that the rate of CTL-mediated killing can be larger than 1/day.

7.3.2 Which model quantitatively describes the ART and CD8-depletion data best?

Recently, Elemans *et al.* [74] studied whether or not the above models (i.e., the basic, early-stage killing, and late-stage killing; Fig. 7.1) can provide a good quantitative description of the CD8 depletion/ART data of Klatt *et al.* [72]. Fitting these models to the data, they found that all three models poorly described the experimental data [74]. This is puzzling as both Klenerman *et al.* [31] and Althaus *et al.* [32] demonstrated that their respective models are qualitatively consistent with the experiments over a wide range of parameters. A potential explanation for these conflicting findings is that Elemans *et al.* [74] required the target cell levels in the model to describe the observed $CD4^+$ T cell counts, and considered the specific CTL response to be proportional to the observed $CD8^+$ T cell counts. Contrary to these assumptions, the frequency of HIV-specific CTLs within the pool of $CD8^+$ T cells could change over time following CD8 depletion, and the total number of $CD4^+$ T cells is probably a poor indicator for the number of susceptible target cells. Thus, it remains possible that the two-stage models shown in Fig. 7.1B can quantitatively account for the viral load data.

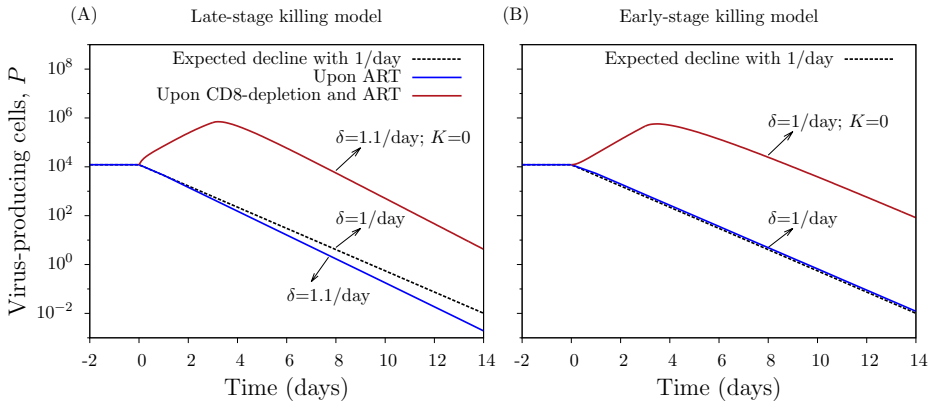

Figure 7.2. Predictions of the decay of virus-producing cells following ART with or without CD8-depletion in the late-stage killing model (A) and in the early-stage killing model (B). Solid blue lines depict the dynamics of productively infected cells, P, upon ART starting at day 0. Solid red lines indicate their dynamics upon CD8-depletion at day 0 followed by ART starting at day 3. Dashed black lines depict the expected decline of virus-producing cells at a rate 1/day. During chronic infection, before CD8-depletion, the actual CTL killing rate in both models was about $K = 4.8$/day. The dynamics were computed with the differential equations corresponding to the scheme of Fig. 7.1B: $T' = \sigma - d_T T - \beta TV, I' = \beta TV - \delta_I I - \gamma I, P' = \gamma I - \delta_P P$ and $V = P$,with $\sigma = 10^6$ cells/day, $d_T = d_I = 0.1$/day, and $\gamma = 1$/day. The CTL dynamics and killing of infected cells obey the same functions and parameters as in [102], i.e., $E' = pEA/(h + A + E) - d_E E$ and $K = kE$, where the amount of antigen, A, is defined by P in the late-stage killing model, and by I in the early-stage killing model, and $p = 1.1$/day, $d_E = 0.1$/day and $k = 4 \times 10^{-5}$. In the early-stage killing model, a death rate of $d_P = 1$/day is used for productively infected cells such that decay rates are consistent with the experimental observations, i.e., $\delta = d_P$, whereas $d_P = 2$/day is used in the late-stage killing model (to guarantee that the eclipse phase remains the slowest time scale even after CD8-depletion). Infection rates, β, for both models are chosen following [109], such that the initial viral growth is 1.5/day (specifically $\beta = 9.1 \times 10^{-7}$ for the late-stage killing model, and 6.5×10^{-7} for the early-stage killing model).

7.4 Estimating killing rates from the increase of the viral load upon CD8-depletion

In all studies where $CD8^+$ cells are depleted in chronically SIV-infected macaques it was consistently found that this results in a rapid transient increase of the viral load [72, 73, 113], suggesting that CD8-depletion results in an imbalance between viral production and clearance. Indeed, there was a negative correlation between the residual $CD8^+$ T cells surviving the depletion and the fold-increase in the viral load [73]. Because the killing rate at steady state was fast, both the early- and late-stage killing models readily account for such a rapid increase of the viral load increase upon CD8 depletion (Fig. 7.2), and both are consistent with the experimental observations. Since the killing rate in the basic model should not be faster than $\delta = 1$/day, the basic model can only account for these data if the major effect of CTLs is non-lytic [114].

A few studies directly estimated the CTL-mediated death rate by equating it to the rate at which the viral load increases upon CD8-depletion [72, 73], and arrived at a killing rate between 0.25-0.8/day [73, 74]. In the basic model of Fig. 7.1A one indeed expects the upslope of the viral load to reflect the killing rate K, but in the multi-stage models of Fig. 7.1B this is more complicated. Generally, the rate at which the viral load increases upon CD8-depletion reflects the effective replication rate of the virus in the chronic steady state just before the $CD8^+$ T cells were depleted. Compared to acute infection, the number of $CD4^+$ T cells is decreased during chronic stage. Therefore, the availability of suitable target cells should also be low at the onset of the CD8-depletion, and the rate at which the viral load increases is expected to be lower than during acute infection, i.e., approximately 1.5/day [76–78, 115]. Indeed, the observed viral load increases of 0.25-0.8/day [73, 74] are consistent with this reasoning. Similar rates of viral load increase, about 0.3–1.2/day, occur in other CD8-depletion studies [113, 114, 116, 117]. In the model simulations of CD8-depletion (Fig. 7.2) the productively infected cells, and hence the viral load, increased at a realistic rate of about 1.3/day, whereas the CTL-mediated killing rate at steady state was almost 5/day. Therefore, the rate at which the viral load increases upon CD8-depletion need not always reflect the killing rate, and rapid killing rates can be consistent with the moderate viral load increase rates observed in the data.

7.5 Killing rates from adoptive transfer studies

More than a decade ago, Brodie *et al.* [57] transferred *ex-vivo* activated HIV-specific CTLs into chronically HIV-1-infected individuals, and followed the resulting dynamics of productively infected cells (defined by the expression of HIV-mRNA) and CTLs in the blood. To our knowledge, this is the only study involving adoptive transfer of CTLs into HIV-1-infected humans, and provides an opportunity to directly estimate the killing rates. Fitting a mathematical model to these measurements, Wick *et al.* [13] estimated the killing rate due to the transferred CTLs as ranging from 1.6/day to 9.8/day [11, 13].

This range thus represents the highest killing rate estimate so far.

However, the model by Wick *et al.* [13] described the data rather poorly, particularly around 4 days post CTL transfer, at which time the CTLs in the blood reached nadir. This could be because the simulations considered only CTLs and infected cells in the blood, ignoring their interactions in lymphoid tissues. Indeed, at day 4 Brodie *et al.* [57] found 10-fold more CTLs in lymph nodes (LNs) than in the blood. Moreover, LN-residing CTLs preferentially co-localized with HIV-infected cells, suggesting that CTLs in the LN continue to kill infected cells at this time point. Because the frequency of CTLs in the LNs was measured at only a single time point, it remains unknown whether they preferentially accumulated in the LN, and what fraction of killing occurs in the LN. Therefore, the estimated death rates are likely inaccurate.

7.6 Conclusions

Over the past decades, researchers have used various experimental and modeling approaches to determine the importance of CTLs in mediating lytic control of HIV-1 infection. In this review, we have examined several estimates for CTL-mediated death rates of HIV-1 infected cells. We conclude that there is currently not a single robust estimate, and have highlighted some of the difficulties associated with inferring killing rates from escape rates. Unfortunately, models where productively infected cells are killed largely at an early stage [32], at a late stage [31], or where CTL action occurs largely through non-lytic effects [74] can all explain the data, and it thus remains unknown which of them is correct. This calls for novel experiments that can distinguish between these mechanisms. In conclusion, published estimates of CTL-mediated killing rates remain uncertain, and we have only added to this uncertainty by arguing that rapid killing rates are also consistent with the data. Thus, CTL killing could after all be the major cause of death of productively infected $CD4^+$ T cells.

Acknowledgements

The authors thank Becca Asquith, Vitaly Ganusov, Marit van Buuren, and Hanneke van Deutekom for critical reading of and comments on an earlier version of the manuscript. This study is supported by NWO grant 819.03.009 (to RJdB) and by NWO grant 864.12.013 (to JBB). This study is also supported by the "Virgo consortium," funded by the Dutch government [project number FES0908] and by the "Netherlands Genomics Initiative (NGI)" [project number 050-060-452]. The authors declared that they have no competing interests.

Chapter 8

Summary and Outlook

8.1 Summary

In all the studies of this thesis, we consistently find that a double saturation (DS) model with two saturation constants (one for CTLs and another for target cells) describes the CTL-mediated killing well. This is true for different modes of interactions, in spatially homogeneous as well as heterogeneous gels, in 2D as well as 3D spaces, and in densely as well as sparsely populated environments. We showed that this DS model can be mechanistically derived for some cases, and that in the other cases it still provides a semi-mechanistic description. Our results suggest that the extent of saturation in CTLs and targets is determined by the stability of the conjugates, spatial dimensionality of the tissue, and mode of CTL-target interactions. The relative differences in the two saturation constants can help us identify underlying CTL-target cell interactions, but factors like the occurrence of a transient to the steady state and spatial heterogeneity of the environment can confound this inference. Nevertheless, any significant deviations from the DS model noticed in cytotoxicity assays do suggest that additional mechanisms are at play. In summary, we propose that the DS model is an excellent default model to describe CTL-mediated killing of target cells.

8.2 Outlook

The primary aim of *in vivo* and *in vitro* cytotoxicity assays is to obtain estimates for CTL-mediated killing rates that are representative of the rate at which CTLs kill target cells *in vivo* during an ongoing viral infection or in a tumor. *In vitro* collagen gel assays provide a first approximation to this *in vivo* aim, and they overcome many of the shortcomings of the '^{51}Cr-release' assays. In our analysis of the data from two independent collagen gel assays [7, 21], we found that CTL-mediated killing rates saturate more pronouncedly in CTL than in target cell densities (Chapters 5-6). Further, the extent of saturation of the killing rate in target cell densities differed between these datasets—we found evidence for saturation in targets in Chapter 6, but no evidence in Chapter 5. The differences in the spatial organization of targets between these two experiments might explain this variation.

In the assays of Budhu *et al.* [7] (and Chapter 5), target cells were uniformly distributed (referred to as 'homogeneous gels' hereafter), whereas in the gels developed by Friedl and colleagues [21] (see Chapter 6) the targets were localized in the bottom layer of the gel (referred to as 'monolayer gels'). Additionally, the target cells were clustered within the monolayer gels [21]. As a result, CTLs in the monolayer gels more often find a cluster of target cells than isolated targets, which could result in saturation of killing at much lower target cell densities.

8.2.1 Towards improved estimation of killing rates and identification of mechanisms

From our analysis of the *in vitro* cytotoxicity data, we gained insights into the circumstances that influence killing rate and functional response estimates that are also applicable to *in vivo* assays. Specifically, we identified two factors that can confound the identification of underlying CTL-target interactions from cytotoxicity assays, namely (1) the spatial organization of cells, and (2) the occurrence of a transient before steady state. Together with the tissue dimensionality and the mode of interactions, these factors determine the extent of saturation of killing rates with increasing CTL and target cell densities. In some cases, they can confound the precise estimation of the extent of saturation, and as a consequence the underlying mechanisms of CTL-target cell interactions. This will also affect the accuracy of estimates of CTL-mediated death rates because they depend on the parameters of the functional response.

In the *in vitro* collagen gels, T cells can migrate and they exhibit similar migration properties [22] to those observed *in vivo* [26]. The spatially homogeneous DS model describes the CTL-mediated killing of tumor cells in the heterogeneous monolayer gels very well, despite the fact that not all the CTLs are readily available to kill the target cells within the monolayer. This bias in the data will lead to an overestimation of the saturation constant in CTLs whenever only a fraction of the total CTLs is present in the bottom mono-layer. This may interfere with the identification of the mode of interactions between CTLs and target cells. For instance, consider a cytotoxicity assay in which each CTL kills multiple target cells simultaneously. From our simulations (Chapter 2), we then expect that the number of target cells killed per unit time (referred to as the killing rate) strongly saturates with increases in the CTL densities (i.e., $h_E < h_T$). Depending on the fraction of CTLs present in the monolayer, we may find in the assays that the killing rate saturates more or less symmetrically with increases in CTL and target cell densities ($h_E \simeq h_T$), or even that it saturates more strongly with increases in target cell than in CTL densities ($h_E > h_T$). Therefore, to accurately quantify the parameters, it is required to quantify the number of CTLs present in the monolayer. Such an approach seems feasible because these monolayer gels support time-lapse imaging [21], by which one could track the arrival and departure of CTLs.

In *in vivo* adoptive transfer assays [12, 23–25], one typically determines the total number of cognate CTLs present in the tissue of interest. However, it is unclear how many CTLs are functional and actually participate in the killing of target cells. Since lymphoid and peripheral tissues are highly organized, the fraction of peptide-specific CTLs that actually participate in the killing of target cells is likely to be less than one. As discussed above, this bias results in an overestimation of the CTL densities at which killing rates saturate, and this might be one of the reasons why there was no evidence for saturation of killing in adoptive transfer assays so far [10, 15]. There are other explanations that can explain lack of saturation [17]; one trivial explanation is that the CTL densities in these *in vivo* experiments are too low to approach saturation of killing rates.

Another factor that can confound the identification of the extent of saturation in killing,

and thus the mode of CTL-target interactions, is the initial transient to steady state. When killing occurs at steady state, the cumulative interaction times that target cells have spent in conjugates (i.e., the killing signal) are uniformly distributed. Since both *in vivo* adoptive transfer and *in vitro* assays employ 'fresh' targets [12, 14, 23–25], the killing signal is not uniformly distributed at the beginning of the assay, resulting in a lack of steady state killing. In such a non-steady state situation, assays of varying duration are expected to result in variable killing rate estimates. Thus, these differences in the estimates mirror and quantify the influence of the transient on the realized killing rates. To reduce the effect of the initial transient on the realized CTL-mediated killing, the duration of the experiment should be much longer than the typical time required to kill a target.

It remains to be determined whether *in vivo* experiments during ongoing CTL-responses to tumors or viral infections have approached a steady state (i.e., uniform) distribution of killing signals. For chronic viral infections and tumor it seems safe to assume that the killing is at steady state, as the viral load remains relatively constant over many years, and tumors typically grow slowly. During an acute viral infection the distribution of killing signals may approach steady state within a few days. However, in the *in vivo* adoptive transfer assays, the transferred CTLs or (peptide-pulsed) target cells gradually accumulate within the tissue of interest, and start at a non-steady state distribution of killing signals. As discussed above, this could result in inaccurate estimates of the saturation constants, and thus of CTL-mediated death rates as well as per-capita killing rates.

Taken together, both the presence of a transient and the uncertainty in the number of peptide-specific CTLs that are actively involved in the killing, can confound relative extents of saturation. Although several studies determined the CTL-mediated killing rates and the functional response of CTL-mediated killing from *in vitro* and *in vivo* assays [10, 12, 14, 15, 25], the relative importance of the above factors in explaining the saturation of killing rates (or the lack of it) remains to be determined. Thus, it is currently unclear whether the parameter estimates of the functional response are truly representative of the underlying mechanisms of the CTL-target interactions, and thereby the CTL-mediated death rates and per-capita killing rates.

In summary, identifying the functional response that is applicable over a wide range of conditions is a proper first step towards a complete quantification of CTL-mediated killed rates, and why they vary between different studies. Still, this approach is incomplete without investigating the relative contributions of various mechanisms in determining the parameters of the functional response—which should be the focus of subsequent steps. We conclude that it is extremely important to device methods that determine the CTL-mediated killing rate without altering the dynamics of viral infection and tumor. This further emphasizes the need of time-lapse imaging in combination with cell-based models in order to achieve both accurate estimates of the CTL-mediated killing rates, and to identify the underlying CTL-target interactions.

Bibliography

[1] Foley MH, Forcier T, McAndrew E, Gonzalez M, Chen H, Juelg B, Walker BD, and Irvine DJ. High avidity CD8+ T cells efficiently eliminate motile HIV-infected targets and execute a locally focused program of anti-viral function. PLoS One 2014;9(2):e87873. (Cited on pages 2, 42, and 65.)

[2] Boissonnas A, Fetler L, Zeelenberg IS, Hugues S, and Amigorena S. In vivo imaging of cytotoxic T cell infiltration and elimination of a solid tumor. J Exp Med 2007; 204(2):345–356. (Cited on pages 2, 3, 13, 54, 55, and 90.)

[3] Ariotti S, Hogenbirk MA, Dijkgraaf FE, Visser LL, Hoekstra ME, Song JY, Jacobs H, Haanen JB, and Schumacher TN. Skin-resident memory CD8+ T cells trigger a state of tissue-wide pathogen alert. Science 2014;346(6205):101–105. (Cited on pages 2 and 54.)

[4] Wang T, Eileen S, Yin Z, Kim JH, Sha W, Yan J, Mamula M, Anderson JF, Craft J, and Fikrig E. IFN-γ-producing $\gamma\delta$ T cells help control murine west nile virus infection. J Immunol 2003;171:2524–2531. (Cited on page 2.)

[5] Jenkins MR, La Gruta NL, Doherty PC, Trapani Ja, Turner SJ, and Waterhouse NJ. Visualizing CTL activity for different CD8+ effector T cells supports the idea that lower TCR/epitope avidity may be advantageous for target cell killing. Cell Death Differ 2009;16(4):537–42. (Cited on page 2.)

[6] La Gruta NL, Turner SJ, and Doherty PC. Hierarchies in cytokine expression profiles for acute and resolving influenza virus-specific CD8+ T cell responses: correlation of cytokine profile and TCR avidity. J Immunol 2004;172(9):5553–5560. (Cited on page 2.)

[7] Budhu S, Loike J, Pandolfi A, Han S, Catalano G, Constantinescu A, Clynes R, and Silverstein S. CD8+ T cell concentration determines their efficiency in killing cognate antigen–expressing syngeneic mammalian cells in vitro and in mouse tissues. J Exp Med 2010;207(1):223. (Cited on pages 2, 3, 10, 13, 14, 55, 77, 78, 81, 82, 83, 86, 87, 90, and 120.)

[8] Yates A, Graw F, Barber DL, Ahmed R, Regoes RR, and Antia R. Revisiting estimates of CTL killing rates in vivo. PLoS One 2007;2(12):e1301. (Cited on pages 2, 4, 5, and 6.)

[9] Ganusov VV, Lukacher AE, and Byers AM. Persistence of viral infection despite similar killing efficacy of antiviral CD8(+) T cells during acute and chronic phases of infection. Virology 2010;405(1):193–200. (Cited on pages 2, 4, 5, 6, and 90.)

[10] Ganusov VV, Barber DL, and de Boer RJ. Killing of targets by $CD8^+$ T cells in the mouse spleen follows the law of mass action. PLoS One 2011;6(1):e15959. (Cited on pages 2, 4, 5, 6, 13, 31, 77, 101, 121, and 122.)

[11] Elemans M, Florins A, Willems L, and Asquith B. Rates of CTL killing in persistent viral infection in vivo. PLoS Comput Biol 2014;10(4):e1003534. (Cited on pages 2, 4, 5, 6, 108, 110, and 117.)

[12] Garcia V, Richter K, Graw F, Oxenius A, and Regoes RR. Estimating the in vivo killing efficacy of cytotoxic T lymphocytes across different peptide-MHC complex densities. PLoS Comput Biol 2015;11(5):e1004178. (Cited on pages 2, 3, 4, 6, 121, and 122.)

[13] Wick WD, Yang OO, Corey L, and Self SG. How many human immunodeficiency virus type 1-infected target cells can a cytotoxic T-lymphocyte kill ? J Virol 2005; 79(21):13579–13586. (Cited on pages 2, 5, 6, 117, and 118.)

[14] Hogan T, Kadolsky U, Tung S, Seddon B, and Yates A. Spatial heterogeneity and peptide availability determine CTL killing efficiency in vivo. PLoS Comput Biol 2014;10(9):e1003805. (Cited on pages 2, 4, 5, 6, and 122.)

[15] Graw F and Regoes RR. Investigating CTL mediated killing with a 3D cellular automaton. PLoS Comput Biol 2009;5(8):e1000466. (Cited on pages 2, 4, 6, 8, 13, 17, 18, 25, 31, 54, 77, 86, 90, 92, 100, 101, 121, and 122.)

[16] Borghans JAM and de Boer RJ. Extending the quasi-steady state approximation by changing variables. Bull Math Biol 1996;58(1):43–63. (Cited on pages 2, 6, 7, 8, 13, 20, 21, 27, 42, 44, 46, 47, 59, 98, and 103.)

[17] Regoes RR, Yates A, and Antia R. Mathematical models of cytotoxic T-lymphocyte killing. Immunol Cell Biol 2007;85(4):274–279. (Cited on pages 2, 4, 7, 42, 108, 109, 110, and 121.)

[18] Perelson AS, Macken A, Gruvim EA, Roos LS, and Bonavida B. Mechanism of cell mediated cytotoxicity at the single cell lymphocyte level. VIII. kinetics of lysis of target cells bound by more than one cytotoxic T lymphocyte. J Immunol 1984; 132(May):2190–2198. (Cited on pages 2 and 101.)

[19] Breart B, Lemaître F, Celli S, and Bousso P. Two-photon imaging of intratumoral $CD8^+$ T cell cytotoxic activity during adoptive T cell therapy in mice. J Clin Invest 2008;118(4):1390–1397. (Cited on pages 2, 3, 54, and 101.)

[20] Ariotti S, Beltman JB, Chodaczek G, Hoekstra ME, van Beek AE, Gomez-Eerland R, Ritsma L, van Rheenen J, Marée AFM, Zal T, de Boer RJ, Haanen JBaG, and Schumacher TN. Tissue-resident memory CD8+ T cells continuously patrol skin epithelia to quickly recognize local antigen. Proc Natl Acad Sci USA 2012; 109(48):19739–44. (Cited on pages 2 and 54.)

[21] Weigelin B and Friedl P. A three-dimensional organotypic assay to measure target

cell killing by cytotoxic T lymphocytes. Biochem Pharmacol 2010;80(12):2087 – 2091. (Cited on pages 3, 77, 86, 90, 91, 94, 102, 104, 120, and 121.)

[22] Wolf K, Müller R, Borgmann, Bröcker EB, and Friedl P. Amoeboid shape change and contact guidance: T-lymphocyte crawling through fibrillar collagen is independent of matrix remodeling by MMPs and other proteases. Blood 2003; 102(9):3262–3269. (Cited on pages 3 and 121.)

[23] Barber DL, Wherry EJ, and Ahmed R. Cutting edge : Rapid in vivo killing by memory CD8 T cells. J Immunol 2003;171:27–31. (Cited on pages 3, 13, 31, 121, and 122.)

[24] Byers AM, Kemball CC, Moser JM, and Luckacher AE. Cutting edge : Rapid in vivo CTL activity by polyoma virus-specific effector and memory CD8+ T cells. J Immunol 2003;171:17–21. (Cited on pages 3, 121, and 122.)

[25] Graw F, Richter K, Oxenius A, and Regoes RR. Comparison of cytotoxic T lymphocyte efficacy in acute and persistent lymphocytic choriomeningitis virus infection. Proc R Soc Lond B Biol Sci 2011;278(1723):3395–3402. (Cited on pages 3, 121, and 122.)

[26] Mempel TR, Pittet MJ, Khazaie K, Weninger W, Weissleder R, von Boehmer H, and von Andrian UH. Regulatory T cells reversibly suppress cytotoxic T cell function independent of effector differentiation. Immunity 2006;25(1):129 – 141. (Cited on pages 3, 14, 15, 17, 18, 31, 42, 54, 55, 56, 66, 67, 82, 101, 104, and 121.)

[27] Ganusov VV and de Boer RJ. Estimating in vivo death rates of targets due to CD8 T-cell-mediated killing. J Virol 2008;82(23):11749–57. (Cited on pages 4, 5, and 108.)

[28] Fernandez CS, Stratov I, Rose RD, Walsh K, Dale CJ, Smith MZ, Michael B, Hu Sl, Krebs K, Watkins DI, David H, Connor O, Davenport MP, Kent SJ, Fernandez CS, Stratov I, Rose RD, Walsh K, Dale CJ, Smith MZ, Agy MB, Hu Sl, Krebs K, Watkins DI, Connor DHO, Davenport MP, and Kent SJ. Rapid viral escape at an immunodominant simian-human immunodeficiency virus cytotoxic T-lymphocyte epitope exacts a dramatic fitness cost. J Virol 2005;79(9):5721–5731. (Cited on page 5.)

[29] Asquith B, Edwards CTT, Lipsitch M, and McLean AR. Inefficient cytotoxic T lymphocyte-mediated killing of HIV-1-infected cells in vivo. PLoS Biol 2006; 4(4):e90. (Cited on pages 5, 6, 108, 109, 110, and 112.)

[30] Wick WD and Yang OO. Biologically-directed modeling reflects cytolytic clearance of SIV-infected cells in vivo in macaques. PLoS One 2012;7(9):e44778. (Cited on pages 6, 112, and 113.)

[31] Klenerman P, Phillips RE, Rinaldo CR, Wahl LM, Ogg G, May RM, McMichael AJ, and Nowak MA. Cytotoxic T lymphocytes and viral turnover in HIV type 1 infection. Proc Natl Acad Sci USA 1996;93(26):15323–8. (Cited on pages 6, 112, 113, 114, 115, and 118.)

[32] Althaus CL and de Boer RJ. Implications of CTL-mediated killing of HIV-infected

cells during the non-productive stage of infection. PLoS One 2011;6(2):e16468. (Cited on pages 6, 114, 115, and 118.)

[33] Merrill SJ. Foundations of the use of an enzyme-kinetic analogy in cell-mediated cytotoxicity. Math Biosci 1982;62(2):219 – 235. (Cited on pages 6, 8, 13, 19, 21, 25, 27, 30, 42, 59, and 100.)

[34] Beddington J. Mutual interference between parasites or predators and its effect on searching efficiency. J Anim Ecol 1975;44(1):331–340. (Cited on pages 6 and 21.)

[35] Segel LA. On the validity of the steady state assumption of enzyme kinetics. Bull Math Biol 1988;50(6):579–593. (Cited on pages 6 and 7.)

[36] Wiedemann A, Depoil D, Faroudi M, and Valitutti S. Cytotoxic T lymphocytes kill multiple targets simultaneously via spatiotemporal uncoupling of lytic and stimulatory synapses. Proc Natl Acad Sci USA 2006;103(29):10985–10990. (Cited on pages 8, 13, 19, 25, and 31.)

[37] Caramalho Í, Faroudi M, Padovan E, Müller S, and Valitutti S. Visualizing CTL/melanoma cell interactions: multiple hits must be delivered for tumour cell annihilation. J Cell Mol Med 2009;13(9b):3834–3846. (Cited on pages 8, 13, 19, 21, and 101.)

[38] Dougan M and Dranoff G. Immune therapy for cancer. Annu Rev Immunol 2009; 27:83–117. (Cited on pages 13 and 90.)

[39] Morgan RA, Dudley ME, Wunderlich JR, Hughes MS, Yang JC, Sherry RM, Royal RE, Topalian SL, Kammula US, Restifo NP, Zheng Z, Nahvi A, de Vries CR, Rogers-Freezer LJ, Mavroukakis SA, and Rosenberg SA. Cancer regression in patients after transfer of genetically engineered lymphocytes. Science 2006;314(5796):126–129. (Cited on pages 13 and 90.)

[40] Rosenberg SA, Packard BS, Aebersold PM, Solomon D, Topalian SL, Toy ST, Simon P, Lotze MT, Yang JC, Seipp CA, Simpson C, Carter C, Bock S, Schwartzentruber D, Wei JP, and White DE. Use of tumor-infiltrating lymphocytes and interleukin-2 in the immunotherapy of patients with metastatic melanoma. New Engl J Med 1988;319(25):1676–1680. (Cited on pages 13 and 90.)

[41] Schmidt NW, Butler NS, Badovinac VP, and Harty JT. Extreme CD8 T cell requirements for anti-malarial liver-stage immunity following immunization with radiation attenuated sporozoites. PLoS Pathog 2010;6(7):e1000998. (Cited on page 13.)

[42] Schmidt NW, Podyminogin RL, Butler NS, Badovinac VP, Tucker BJ, Bahjat KS, Lauer P, Reyes-Sandoval A, Hutchings CL, Moore AC, Gilbert SC, Hill AV, Bartholomay LC, and Harty JT. Memory CD8 T cell responses exceeding a large but definable threshold provide long-term immunity to malaria. Proc Natl Acad Sci USA 2008;105(37):14017–14022. (Cited on page 13.)

[43] Glazier JA and Graner F. Simulation of the differential adhesion driven rearrangement of biological cells. Phys Rev E 1993;47(3):2128–2154. (Cited on pages 13,

17, 54, and 55.)

[44] Graner F and Glazier JA. Simulation of biological cell sorting using a two-dimensional extended potts model. Phys Rev Lett 1992;69(13):2013–16. (Cited on pages 13, 17, 54, and 55.)

[45] Beltman JB, Marée AFM, Lynch JN, Miller MJ, and de Boer RJ. Lymph node topology dictates T cell migration behavior. J Exp Med 2007;204(4):771–780. (Cited on pages 14, 15, 18, 19, 55, 65, 95, and 104.)

[46] Beltman JB, Marée AFM, and de Boer RJ. Spatial modelling of brief and long interactions between T cells and dendritic cells. Immunol Cell Biol 2007;85(4):306–14. (Cited on pages 14, 15, 18, 19, and 55.)

[47] Katakai T, Hara T, Sugai M, Gonda H, and Shimizu A. Lymph node fibroblastic reticular cells construct the stromal reticulum via contact with lymphocytes. J Exp Med 2004;200(6):783–795. (Cited on page 14.)

[48] Miller MJ, Wei SH, Parker I, and Cahalan MD. Two-photon imaging of lymphocyte motility and antigen response in intact lymph node. Science 2002; 296(5574):1869–1873. (Cited on pages 14 and 15.)

[49] Parkhurst M and Saltzman W. Quantification of human neutrophil motility in three-dimensional collagen gels: Effect of collagen concentration. Biophys J 1992; 61(2):306–15. (Cited on pages 15 and 35.)

[50] Mrass P, Takano H, Ng LG, Daxini S, Lasaro MO, Iparraguirre A, Cavanagh LL, von Andrian UH, Ertl HCJ, Haydon PG, and Weninger W. Random migration precedes stable target cell interactions of tumor-infiltrating T cells. J Exp Med 2006;203(12):2749–61. (Cited on page 15.)

[51] Sumen C, Mempel TR, Mazo IB, and von Andrian UH. Intravital microscopy: Visualizing immunity in context. Immunity 2004;21(3):315 – 329. (Cited on pages 15, 56, and 95.)

[52] Huisman G and de Boer RJ. A formal derivation of the "Beddington" functional response. J Theor Biol 1997;185(3):389 – 400. (Cited on page 21.)

[53] Schnell S and Maini PK. Enzyme kinetics at high enzyme concentration. Bull Math Biol 2000;62(3):483–99. (Cited on page 21.)

[54] Malka R, Wolach B, Gavrieli R, Shochat E, and Rom-Kedar V. Evidence for bistable bacteria-neutrophil interaction and its clinical implications. J Clin Invest 2012; 122(8):3002–3011. (Cited on pages 31, 100, and 101.)

[55] Gadhamsetty S, Marée AF, Beltman JB, and de Boer RJ. A general functional response of cytotoxic T lymphocyte-mediated killing of target cells. Biophys J 2014;106(8):1780–1791. (Cited on pages 42, 43, 44, 45, 46, 47, 48, 49, 51, 54, 55, 59, 60, 63, 65, 66, 77, 78, 83, 86, 90, 91, 92, 96, 98, 100, 102, and 103.)

[56] Hickman H, Reynoso G, Ngudiankama B, Cush S, Gibbs J, Bennink J, and Yewdell J. CXCR3 chemokine receptor enables local CD8+ T cell migration for the destruction of virus-infected cells. Immunity 2015;42(3):524 – 537. (Cited on page 49.)

[57] Brodie SJ, Lewinsohn DA, Patterson BK, Jiyamapa D, Krieger J, Corey L, Greenberg PD, and Riddell SR. In vivo migration and function of transferred HIV-1-specific cytotoxic T cells. Nat Med 1999;5:34–41. (Cited on pages 54, 65, 117, and 118.)

[58] Marée AFM and Hogeweg P. How amoeboids self-organize into a fruiting body: multicellular coordination in Dictyostelium discoideum. Proc Natl Acad Sci USA 2001;98(7):3879–83. (Cited on page 65.)

[59] Vroomans RMA, Hogeweg P, and ten Tusscher KHWJ. Segment-specific adhesion as a driver of convergent extension. PLoS Comput Biol 2015;11(2):e1004092. (Cited on page 65.)

[60] Ochalek T, Nordt FJ, Tullberg K, and Burger MM. Correlation between cell deformability and metastatic potential in B16-F1 melanoma cell variants. Cancer Res 1988;48(18):5124–5128. (Cited on pages 67, 81, and 82.)

[61] Gunzer M, Schäfer A, Borgmann S, Grabbe S, Zänker KS, Bröcker EB, Kämpgen E, and Friedl P. Antigen presentation in extracellular matrix: Interactions of T cells with dendritic cells are dynamic, short lived, and sequential. Immunity 2000; 13(3):323 – 332. (Cited on page 77.)

[62] Freedman VH, Gorrell TE, Nathan CF, Copeland CS, and Silverstein SC. Bacillus calmette-guérin-activated murine macrophages kill syngeneic melanoma cells under strict anaerobic conditions. J Exp Med 1984;160(1):94–107. (Cited on pages 78 and 87.)

[63] Mrass P, Kinjyo I, Ng LG, Reiner SL, Puré E, and Weninger W. CD44 mediates successful interstitial navigation by killer T cells and enables efficient antitumor immunity. Immunity 2008;29(6):971 – 985. (Cited on page 82.)

[64] Deguine J, Breart B, Lemaître F, Santo JPD, and Bousso P. Intravital imaging reveals distinct dynamics for natural killer and CD8+ T cells during tumor regression. Immunity 2010;33(4):632 – 644. (Cited on page 82.)

[65] Wolf K, te Lindert M, Krause M, Alexander S, te Riet J, Willis AL, Hoffman RM, Figdor CG, Weiss SJ, and Friedl P. Physical limits of cell migration: Control by ECM space and nuclear deformation and tuning by proteolysis and traction force. J Cell Biol 2013;201(7):1069–1084. (Cited on page 82.)

[66] Dustin ML and Long EO. Cytotoxic immunological synapses. Immunol Rev 2010; 235(1):24–34. (Cited on pages 86 and 95.)

[67] Deguine J, Breart B, Lemaître F, Di Santo JP, and Bousso P. Intravital imaging reveals distinct dynamics for natural killer and CD8(+) T cells during tumor regression. Immunity 2010;33(4):632–44. (Cited on page 101.)

[68] DeVico AL and Gallo RC. Control of HIV-1 infection by soluble factors of the immune response. Nat Rev Microbiol 2004;2(5):401–413. (Cited on page 108.)

[69] Saunders KO, Ward-Caviness C, Schutte RJ, Freel SA, Overman RG, Thielman NM, Cunningham CK, Kepler TB, and Tomaras GD. Secretion of MIP-1beta and MIP-1alpha by $CD8^+$ T-lymphocytes correlates with HIV-1 inhibition independent of coreceptor usage. Cell Immunol 2011;266(2):154–164. (Cited on page 108.)

[70] Ho DD, Neumann AU, Perelson AS, Chen W, Leonard JM, and Markowitz M. Rapid turnover of plasma virions and CD4 lymphocytes in HIV-1 infection. Nature 1995; 373(4):123–126. (Cited on pages 108 and 111.)

[71] Wei X, Ghosh SK, Taylor ME, Johnson VA, Emini EA, Deutsch P, Lifson JD, Bonhoeffer S, Nowak MA, Hahn BH, Saag MS, and Shaw GM. Viral dynamics in human-immunodeficiency-virus type-1 infection. Nature 1995;373(6510):117–22. (Cited on pages 108, 111, and 114.)

[72] Klatt NR, Shudo E, Ortiz AM, Engram JC, Paiardini M, Lawson B, Miller MD, Else J, Pandrea I, Estes JD, Apetrei C, Schmitz JE, Ribeiro RM, Perelson AS, and Silvestri G. CD8+ lymphocytes control viral replication in SIVmac239-infected rhesus macaques without decreasing the lifespan of productively infected cells. PLoS Pathog 2010;6(1):e1000747. (Cited on pages 108, 112, 113, 115, and 117.)

[73] Wong JK, Strain MC, Porrata R, Reay E, Sankaran-Walters S, Ignacio CC, Russell T, Pillai SK, Looney DJ, and Dandekar S. In vivo CD8+ T-cell suppression of SIV viremia is not mediated by CTL clearance of productively infected cells. PLoS Pathog 2010;6(1):e1000748. (Cited on pages 108, 112, and 117.)

[74] Elemans M, Seich Al Basatena NK, Klatt NR, Gkekas C, Silvestri G, and Asquith B. Why don't CD8+ T cells reduce the lifespan of SIV-infected cells in vivo? PLoS Comput Biol 2011;7(9):e1002200. (Cited on pages 108, 115, 117, and 118.)

[75] Seich Al Basatena NK, Chatzimichalis K, Graw F, Frost SD, Regoes RR, and Asquith B. Can non-lytic $CD8^+$ T cells drive HIV-1 escape? PLoS Pathog 2013; 9(11):e1003656. (Cited on pages 108 and 109.)

[76] Little SJ, McLean AR, Spina CA, Richman DD, and Havlir DV. Viral dynamics of acute HIV-1 infection. The Journal of Experimental Medicine 1999;190(6):841–850. (Cited on pages 108 and 117.)

[77] Davenport MP, Ribeiro RM, and Perelson AS. Kinetics of virus-specific CD8+ T cells and the control of human immunodeficiency virus infection. J Virol 2004; 78(18):10096–103. (Cited on pages 108 and 117.)

[78] Nowak MA, Lloyd AL, Vasquez GM, Wiltrout TA, Wahl LM, Bischofberger N, Williams J, Kinter A, Fauci AS, Hirsch VM, and Lifson JD. Viral dynamics of primary viremia and antiretroviral therapy in simian immunodeficiency virus infection. J Virol 1997;71(10):7518–7525. (Cited on pages 108 and 117.)

[79] Murray JM, Emery S, Kelleher AD, Law M, Chen J, Hazuda DJ, Nguyen BYT, Teppler H, and Cooper DA. Antiretroviral therapy with the integrase inhibitor raltegravir alters decay kinetics of HIV, significantly reducing the second phase. AIDS 2007;21(17):2315–21. (Cited on page 108.)

[80] Markowitz M, Louie M, Hurley A, Sun E, Di Mascio M, Perelson AS, and Ho DD. A novel antiviral intervention results in more accurate assessment of human immunodeficiency virus type 1 replication dynamics and T-cell decay in vivo. J Virol 2003;77(8):5037–5038. (Cited on pages 108, 109, 111, and 112.)

[81] Bonhoeffer S, Funk GA, Günthard HF, Fischer M, and Müller V. Glancing behind

virus load variation in hiv-1 infection. Trends in Microbiology 2003;11(11):499 – 504. (Cited on pages 108 and 112.)

[82] Elemans M, Seich Al Basatena NK, and Asquith B. The efficiency of the human CD8+ T cell response: How should we quantify it, what determines it, and does it matter? PLoS Comput Biol 2012;8(2):e1002381. (Cited on pages 108 and 114.)

[83] Liu D, Zuo T, Hora B, Song H, Kong W, Yu X, Goonetilleke N, Bhattacharya T, Perelson AS, Haynes BF, McMichael AJ, and Gao F. Preexisting compensatory amino acids compromise fitness costs of a HIV-1 T cell escape mutation. Retrovirology 2014;11(1):101. (Cited on pages 109 and 110.)

[84] Song H, Hora B, Bhattacharya T, Goonetilleke N, Liu MK, Wiehe K, Li H, Iyer SS, McMichael AJ, Perelson AS, and Gao F. Reversion and T cell escape mutations compensate the fitness loss of a $CD8^+$ T cell escape mutant in their cognate transmitted/founder virus. PLoS One 2014;9(7):e102734. (Cited on pages 109 and 110.)

[85] Song H, Pavlicek JW, Cai F, Bhattacharya T, Li H, Iyer SS, Bar KJ, Decker JM, Goonetilleke N, Liu MK, Berg A, Hora B, Drinker MS, Eudailey J, Pickeral J, Moody MA, Ferrari G, McMichael A, Perelson AS, Shaw GM, Hahn BH, Haynes BF, and Gao F. Impact of immune escape mutations on HIV-1 fitness in the context of the cognate transmitted/founder genome. Retrovirology 2012;9(1):89. (Cited on pages 109 and 110.)

[86] Ganusov VV and de Boer RJ. Estimating costs and benefits of CTL escape mutations in SIV/HIV infection. PLoS Comput Biol 2006;2(3):182–187. (Cited on page 109.)

[87] Chopera DR, Woodman Z, Mlisana K, Mlotshwa M, Martin DP, Seoighe C, Treurnicht F, De Rosa DA, Hide W, Karim SA, Gray CM, and Williamson C. Transmission of HIV-1 CTL escape variants provides HLA-mismatched recipients with a survival advantage. PLoS Pathog 2008;4(3):e1000033. (Cited on pages 109 and 110.)

[88] Goonetilleke N, Liu MK, Salazar-Gonzalez JF, Ferrari G, Giorgi E, Ganusov VV, Keele BF, Learn GH, Turnbull EL, Salazar MG, Weinhold KJ, Moore S, Letvin N, Haynes BF, Cohen MS, Hraber P, Bhattacharya T, Borrow P, Perelson AS, Hahn BH, Shaw GM, Korber BT, and McMichael AJ. The first T cell response to transmitted/founder virus contributes to the control of acute viremia in HIV-1 infection. J Exp Med 2009;206(6):1253–72. (Cited on page 109.)

[89] Ganusov VV, Goonetilleke N, Liu MK, Ferrari G, Shaw GM, McMichael AJ, Borrow P, Korber BT, and Perelson AS. Fitness costs and diversity of the cytotoxic T lymphocyte (CTL) response determine the rate of CTL escape during acute and chronic phases of HIV infection. J Virol 2011;85(20):10518–10528. (Cited on pages 109, 110, and 111.)

[90] Liu MK, Hawkins N, Ritchie AJ, Ganusov VV, Whale V, Brackenridge S, Li H, Pavlicek JW, Cai F, Rose-Abrahams M, Treurnicht F, Hraber P, Riou C, Gray C, Ferrari G, Tanner R, Ping LH, Anderson JA, Swanstrom R, Cohen M, Karim SS, Haynes B, Borrow P, Perelson AS, Shaw GM, Hahn BH, Williamson C, Korber BT,

Gao F, Self S, McMichael A, and Goonetilleke N. Vertical T cell immunodominance and epitope entropy determine HIV-1 escape. J Clin Invest 2013;123(1):380–393. (Cited on page 109.)

[91] Roberts HE, Hurst J, Robinson N, Brown H, Flanagan P, Vass L, Fidler S, Weber J, Babiker A, Phillips RE, McLean AR, and Frater J. Structured Observations Reveal Slow HIV-1 CTL Escape. PLoS Genet 2015;11(2):e1004914. (Cited on pages 109 and 110.)

[92] Ganusov VV, Neher RA, and Perelson AS. Mathematical modeling of escape of HIV from cytotoxic T lymphocyte responses. J Stat Mech 2013;2013:P01010. (Cited on pages 110 and 111.)

[93] Miralles R, Gerrish PJ, Moya A, and Elena SF. Clonal interference and the evolution of RNA viruses. Science 1999;285(5434):1745–1747. (Cited on page 110.)

[94] Strelkowa N and Lässig M. Clonal interference in the evolution of influenza. Genetics 2012;192(2):671–82. (Cited on page 110.)

[95] Leviyang S. Computational inference methods for selective sweeps arising in acute HIV infection. Genetics 2013;194(3):737–752. (Cited on pages 110 and 111.)

[96] Kessinger TA, Perelson AS, and Neher RA. Inferring HIV Escape Rates from Multi-Locus Genotype Data. Front Immunol 2013;4(September):252. (Cited on pages 110 and 111.)

[97] Leviyang S. Constructing lower-bounds for CTL escape rates in early SIV infection. J theor Biol 2014;352:82–91. (Cited on pages 110 and 111.)

[98] Garcia V and Regoes RR. The effect of interference on the CD8+ T cell escape rates in HIV. Front Immunol 2015;5(661). (Cited on pages 110 and 111.)

[99] Althaus CL and de Boer RJ. Dynamics of immune escape during HIV/SIV infection. PLoS Comput Biol 2008;4(7):e1000103. (Cited on pages 110 and 111.)

[100] Henn MR, Boutwell CL, Charlebois P, Lennon NJ, Power KA, Macalalad AR, Berlin AM, Malboeuf CM, Ryan EM, Gnerre S, Zody MC, Erlich RL, Green LM, Berical A, Wang Y, Casali M, Streeck H, Bloom AK, Dudek T, Tully D, Newman R, Axten KL, Gladden AD, Battis L, Kemper M, Zeng Q, Shea TP, Gujja S, Zedlack C, Gasser O, Brander C, Hess C, Gunthard HF, Brumme ZL, Brumme CJ, Bazner S, Rychert J, Tinsley JP, Mayer KH, Rosenberg E, Pereyra F, Levin JZ, Young SK, Jessen H, Altfeld M, Birren BW, Walker BD, and Allen TM. Whole genome deep sequencing of HIV-1 reveals the impact of early minor variants upon immune recognition during acute infection. PLoS Pathog 2012;8(3):e1002529. (Cited on pages 110 and 111.)

[101] Pandit A and de Boer RJ. Reliable reconstruction of HIV-1 whole genome haplotypes reveals clonal interference and genetic hitchhiking among immune escape variants. Retrovirology 2014;11(1):56. (Cited on pages 110 and 111.)

[102] van Deutekom HW, Wijnker G, and de Boer RJ. The rate of immune escape vanishes when multiple immune responses control an HIV infection. J Immunol 2014; 191:3277–3286. (Cited on pages 111 and 116.)

[103] Radebe M, Gounder K, Mokgoro M, Ndhlovu ZM, Mncube Z, Mkhize L, van der Stok M, Jaggernath M, Walker BD, and Ndung'u T. Broad and persistent Gag-specific CD8+ T-cell responses are associated with viral control but rarely drive viral escape during primary HIV-1 infection. AIDS 2015;29(1):23–33. (Cited on page 111.)

[104] Bonhoeffer S, May RM, Shaw GM, and Nowak MA. Virus dynamics and drug therapy. Proc Natl Acad Sci USA 1997;94(13):6971–6976. (Cited on pages 111 and 115.)

[105] Perelson AS, Essunger P, Cao Y, Vesanen M, Hurley A, Saksela K, Markowitz M, and Ho DD. Decay characteristics of HIV-1-infected compartments during combination therapy. Nature 1997;387:188–91. (Cited on page 111.)

[106] Dixit NM, Markowitz M, Ho DD, and Perelson AS. Estimates of intracellular delay and average drug efficacy from viral load data of HIV-infected individuals under antiretroviral therapy. Antivir Ther 2004;9(2):237–246. (Cited on page 112.)

[107] Sacha JB, Buechler MB, Newman LP, Jason R, Wallace LT, Loffredo JT, A WN, and I WD. Simian immunodeficiency virus-specific CD8+ T cells recognize Vpr- and Rev-derived epitopes early after infection. J Virol 2010;84(20):10907–10912. (Cited on page 113.)

[108] Perelson AS, Neumann AU, Markowitz M, Leonard JM, and Ho DD. HIV-1 dynamics in vivo: Virion clearance rate, infected cell life-span, and viral generation time. Science 1996;271(5255):1582–86. (Cited on page 114.)

[109] de Boer RJ. Understanding the failure of CD8+ T-cell vaccination against simian/human immunodeficiency virus. J Virol 2007;81(6):2838–48. (Cited on page 116.)

[110] Funk GA, Fischer M, Joos B, Opravil M, Günthard HF, Ledergerber B, and S B. Quantification of in vivo replicative capacity of HIV-1 in differrent compartments of infected cells. J Acq Imm Def Syn 2001;26:397–404. (Cited on page 115.)

[111] Grosssman Z, Feinberg M, Kuznetsov V, Dimitrov D, and Paul W. HIV infection: how effective is drug combination treatment? Immnol Today 1998;19(11):528–32. (Cited on page 115.)

[112] Althaus CL, Joos B, Perelson AS, and Günthard HF. Quantifying the turnover of transcriptional subclasses of HIV-1-infected cells. PLoS Comput Biol 2014; 10(10):e1003871. (Cited on page 115.)

[113] Schmitz JE, Kuroda MJ, Santra S, Sasseville VG, Simon MA, Lifton MA, Racz P, Tenner-Racz K, Dalesandro M, Scallon BJ, Ghraye J, Forman MA, Montefiori D, Peter Rieber E, Letvin NL, and Reimann KA. Control of viremia in simian immunodeficiency virus infection by CD8+ lymphocytes. Science 1999;283(5403):857–60. (Cited on page 117.)

[114] Jin X, Bauer DE, Tuttleton SE, Lewin S, Gettie A, Blanchard J, Irwin CE, Safrit JT, Mittler J, Weinberger L, Kostrikis LG, Zhang L, Perelson AS, and Ho DD. Dramatic rise in plasma viremia after CD8+ T cell depletion in simian immunodeficiency

virus-infected macaques. J Exp Med 1999;189(6):991–998. (Cited on page 117.)

[115] Davenport MP, Zhang L, Bagchi A, Fridman A, Fu Tm, Schleif W, Shiver JW, and Ribeiro AS Ruy M Perelson. High-potency human immunodeficiency virus vaccination leads to delayed and reduced $CD8^+$ T-cell expansion but improved virus control 2005;79(15):10059–10062. (Cited on page 117.)

[116] Chea S, Dale CJ, de Rose R, Ramshaw IA, and Kent SJ. Enhanced cellular immunity in macaques following a novel peptide immunotherapy. J Virol 2005; 79(6):3748–3757. (Cited on page 117.)

[117] Fukazawa Y, Lum R, Okoye AA, Park H, Matsuda K, Bae JY, Hagen SI, Shoemaker R, Deleage C, Lucero C, Morcock D, Swanson T, Legasse AW, Axthelm MK, Hesselgesser J, Geleziunas R, Hirsch VM, Edlefsen PT, Piatak M Jr, Estes JD, Lifson JD, and Picker LJ. B cell follicle sanctuary permits persistent productive simian immunodeficiency virus infection in elite controllers. Nat Med 2015;21(2):132–139. (Cited on page 117.)

Summary

Cytotoxic T lymphocytes (CTLs) are cells of the immune system that continuously search for and kill virus-infected and tumor cells, and thus play an important role in the control of viral infections and tumors. An important parameter in determining the efficiency of CTL-mediated control is the rate at which a CTL kills target cells and how it varies with CTL and target cell densities, which is referred to as functional response of CTL-mediated killing. There have been numerous attempts to quantify the CTL-mediated killing rates involving different pathogens and tumors, using different experimental setups. However, there is no clear agreement on how the CTL-mediated killing rates vary with CTL and target cell densities.

In this thesis, I investigate what is the general functional response of CTL-mediated killing, and how do different factors alter this functional response. To this end, I employ computational and mathematical models, and analysis of experimental data to determine the general functional response that is applicable over a wide range of conditions. I first aim to determine the general functional response resulting from different CTL-target cell interactions (Chapter 2) using simulations of CTL-mediated killing of target cells in two-dimensional environments. I consider four simple scenarios of such cellular interactions that differ in the types of CTL-target conjugates allowed. For all the scenarios I find that the CTL-mediated killing saturates both with increasing CTL and target cell densities, and the relative extent of saturation depends on the nature of the CTL-target interactions. Furthermore, I show that CTL-mediated killing resulting from the simulations of all the CTL-target cell interactions can be well described by a double saturation (DS) model with two different saturation constants—one for saturation in CTLs and the other for saturation in target cells.

In Chapter 3, I examine how the stability of the synapses between CTLs and target cells affects the functional response of CTL-mediated killing. For this purpose, I consider that target cells are killed when their accumulated 'killing signal' from short-living synapses reaches a threshold (i.e., equivalent to multi-stage killing). I find that the killing rate in this case saturates at much higher CTL and target cell densities as compared to when synapses are stable. Therefore for a given killing time, CTL killing rate decreases as the synapses become less stable. Next in Chapter 4, I compare the CTL-mediated killing in the 2D-like and 3D spatial environments, and find that the CTL-mediated killing in 3D

environments is more efficient than in 2D as the CTLs are in contact with more target cells at any given time.

After building the expectation for the general functional response using computational models, I examine the data from *in vitro* cytotoxicity assays in collagen-gels to determine the CTL-mediated killing rates and the mechanisms of CTL-target interactions. I analyze data from two independent experiments of CTL-mediated killing in collagen-fibrin gels: killing of melanoma cells that are homogeneously distributed in the gels (Chapter 5), and killing of BOK cells that exists as a mono-layer in the gels (Chapter 6). I argue that the DS model with more pronounced saturation in CTL densities is the best descriptor of the CTL-mediated killing in both the experimental systems. Furthermore, I perform simulations that mimic these experiments and identify several mechanisms that reverse the saturation, namely to saturate strongly in target cell densities.

In Chapter 7, I focus on the extent of CTL-mediated control of HIV-1-infection. I compile published estimates of CTL-mediated death rates during HIV-1-infection, and examine whether these studies permit determining the rate at which CTLs kill HIV-1 infected cells. I highlight potential misinterpretations of the CTL-killing rates from the escape rates of mutants, and from perturbations of the steady state viral load during chronic infection. Our major conclusion is that CTL-mediated killing rates remain unknown. But contrary to current consensus, I argue that CTLs killing a majority of the productively infected cells is perfectly consistent with the experimental data.

Taken together, the results in this thesis together suggest that the double saturation model is a generic model that can describe CTL-mediated killing over a wide range of conditions; and this work sheds light on the difficulties associated with inferring the CTL-mediated killing rates and the CTL-target cell interactions from the cytotoxicity assays.

Samenvatting

Cytotoxische T lymfocyten (CTLs) zijn cellen van het immuunsysteem die geïnfecteerde cellen en tumorcellen opsporen en doden. De snelheid waarmee CTLs deze afwijkende cellen doden, oftewel de functionele respons, wordt bepaald door zowel de dichtheid van CTLs als die van de afwijkende cellen ("target cellen"). Er zijn al veel pogingen gedaan om deze snelheid te bepalen in de aanwezigheid van verscheidene pathogenen en tumoren, en met verschillende experimentele opstellingen. Uit deze experimenten is echter nog geen eenduidig beeld ontstaan van hoe de functionele respons precies afhangt van het aantal CTLs en dichtheid van target cellen.

In dit proefschrift onderzoek ik de algemene functionele respons van CTL-gedreven vernietiging van target cellen, en kijk ik naar hoe verschillende factoren deze respons beïnvloeden. Ik gebruik computationele en wiskundige modellen om een algemene functionele respons te vinden die breed van toepassing is. Daarnaast analyseer ik experimentele data en test welke vorm van de functionele respons de experimentele data het beste beschrijft en wat dit ons leert over interacties tussen CTL en target cellen.

In hoofdstuk 3 bepaal ik allereerst hoe de algemene functionele respons afhangt van het type interactie tussen CTLs en target cellen; hiervoor gebruik ik simulaties van CTLs en target cellen in een 2-dimensionale modelomgeving. Ik bestudeer vier eenvoudige scenario's die verschillen in het aantal mogelijke verbindingen tussen CTLs en target cellen. Mijn simulaties tonen aan dat in alle scenario's het vernietigen van target cellen verzadigt met zowel het aantal CTLs als het aantal target cellen, maar dat de vorm van de verzadiging wel afhangt van het soort interactie tussen CTL en target cel. Verder laat ik zien dat de functionele respons in alle simulaties goed kan worden beschreven met een model met twee verschillende saturatie constanten (het dubbele saturatie (DS) model) - de één voor de verzadiging in het aantal CTLs en de ander voor de verzadiging in het aantal target cellen.

Na deze algemene beschrijving van de functionele respons, onderzoek ik in hoofdstuk 3 hoe de functionele respons specifiek afhangt van de stabiliteit van de verbindingen (synapsen) die gevormd worden tussen CTLs en target cellen. De target cellen worden vernietigd als zij in totaal voldoende 'vernietigingssignaal' hebben ontvangen, ofwel van een stabiele synaps ofwel van meerdere opeenvolgende kortdurende synapsen. De snel-

heid van vernietiging verzadigt bij een veel hogere CTL en target cel dichtheid als er slechts kortdurende synapsen worden gevormd dan wanneer de synapsen stabiel zijn. Dit verklaart waarom de snelheid van vernietiging omlaag gaat als de synapsen minder stabiel zijn. In hoofdstuk 4 vergelijk ik vervolgens de functionele respons in 2D en 3D weefsels, en laat zien dat CTL-gedreven vernietiging efficiënter is in 3D omdat de CTLs dan met meer target cellen tegelijk in contact kunnen zijn.

Na de functionele respons met modellen te hebben gekarakteriserd, onderzoek ik data van *in vitro* cytotoxiciteits analyses in collageen gels om hieruit de vernietigingssnelheid van CTLs te bepalen, en vast te stellen welk type CTL-target cel interacties er plaatsvindt. Ik bestudeer twee onafhankelijke experimenten: de vernietiging van melanoomcellen die homogeen verdeeld zijn in de gel (hoofdstuk 5) en de vernietiging van BOK cellen die een enkele laag vormen op de bodem van de gel (hoofdstuk 6). Het DS model met een sterkere verzadiging als functie van CTL dan van de target cel dichtheid blijkt de resultaten van beide experimenten zeer goed te beschrijven. In mijn simulaties uit Hoofdstuk 2-4 treedt zo'n vroege verzadiging van de functionele respons ook op wanneer CTLs meerdere target cellen tegelijk doden. Het blijft helaas onduidelijk of dit ook daadwerkelijk plaatsvindt in de experimenten. In parallel heb ik de experimenten waarin de target cellen een enkele laag vormen in realistische simulaties nagebootst. Deze simulaties voorspellen juist het omgekeerde van wat de experimentele data laten zien, namelijk een sterkere verzadiging van de vernietigingssnelheid als functie van de target cel dan van de CTL dichtheid. Ik beschrijf een aantal mechanismen die dit omgekeerde resultaat kunnen verklaren.

In hoofdstuk 7 focus ik op de rol van CTLs in het beheersen van HIV-1 infecties. Ik verzamel gepubliceerde schattingen van CTL-gedreven vernietigingssnelheden tijdens een HIV-1 infectie, en onderzoek of deze studies het mogelijk maken om de snelheid te bepalen waarmee CTLs de geïnfecteerde cellen doden. Ik breng mogelijke misinterpretaties van de vernietigingssnelheid aan het licht, zoals wanneer deze geschat wordt met behulp van de snelheid waarmee HIV mutanten ontstaan die het immuunsysteem ontduiken, of met behulp van experimenten die de hoeveelheid virus verstoren tijdens een chronische infectie. Onze voornaamste conclusie is dat door al deze haken en ogen de snelheid waarmee CTLs HIV-geinfecteerde cellen vernietigen erg onzeker is. In tegenstelling tot de huidige consensus, beargumenteer ik dat de experimentele data in overeenstemming zijn met de hypothese dat het merendeel van de geïnfecteerde cellen sterft door toedoen van CTLs.

Al met al suggereren de resultaten in dit proefschrift dat het dubbele saturatie model van algemene toepassing is op het vernietigen van target cellen door CTLs in een brede reeks van omstandigheden. Verder brengt mijn werk de moeilijkheden boven tafel die komen kijken bij het bepalen van de vernietigingssnelheid en de interacties tussen CTLs en target cellen uit cytotoxiciteits analyses.

Curriculum Vitae

Saikrishna Gadhamsetty was born in Nellore, India, on December 5th 1985. In 2007, he received his bachelor diploma in chemical engineering from Osmania University, Hyderabad, India. He then enrolled to master program in chemical engineering at Indian Institute of Science (IISc), Bangalore, India. Under the supervision of Dr. Narendra M. Dixit, he studied for his master thesis the evolution drug resistant mutants in HIV-infected individuals. After defending his master thesis in 2009, he briefly worked as a junior research fellow in the group of Dr. Narendra M. Dixit, IISc.

In April 2010, he started his PhD research at the Theoretical Biology and Bioinformatics group at Utrecht University, under the supervision of Prof. dr. Rob J. de Boer and Dr. Joost B. Beltman. During his PhD, he studied what is the general functional response of CTL-mediated killing and how various factors influence it. The results of his PhD research are described in this thesis.

List of Publications

Gadhamsetty S, Marée AFM, Beltman JB, de Boer RJ. Determinants of the functional response of cytotoxic T lymphocyte-mediated killing. *In preparation*

Gadhamsetty S, Marée AFM, Beltman JB, de Boer RJ. Tissue dimensionality influences the functional response of cytotoxic T lymphocyte mediated killing. *In preparation*

Gadhamsetty S, Beltman JB, Ganusov VV, Budhu S, Silverstein SC, de Boer RJ. Quantifying the cytotoxic T lymphocyte killing rate of B16 melanoma cells in collagen-fibrin gels. *In preparation*

Gadhamsetty S, Dieteren C, Beltman JB, Friedl P, de Boer RJ. Cytotoxic T lymphocyte-mediated killing of tumor cells in collagen gels saturates strongly with CTL density. *In preparation*

Gadhamsetty S, Beltman JB, de Boer RJ. What do mathematical models tell us about cytotoxic T lymphocyte-mediated killing rates during HIV-infection? (2015) *Immunol Lett.* (Review in press)

Gadhamsetty S, Marée AFM, Beltman JB, de Boer RJ. A general functional response of cytotoxic T lymphocyte-mediated killing of target cells. (2014) *Biophys J.* Apr;106(8):1780-91.

Gadhamsetty S, Dixit NM. Estimating Frequencies of minority nevirapine-resistant strains in chronically HIV-1-infected individuals naïve to nevirapine by using stochastic simulations and a mathematical model. (2010) *J Virol.* Oct;84(19):10230-40.

Acknowledgements

During my five years of PhD here in Utrecht, there are lots of people who helped me in one way or another; I consider myself lucky for having been surrounded by amazing people. Since acknowledgements should not be longer than the chapters of my thesis, I will try to keep it short (relatively).

First of all, my deep gratitude goes to my supervisors Rob and Joost. Your support has been incredible all these years, and you both guided me through many hurdles during my PhD years (and there was no shortage of them).

Rob, you taught me how to qualitatively understand the effect of a mechanism before examining it in detail and how to show model assumptions in a better light. I loved to brainstorm and discuss with you (and to debate the choice between δ or d_P) and I always looked forward to our Wednesday meetings. You always made time for me, even during weekends and traveling, without which I could not have finished my thesis in time. You have set for me a good example of a supervisor. Thank you for forwarding all the mails about potential employment opportunities, for helping me solve my visa troubles, and for finding funding sources (so that I can finish my PhD without breaking myself). In short, I could not have asked for a better PhD *promotor*.

Joost, I loved the discussions and debates with you, and you taught me to critically analyze hypotheses (we required a lot of them for Chapter 5). I like very much the way you come up with new mechanisms to explain many of the surprising, difficult results. I appreciate your help with the simulations. We managed to find solutions to work and communicate from different locations (Utrecht and Leiden)—thank you for taking time to meet in the city and to read and edit many drafts of my thesis. I wish you success with your new group at Leiden.

I have been in this group for more than 5 years. It amazes me how fast time flies in TBB: Discussions over coffee, meticulously prepared dinners, drinks to welcome new members, and basking in the sun. Thank you Paulien, Can, Berend, Ronald, Kirsten, Jan Kees, Rutger, and Bas. You all made this group and my experience here wonderful. Jan Kees, you made the machines so reliable that we never have to worry about months-long simulations; you are a *genie* to this group! Thank you very much for keeping a close

watch on failing hard disks, for persuading people to clear the *mutants*, for wonderful discussions (under sun). I hope that the next-generation PhD students will be better organized and will clean up their 'act' on the *mutants*.

I would like to thank Paola and Lidija, my paranymphs, for bearing, beering, and burgering with me, and for looking out for me at all times. We have spent considerable amount of time together, from the times of Paulien's course to recent times of being lazy last year PhD students (LLYPS). It was wonderful to sail with you in the ship of LLYPS, and I am very happy that we never learned to keep the promise 'one-drink at *The Basket*, just one'. Paola, there are innumerable things to thank you for, to name a few, 'be there' parties, Christmas dinners, cakes on random fridays, your assurances, and your secrets of thesis writing. I am not exaggerating, believe me, you were the 'social-glue' that brought and bound together most people of the TBB. Lidija, your spot-on points with so well chosen words makes me more often speechless. I loved the long discussions about science and career during the strolls. Thank you very much for helping me with writing many, many mails and cover letters, for giving the chance to experience defense ceremony beforehand as your paranymph, for suggesting wonderful articles and books (feedback will never be the same again to me), and for sharing your experiences of the interviews. To put simply, I am very happy to have known you.

No theory can stand on its own, without the supporting experiments. My sincere thanks to Samuel Silverstein, Sadna Budhu, Peter Friedl, and Cindy Dieteren for generously sharing their published and unpublished data with us and for taking their time to explain a lot of the experimental details. I would like to thank Becca Asquith, Vitaly Ganusov, Hans Heesterbeek, Roland Regoes, and Roeland Merks for taking their time to read my thesis and for their valuable comments and suggestions.

TBB is a wonderful group to be in, and multi-purpose room (coffee room, only name changed to reflect its purpose) is the best place if you are in TBB: analysis of new scientific developments, and amazing (and sometimes inappropriate) lunch conversations. I will miss many traditions of this group: walks to *Gutenberg*; shouts of 'coffee' at a wide range of frequencies; singing for birthdays, publications, and what-not; and *borrels*. Thank you all TBB people, and particularly, Aridaman, Sandro, Paola, Lidija, Hanneke, Michael, Nobuto, Johannes, Thomas, Daniel, Folkert, Chris, 'pipeline' Bram, Bram, Renske, Alessia, Henk-Jan, Bruno, Rutger, Diego, Felipe, and Julien. Sandro, thank you for a lot of things (for obvious reasons, I can only mention few here): wonderful discussions, your sarcasm-loaded comments, and your extra-ordinary analysis of everything. Michael, I have lots of fun talking to you, traveling with you, and sharing a lot of stories about science and the related issues. Thank you very much and wish you all the best! Nobuto, you were also my flatmate for sometime. I enjoyed the conversations we had and the beers and *biryanis* we shared. You were very helpful to brainstorm about work and to identify the better ways in dealing with people. I wish that you will come back to NL for a longer stay. Thank you Chris, Johannes, Rutger (Hermsen) and Ioana for helping me out with CPM, brain-storming, analysis, and approximations. I wish you all success!

Thanks to Hanneke, Lidija, Renske, Alessia, and Rutger (Bos) for organizing group-uitjes,

dinners, canoeing, movie-nights, trips to *proeflokaal*, and other recreational activities for the group. You people made sure that TBB group had enough fun together. Thomas, Sandro, and Bram (van Dijk), the current and former Coffee czars, I greatly appreciate your efforts in making sure that our group has sufficient coffee, and in making TBB simply an exhilarating, caffeine-filled place.

I would like thank the people who made the wonderful cover of my thesis possible: Alessia and Bram. I am sure your designs would make my thesis stick with people a little longer. Alessia, thank you for taking time to make the sketches for my cover, despite the thesis-induced stress; I love the sketches you made. You brought people together (and the BBQ) for barbecue-ing on sunny afternoons. I wish you all the very best in finishing your thesis. Bram, thank you for converting the sketches to an even-more wonderful cover. I am glad that I could share office with you, and I loved the spontaneous discussions on different topics. Thank you for believing me to be the Batman!

I have shared office with wonderful people: Paola, Hanneke, Ilka, Jorg, Julia, Bram (pipeline), Ioana, Bram, Renske, and Gijs. You were all very helpful and cheerful to work with. Thank you all. Jorg, thank you for helping me with moving, for the wonderful discussions, and for the 4-times pdflatex solution. Hanneke, thank you for the dinners and always being there to help me out. Renske, thank you very much for your help with Dutch translation of summary and with CPM and excalib. Julia, your presence made Wednesdays in the office very nice.

Thanks to the lovely people from the extended-TBB: Lex, Oussama, and Sanja. Lex and Oussama, you are wonderful to hang out with, just like your better halves! Sanja, I wish I had a fraction of your boundless optimism, and I had lot of fun talking to you. Thank you for sharing ideas about future employment.

There are several people with whom I shared my flat with. Thank you Suresh, Das, and Jeba for taking me into your house when my visa processing took longer than I anticipated. Suresh, thank you for assuring that I can count on you if I need a place to stay temporarily; this really took pressure off of me. You were also very helpful around my thesis submission, sharing your food with me, assuring me that there is lot of room to maneuver around the submissions of forms 2 and 3, and suggesting me new movies to watch (we may soon be able to talk to each other in a language that is not native to both of us: Malayalam!). I wish you very best at Göttingen. Das, you are full of energy and a lot of fun to talk to. I could practice my *Hyderbadi* Hindi with you. Thank you for your company, and I wish you all the best your thesis and defense.

Ram, thank you for sharing your cooking-secrets, tips, and your trademark recipes. I also learned from you a lot about politics, and I hope all of these will come of help in future. I wish you success in future endeavors. Deepa, thank you for helping me to familiarize with Utrecht (and Zeist) in my very beginning days in NL. You were a pseudo-flatmate when I moved to Bunnik, and I had wonderful time hanging out with you.

I have met several compatriots in Utrecht. Raja and Brijesh, unforgettable memories of pongs of many sorts and barbecues at UCU. I wish you all the best with your respective

groups. Vamshi and Sada, thank you very much for all the beers and *biryanis*, and for helping me with moving houses. It was a lot of fun watching movies together and sharing about the books we read. Umesh and Jyotsna, you are among the most kind and generous people I have come across. Your helpful and caring nature has set a good example for me. Prajakta, Akshatha, Sankar and Sonu, it was a lot of fun traveling with you. Thanks to my dear movie-lovers: Aridaman, Tanmoy, Sudhanshu and Amol. I loved hanging out with you all people.

There are several other people who played an important role in my happiness, long before I moved to NL. Narendra Dixit, my master-thesis adviser, I enjoyed visiting your group during my trips to India. I am amazed by the changes happening in the group every year, including how many new faces replace the familiar ones. I appreciate that you took time to discuss recent research of your group. Thank you for sharing your wisdom on how the job description changes as one climbs up the ladder, and the new problem solving techniques you employ. I wish you and your group very best.

Sheeja, Shivanaresh, Gajendra, Pranesh, and Pradeep, thank you for making feel like at home whenever and wherever I meet you. Pranesh, thank you for taking care of my stay in IISc during my visits. Simna and Bindu, it is amazing that you trust me so much in so little time. You both made my second stay in Bangalore wonderful. I had a lot of fun talking to you all, hanging out in the tea-board, and many all-you-can-eat lunches. Wish you all the best with your future endeavors.

Subbu, thank you for being a wonderful host whenever I came for Dutch visas in India. I enjoyed meeting you and traveling with you. Vinod, Rajasekhar, and Mohan, I had lot of fun visiting you in Hyderabad and Bangalore. Rajesh, there are innumerable times where we talk for hours about the latest and upcoming gadgets, about the developments in our respective PhDs, and about other aspects of life. It was a lot of fun to extensively debate and discuss pros and cons of the new software we use. Thank you very much for introducing Linux and many other things that stuck with me even today. Kesari, it is a lot of fun every time catching up with you. I am glad to have your trust and support at all times. Thank you for being there for me! Sravan, we managed to keep in touch despite being miles away. It is unbelievable to me how long we known each other. Except the differences in the time zones, I am glad that everything remained the same between us, and I hope it stays the same in future.

Satya, you taught me to see the silver linings that exists everywhere, and stood by me in happy and difficult times. To say the least I am a more cheerful and positive person because of you. I wish you very best with finishing your thesis and with your future endeavors.

Last but never the least, I would like to thank Saroja (my mother), Subbaiah (my father) and Sainath (my brother) for their unconditional love and support at all times and for understanding many things without much explanations.